SINGLE-CRYSTAL $^{40}AR/^{39}AR$ PROVENANCE AGES AND POLARITY STRATIGRAPHY OF RHYOLITIC TUFFACEOUS SANDSTONES OF THE THURMAN FORMATION (LATE OLIGOCENE), RIO GRANDE RIFT, NEW MEXICO

Jenny Docherty Boryta

Submitted in partial fulfillment
of the requirements for the degree
of Master of Science in Geochemistry

Department of Geoscience
New Mexico Institute of Mining and Technology
Socorro, New Mexico
April 1994

ACKNOWLEDGEMENTS

I thank Bill McIntosh for suggesting this project and Martyne Kieling, John Kieling, Greg Mack, and Bill McIntosh for help in the field and guidance in selecting the appropriate units for sampling. I also thank John Geissman of UNM for the field gear and laboratory support during the months that followed. Roberto Molino and Gary Acton helped to show me paleomagnetic laboratory techniques at UNM and Matt Heizler of the New Mexico Bureau of Mines and Mineral Resources helped to supervise the laser fusion of sanidines in the Geochronology Laboratory at New Mexico Tech. The New Mexico Bureau of Mines and Mineral Resources provided financial support for this project during the spring and summer of 1993 when the data were analyzed. I especially thank Dr. Chapin of the Bureau for help with tuition and employment during my tenure as a master student at New Mexico Tech.

ABSTRACT

The Thurman Formation was sampled in two localities along the Rio Grande rift for paleomagnetic and single-crystal $^{40}Ar/^{39}Ar$ geochronology to determine the timing and duration of deposition and sanidine provenance of the synrift basin fill. More than 300 paleomagnetic specimens (32 sites) were drilled in 25-m intervals from two approximately 400-m-thick sections of sandstones, conglomeratic sandstones, and debris flows near Johnson Spring in the Rincon Hills and Apache Canyon in the Caballo Mountains. About 60 sanidines were analyzed by $^{40}Ar/^{39}Ar$ single-crystal laser fusion from three stratigraphic horizons at both localities to determine the age and provenance of individual grains. Provenance ages span 34.9 to 27.4 Ma but cluster at ages of 34.7, 33.3-33.5, 27.6, and 27.4 Ma.

Petrographic examinations show that the tuffaceous sandstones have detrital grains of sanidine, quartz, and plagioclase and detrital volcanic rock fragments of rhyolitic tuff, pumice, and deuterically altered or oxidized andesite. Opaque minerals in the rock fragments include magnetite, titanomagnetite, pyrite, ilmenite, and hematite. Authigenic cement of clay, zeolites, and hydroxides coat rims of grains and rock fragments. Clay and zeolites delicately line relict textures of pumice and tuff fragments and partially infill dissolved plagioclase grains.

Specimens collected for paleomagnetic studies were examined by reflected light microscopy and by alternating field and thermal demagnetization methods to assess the magnetic mineralogy, components of remanent magnetism, and the nature of the variations in remanence. Within the Apache Canyon section of the Thurman Formation, two magnetic polarity zones are identified and, based on the position of sanidine provenance ages within pumice and matrix of debris flows, the zones may span the time near the reversal at 27.4 Ma.

The sanidine provenance ages in the Thurman Formation can be correlated with high-precision $^{40}Ar/^{39}Ar$ sanidine geochronology of rhyolitic ash-flow tuffs in the Mogollon-Datil volcanic field. Sanidines dated at ~27.6 Ma from fluvial sandstones may represent reworked fall material from the Weatherby Tuff (27.6 ± .04 Ma) of the Boot Heel volcanic field and sanidines dated at 27.4 ± .21 Ma from pumice in a debris flow may represent fall material from South Canyon Tuff (27.4 ± .07 Ma). Sanidines from matrix in debris flows dated at 28.0, 33.3-33.5, and 34.7-34.9 may represent reworked tuff from Lemitar Tuff, Box Canyon Tuff, and Kneeling Nun Tuff. Sanidines from South Canyon Tuff and Lemitar Tuff were derived from an area more than 20 km to the west and north, where the vents and areal extent of the ash-flow tuffs are located.

Correlation of the sanidine dates with the regional extent of dated tuffs, independently established paleocurrent directions, and the magnetic polarity stratigraphy show that the rhyolitic tuffaceous sands of the Thurman were largely derived by the erosion of Box Canyon Tuff (33.5 Ma) and then Kneeling Nun Tuff (34.9 Ma) during and soon after the catastrophic eruption of South Canyon Tuff (27.4 Ma) from the Mount Withington caldera. The Thurman Formation is a syn- to posteruptive distal alluvial fan sequence of stacked debris flows and conglomeratic sands that rapidly accumulated in an early rift basin of the Rio Grande rift at an average rate of 1 mm/y. The Thurman Formation records the erosion and unroofing of Oligocene andesitic and rhyolitic volcanic rocks which were disrupted during the explosion of Mount Withington caldera at 27.4 Ma and which continued to be deposited as the lower Santa Fe Group through the late Oligocene. Throughgoing late Oligocene paleodrainage in central New Mexico was southward.

TABLE OF CONTENTS

LIST OF TABLES

LIST OF FIGURES

LIST OF FIGURES (continued)

Introduction

Age-dating and provenance work on single sanidine grains presented in this work help to resolve the timing, duration, and source of alluvial fan deposition and elucidate the mechanics of volcanism and faulting along the southern Rio Grande rift. Prior to this study, the duration and provenance of Cenozoic alluvial fan deposition along the Rio Grande rift have been examined (Barghoorn, 1981; Harrison and Burke, 1989; Waresback and Turbeville, 1990), but not directly dated. Primary pyroclastic tephra and ignimbrites intercalated with rift-basin alluvial sediments have been dated, but the dating of reworked volcaniclastic material has been largely ignored. High-precision, accurate geochronologic dates on synrift basin fill have been difficult to obtain because source units are diverse in age and undergo alteration during transport and diagenesis.

A number of new approaches to dating sedimentary sequences has recently been developed. With the design of rare-gas mass spectrometers (>10-3 A/torr) to allow precise measurements of small amounts of gas, laser fusion of single grains is now possible (Deino and Dalrymple, 1990; York and others, 1981; Lo Bello and others, 1987; Bogaard and others, 1987;) and is now being used with paleomagnetism to correlate ash-flow tuffs (Deino and Best, 1988; Deino, 1989) and to identify multiple provenance ages in sandstones (Renne and others, 1989; Heizler and Harrison, 1991; Harrison and Burke, 1989). A greater understanding of chemical and magnetic overprinting of marine and terrigenous sedimentary rock during burial and diagenesis (Heider and Dunlop, 1987; Walker and others, 1981; Larson and others, 1982; Mack and Grigsby, 1985; Welty, 1988; Karlin, 1990; Heider and others, 1993; Banerjee, 1987) have aided the interpretation of magnetostratigraphy in sedimentary sequences (Johnson and others,

1988; Johnson and McGee, 1983; Hillhouse and others, 1977). Magnetostratigraphy combined with single-crystal $^{40}Ar/^{39}Ar$ laser fusion of terrestrial volcanic rocks are being used to recalibrate the Geomagnetic Polarity Time Scale (Swisher and Prothero, 1990). Within the last decade, careful field mapping and paleomagnetic work in southern New Mexico (Ferguson, 1985; Harrison, 1990; Osburn and Chapin, 1983; Seager and Mack, in prep; McIntosh, 1989) and the accumulation of high-precision $^{40}Ar/^{39}Ar$ sanidine geochronology of volcanic units erupted at intervals of 0.2 Ma or less (Dalrymple and Deino, 1989; McIntosh and others, 1990) have allowed the development of a time-stratigraphic framework for the more than 30 major ignimbrites of the Mogollon-Datil volcanic field. Provenance ages of individual sanidines can now be used to determine which ignimbrites have been eroded and incorporated as detritus into synrift basin fill. All these advances have led to the possibility of using magnetic polarity stratigraphy and $^{40}Ar/^{39}Ar$ laser fusion of single grains for provenance and geochronologic work on volcaniclastic sediments.

This study combines $^{40}Ar/^{39}Ar$ laser fusion and magnetic polarity stratigraphy to examine the geochronology of the mid-Tertiary Thurman Formation in New Mexico. Results primarily bear on the provenance of volcaniclastic detritus shed into the Thurman Formation but also help elucidate the timing and processes of rift basin formation and the timing, duration, and sedimentation rate of synrift basin fill along the Mogollon-Datil volcanic field. Paleomagnetism is used to recover the polarity sequence in the Thurman Formation with the hope that the polarity sequence of normal and reversed polarity zones can be matched with the Geomagnetic Polarity Time Scale. Complex paleomagnetic behavior observed in the volcaniclastic sediments is investigated to determine the diagenetic processes that have affected the primary remanent magnetism. The age dates, provenance work, and magnetic polarity stratigraphy of reworked volcanic pumice and ash in the Thurman Formation reported here help to elucidate the dynamics of basin development alongside large volcanic fields. The geochronologic work explains how and

when the basin that accumulated the detritus of the Thurman Formation formed after development of the extensive Mogollon-Datil volcanic field. The provenance ages and the timing of deposition show that the nature of this accumulation is different from older and thinner sedimentary sequences in the Mogollon-Datil volcanic field and that the denudation of andesitic and silicic volcanic rocks and their accumulation in the Thurman Formation set the stage for the beginning of rifting in the Rio Grande rift.

Geologic Setting

The Mogollon-Datil volcanic field and Rio Grande rift

Previous workers have suggested that the beginning stages of rifting in the Rio Grande rift coincided with the late Oligocene 1.6-my interval of volcanism in the Mogollon-Datil volcanic field from 29.0 to 27.4 Ma during collapse of more than four caldera complexes (Chapin and Seager, 1975; Chamberlin, 1983; Seager and others, 1984; McIntosh and others, 1986, 1992). La Jencia Tuff (1250 km^3) erupted from collapse of the Sawmill-Magdalena cauldron at 28.8 Ma, Vicks Peak Tuff (1050 km^3) from Nogal Canyon cauldron at 28.6 Ma, Bloodgood Canyon Tuff (1000 km^3) from Bursum cauldron at 28.1 Ma, and South Canyon Tuff (700 km^3) from the Mount Withington cauldron at 27.4 Ma (Figure 1; McIntosh and others, 1990). These catastrophic eruptions followed more than 2.5 my of quiescence in volcanism (McIntosh and others, 1986, 1992) and coincided with local faulting. Syn- and posteruptive faulting during the 1.6-my interval from 29.0 to 27.4 Ma have been documented in the Lemitar Mountains, where angular unconformities separate the ignimbrite sheets of La Jencia, Vicks Peak, and South Canyon Tuffs (Chamberlin, 1983). Extrusion of basaltic andesites and smaller outbursts from rhyolite domes also spread andesitic flows and block-and-ash and pyroclastic deposits locally throughout the Mogollon-Datil volcanic field during this time.

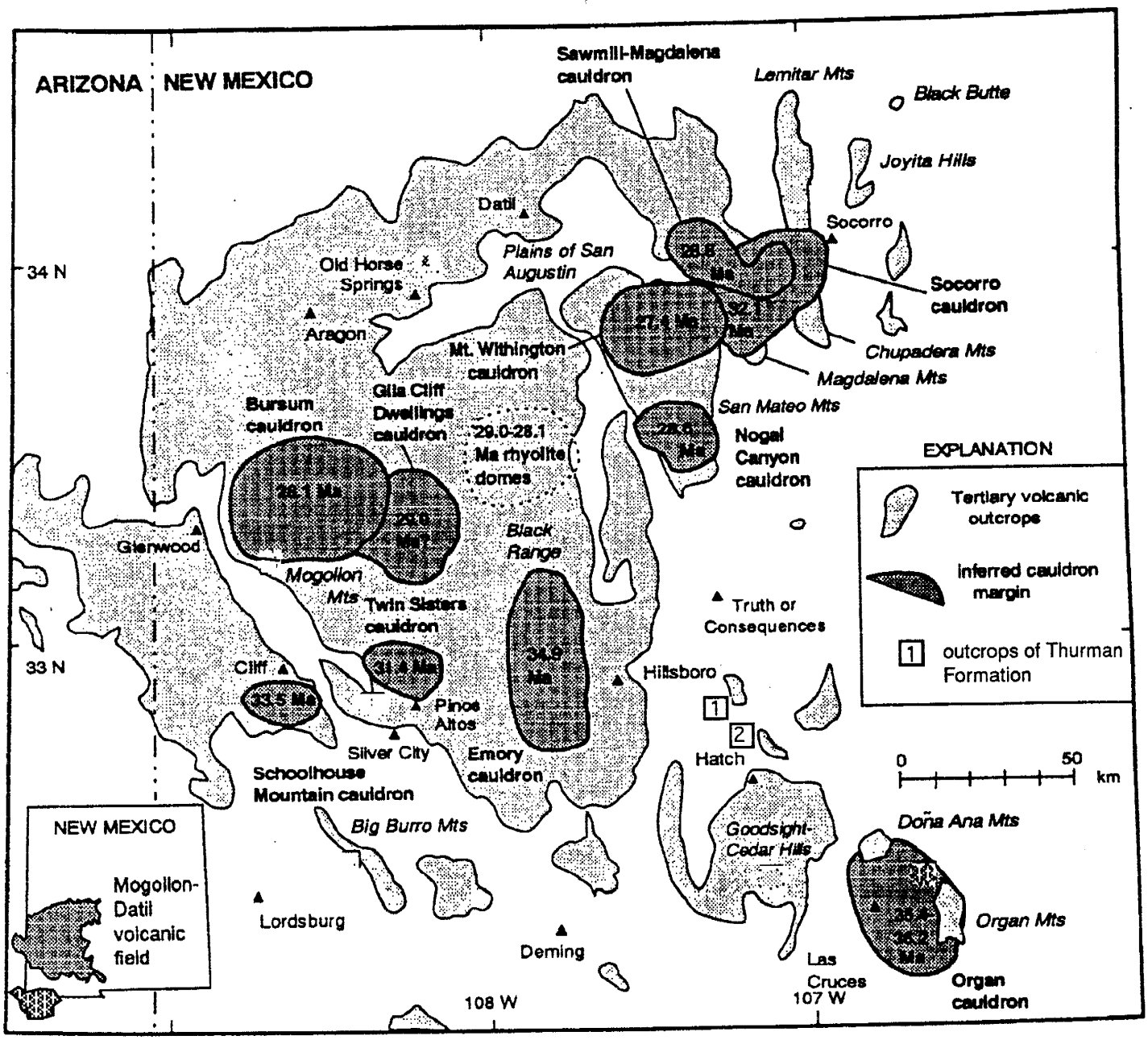

Boot Heel volcanic field

Figure 1 – Location of Tertiary volcanic rocks and calderas and Thurman Formation outcrops (from McIntosh et al., 1991).

The location of the Rio Grande rift on the eastern edge of the Mogollon-Datil volcanic field is controlled by pre-existing north-trending zones of weakness formed during deformations from at least as far back as the Paleozoic when the ancestral Rocky Mountains formed, through the Laramide (late Cretaceous to mid-Eocene), to the voluminous intermediate volcanism in the late Eocene-early Oligocene (Chapin and Seager, 1975; Christiansen and Lipman, 1972). Volcaniclastic sedimentary rocks eroded from the late Eocene-early Oligocene intermediate volcanism in the Mogollon-Datil volcanic field and deposited as detritus from about 37 to 32 Ma are preserved as thick sequences of intercalated purplish red to brown mudstones, debris flows, and conglomeratic sandstones. The 670-900-m-thick Spears Formation of the Datil Group of the northern Mogollon-Datil volcanic field lies below the Hells Mesa Tuff (32.1 Ma) that erupted from the Socorro cauldron (Osburn and Chapin, 1983; Cather and Chapin, 1989). Regional ignimbrites are interbedded with this thick sedimentary sequence of andesitic to rhyodacitic detritus that was shed into the 150-km wide Baca basin near Datil and the 100-km long Carthage-La Joya basin near Socorro (Cather and Chapin, 1989). The Rubio Peak Formation and Palm Park Formation of the southeastern Mogollon-Datil volcanic field are also up to 1000 m thick and consist mostly of andesitic to dacitic volcaniclastic sediments that were deposited in broad basins prior to eruption of the Kneeling Nun Tuff (34.9 Ma) from the Emory caldera (Harrison, 1990). These thick sedimentary sequences were eroded from the pre-SCORBA (Southern Cordilleran Basaltic Andesite) porphyritic basaltic andesites, smaller volume ignimbrites (36.2-35.0 Ma), and dominantly intermediate volcanic rocks of the late Eocene-early Oligocene Mogollon-Datil volcanic field (Cameron and others, 1989; McIntosh and others, 1992).

By the late Oligocene (32 to 27 Ma) thinner sedimentary sequences of a few to 30 m thick were deposited and preserved beneath basaltic andesites of the SCORBA suite and thick outflow sheets of rhyolitic to rhyodacitic ignimbrites. Correlative sedimentary units of these early rift sediments are found scattered west of the Rio Grande as thin

wedges in the Black Range, Magdalena and San Mateo Mountains, and Gallinas Range. In the Black Range, the sandstone of Monument Park, which contains clasts of Kneeling Nun Tuff, plagioclase, quartz, sanidine, and biotite, lies below basaltic andesite of Poverty Creek (29-28 Ma?) and is found beneath Rock House Canyon Tuff (34.4 Ma) and intercalated with Caballo Blanco Tuff (31.7 ± .06 Ma) in scattered outcrops about 15 m thick (Woodard, 1982; Harrison, 1990). In the Gallinas Peak area of the northern Mogollon-Datil volcanic field, the sandstones and conglomeratic sandstones of the sedimentary rocks of Antelope Flats lie above Vicks Peak Tuff (28.6 Ma), are intercalated with La Jara Peak Basaltic Andesite (28-24 Ma?) in a 55 m thick section, and then are conformably overlain by the South Canyon Tuff (27.4 Ma; LaRoche, 1980). Volcaniclastic sandstones are found thinly bedded between flows of La Jara Peak Basaltic Andesite east of Datil along the edge of the Bear Mountains (Mayerson, 1979). Thin outcrops of similar volcaniclastic sedimentary units exposed along the southern Rio Grande rift include upper Oligocene conglomeratic sands sandwiched between flows of La Jara Peak Basaltic Andesite and the Lemitar Tuff (28.0 Ma) and overlain by the South Canyon Tuff (27.4 Ma) in the Joyita Hills. Brownish red conglomeratic sands of the Bell Top Formation are overlain by the Uvas Basaltic Andesite (28-27 Ma?) in the Rincon Hills and a 3-m-thick wedge lies between the Kneeling Nun Tuff (34.9 Ma) and Vicks Peak Tuff (28.6 Ma) at Apache Canyon in the Caballo Mountains.

By 25-27 Ma normal faulting had disrupted the voluminous sheets of ignimbrites and basalt flow along the edges of the Mogollon-Datil volcanic field and sedimentary basins had formed and were accumulating detritus along the entire length of the Rio Grande rift (Chapin, 1988). In southern New Mexico, north and northwest-trending fault-bounded extensional sedimentary basins of late Oligocene to Miocene time have been preserved east of the Gallinas Range east of Datil in the Abbe Spring basin (also known as northern Milligan Gulch graben) and north of Hatch in the Rincon Hills and Caballo Mountains fault blocks, areas far from the center of Mogollon-Datil volcanic activity

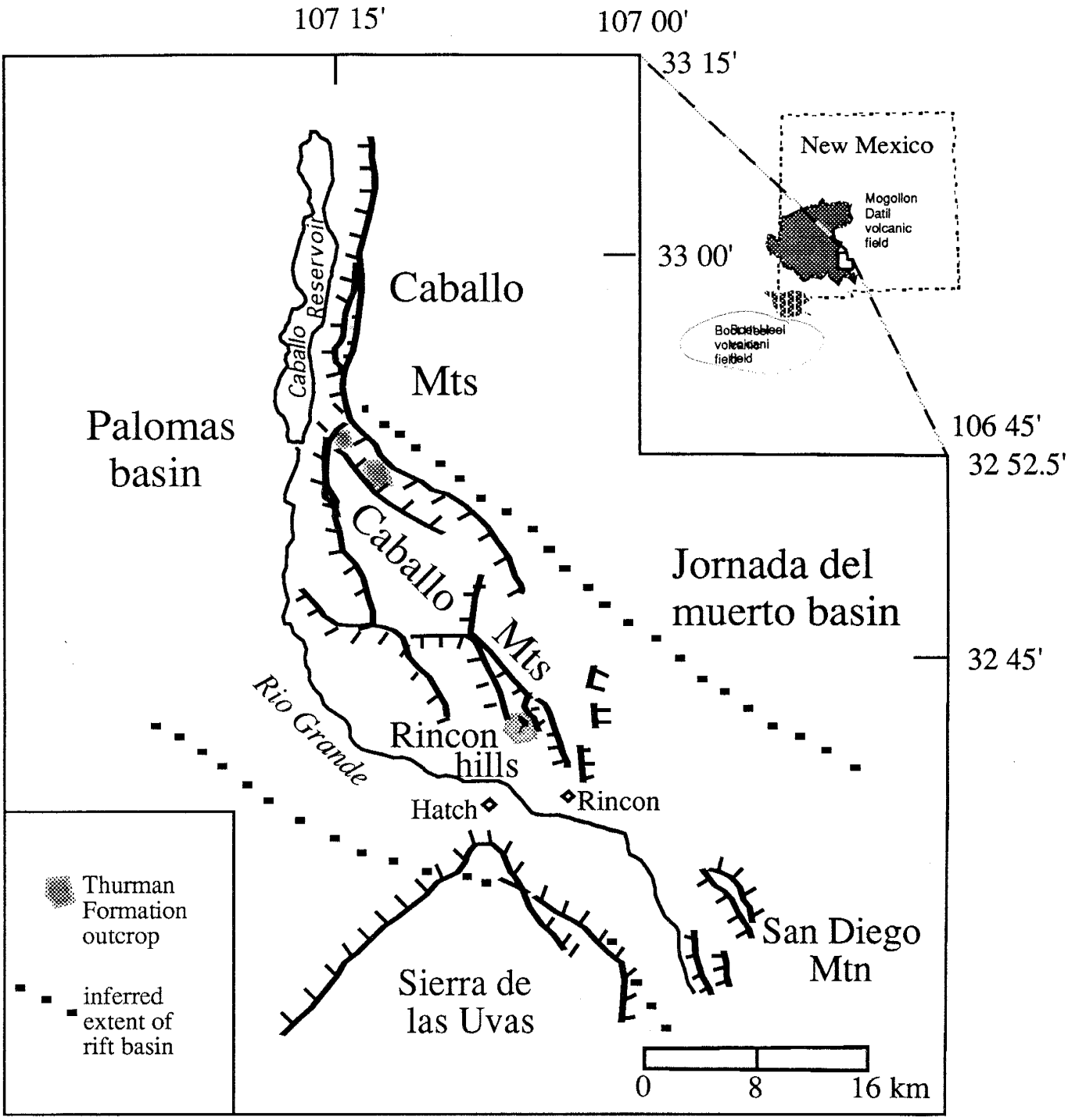

Figure 2- **Location of Thurman Formation outcrops**

(from Seager et al.,1984; Seager and Hawley,1973).

(Chapin and Seager, 1975; Seager and others, 1984; Figure 2). Late Oligocene andesite complexes such as the Sierra de las Uvas south of Hatch and the Bear Mountains east of Datil formed from the extrusion of (28-27 Ma?) Uvas Basaltic Andesite and (28-24 Ma?) La Jara Peak Basaltic Andesite, along the edges and near the sites of future basins (Chapin and Seager, 1975; Seager and others, 1984; Chapin, 1972). SCORBA magmas had leaked near faults that were reactivated as basin-bounding faults (Chapin and Seager, 1975; Chapin, 1988; Cameron and others, 1989) and the SCORBA suite and ignimbrites were then eroded and shed as detritus into these early rift basins of the Rio Grande rift (Chapin and Seager, 1975). The early rift basins were later disrupted by late Miocene-Pliocene extensional basin-and-range faulting that resulted in the closely spaced grabens and fault blocks seen today along the Rio Grande (Chapin and Seager, 1975).

Thurman Formation

The Thurman Formation is located in the early rift basin north of Hatch that lies at the eastern edge of the Mogollon Datil volcanic field (Seager and others, 1984). The only exposures of the Thurman Formation are preserved in two localities east of the Rio Grande in the Rincon Hills and Caballo Mountains (Figure 2). They lie north of the Sierra de las Uvas north of Las Cruces among deformed Paleozoic and Mesozoic beds, where the 20-km-long fault block of the southern Caballo Mountains divides the southwest-tilted sandstone beds at Johnson Spring in the Rincon Hills from the southeast-tilted beds at Apache Canyon in the Caballo Mountains. Kelley and Silver (1952) named these beds as part of the Thurman Formation and Seager and Hawley (1973) described its type section near Johnson Spring as a 600-m-thick exposure of rhyolitic volcaniclastic sandstones, ash-flow tuffs, and andesitic flows. Seager and Mack (in preparation) have redefined the Thurman Formation as the uppermost Thurman of Seager and Hawley (1973), a 400-m-thick unit of volcaniclastic sandstones that lies above a tongue of the Uvas Basaltic Andesite, which has been dated near Hillsboro at 28.1 ± 1.6 Ma by K/Ar

(Seager and others, 1984). Whereas tongues of the Uvas Basaltic Andesite lie beneath the Thurman Formation in the Rincon Hills, the Vicks Peak Tuff (also known as Bell Top 7 tuff; Clemons, 1976) dated at 28.6 ± 0.04 Ma by $^{40}Ar/^{39}Ar$ (McIntosh and others, 1992) lies beneath the Thurman Formation at the Apache Canyon section in the Caballo Mountains (Figure 3). An angular unconformity separates the Thurman Formation from the Vicks Peak Tuff (Figure 4). At the Johnson Spring section in the Rincon Hills, the Thurman Formation is unconformably overlain by the Camp Rice Formation (Pliocene) of the Santa Fe Group. Elsewhere in the Rincon Hills and in the Caballo Mountains the Thurman Formation is conformably overlain by the Haynor Ranch Formation (Miocene) of the Santa Fe Group (Seager and Hawley, 1973).

These outcrops in the Rincon Hills and the Caballo Mountains are the only two localities in New Mexico where the Thurman Formation has been exposed by basin-and-range faulting along the Rio Grande. Uplift of the Rincon Hills probably occurred after initial uplift of the Caballo Mountains; the continued uplift of the southern Caballo Mountains during late Miocene-Pliocene time is indicated by the offset of Rincon Valley Formation along boundary faults (Chapin and Seager, 1975).

The Thurman Formation has been described as a volcaniclastic alluvial fan sequence of rhyolitic tuffaceous sandstone accumulated in an early rift basin of the Rio Grande rift that extended 20 km from the Rincon Hills to the Caballo Mountains (Seager and others, 1984; Figure 2). Together with the overlying rocks of the Santa Fe Group the deposits of this rift basin are 1900 m thick. The sandstones of the Thurman Formation have been interpreted as debris flows, sheetflood, and streamflow deposits of a medial to distal alluvial fan (Kieling, 1993). The sediments consist of andesitic and silicic volcaniclastic material that was redistributed through gravity and stream-flow sedimentary processes (Kieling, 1993; Figure 5).

The Thurman Formation is the thickest sedimentary unit exposed among volcanic units erupted after 34.9 Ma in the southern Mogollon-Datil volcanic field and after 32 Ma

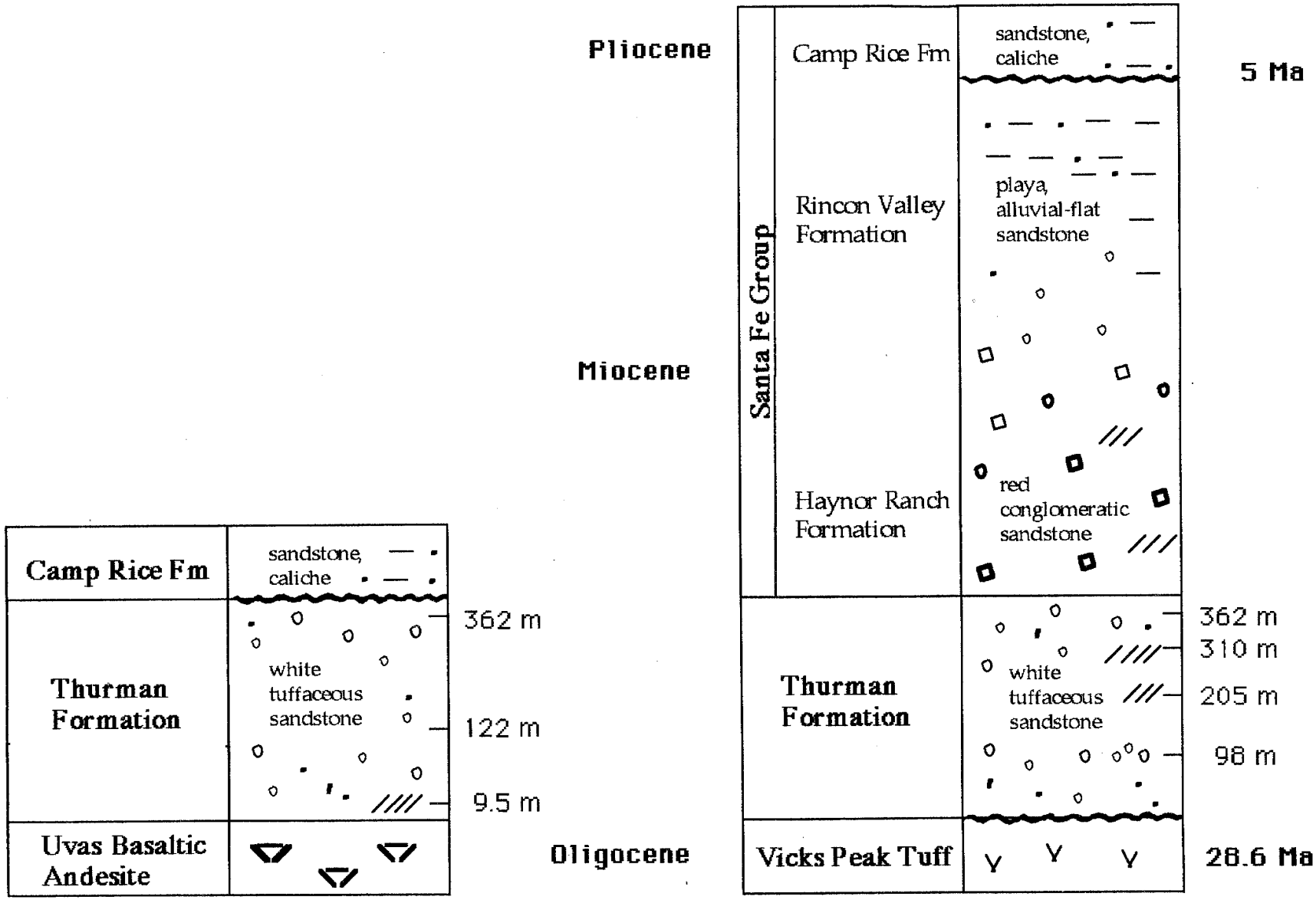

Figure 3--Stratigraphic sections of the Thurman Formation at two localities.

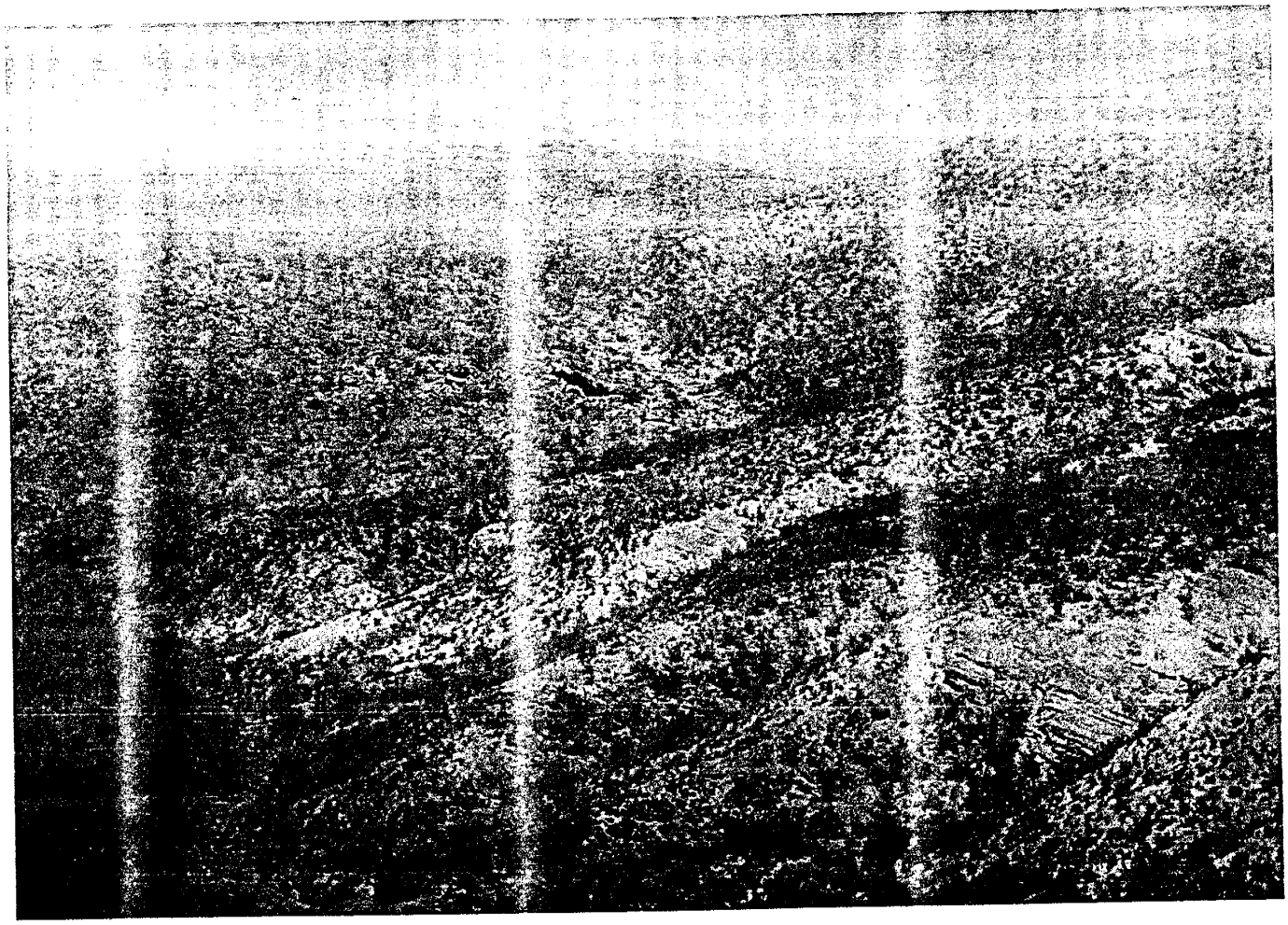

Figure 4- Beds of Thurman Formation in contact with underlying Vicks Peak Tuff, Apache Canyon, Caballo Mountains. Site nm1004 was drilled into southeast-tilted beds in right corner. Sanidine was sparse at this basal site. View is northward.

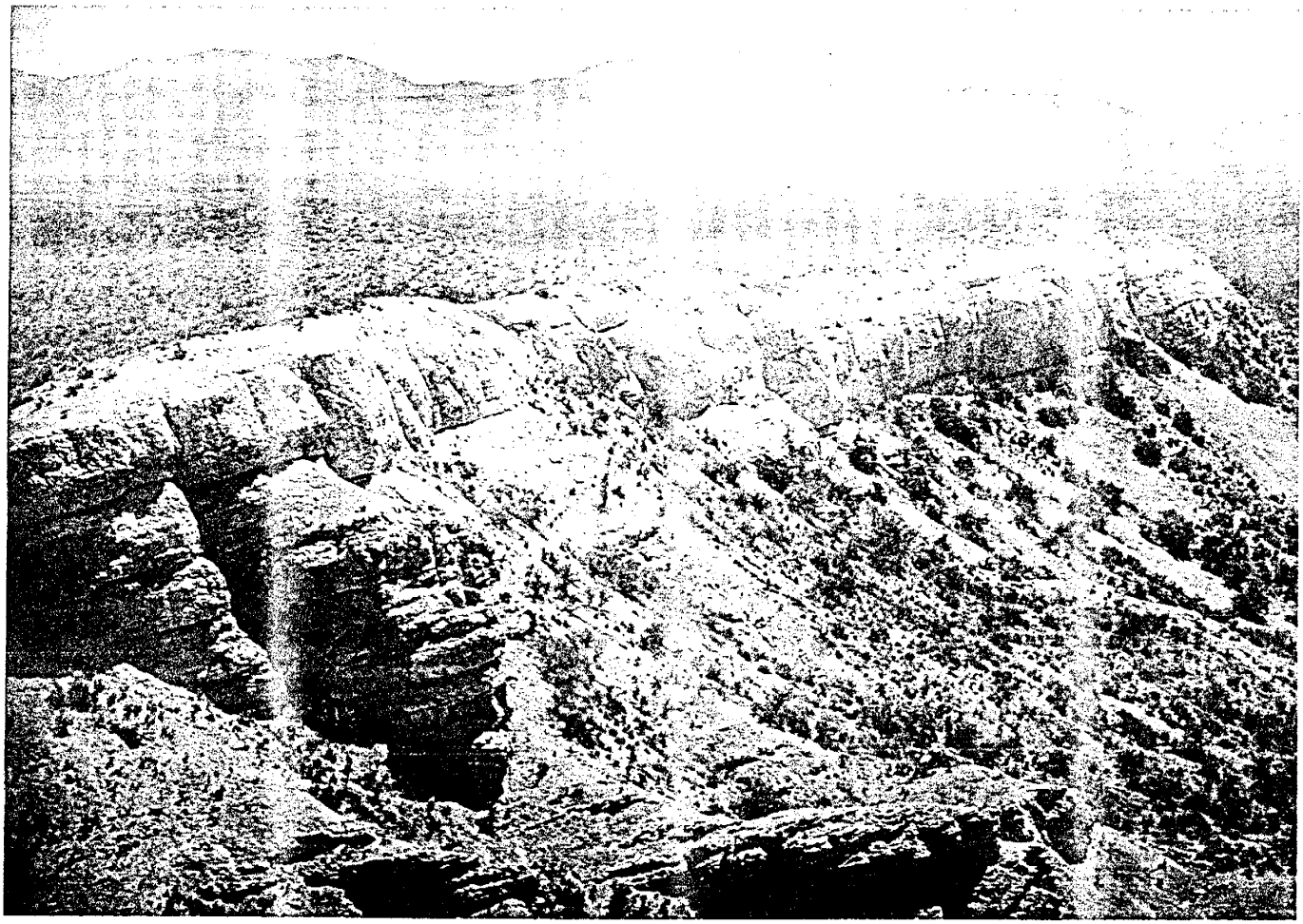

Figure 5- Beds of the Thurman formation, tilted to the Southeast. View is south toward Apache Canyon and the Southern Caballo Mountains.

in the northern Mogollon-Datil volcanic field. The Thurman Formation was deposited immediately prior to deposition of the 1-2 km thick synrift Santa Fe Group and its thickness and apparent lack of paleosols suggest it aggraded during a catastrophic event of high-sediment supply (Kieling, 1993). Its site of deposition is more than 70 km from the sites of caldera complexes of the Mogollon-Datil volcanic field; this location far from the center of volcanic activity, on the edge of a relatively high plateau bounded by normal faults, is appropriate for sedimentation and preservation. The geothermal gradient was relatively steep this far from the caldera complexes until 10 Ma, when it locally began to shallow (Morgan and others, 1986). The Thurman Formation was never buried deep enough to have experienced temperatures greater than 100 °C. The well preserved, nearly complete, continual exposure of the sands make the Thurman Formation an ideal unit for geochronologic study.

The primary goal of this project was to investigate the provenance, timing, and duration of deposition of the debris flows and sheetflood deposits of the Thurman Formation using $^{40}Ar/^{39}Ar$ single-crystal laser fusion of sanidines and magnetic polarity stratigraphy. Magnetic polarity stratigraphy has been used as a correlation and geochronologic tool (Khramov, 1958; Opdyke, 1972; Johnson and others, 1975; Johnson and McKee, 1983) and magnetic polarity stratigraphy and radioisotopic dating have been used together for dating the duration of alluvial fan deposition and for basin analysis (Hillhouse and others, 1977; Johnson and others, 1983, 1988). Sanidine is ideal for provenance and geochronologic studies because it is common in many tuffaceous sandstones, resists diagenetic alteration, is anhydrous, highly retentive of argon, and K rich, and has fairly flat plateau ages that agree with total gas ages. The time-stratigraphic framework of regional ignimbrites of the Mogollon-Datil volcanic field developed by McIntosh and others (1992) and based on a large collection of high-precision sanidine dates also made the choice of sanidine highly favorable. Previous geochronologic work using bulk sanidine separates on an ash unit near the top of the Thurman Formation at an

outcrop in Apache Canyon, Caballo Mountains suggested that $^{40}Ar/^{39}Ar$ single-crystal laser fusion is the best method to use to investigate the geochronology of the Thurman Formation; the age spectra results indicated a mixed population of sanidines of different ages (W. McIntosh, unpublished data, 1989; Figure 6). Advantages of using paleomagnetic techniques as a geochronologic tool on sandstones are that they are inexpensive and nondestructive. This paper presents $^{40}Ar/^{39}Ar$ results of 63 sandines and paleomagnetic results from 280 specimens collected from two sections in the Thurman Formation to help to elucidate the depositional history and provenance ages of the sands.

Methods

Paleomagnetism

The Thurman Formation was sampled near Johnson Spring in the Rincon Hills and along Apache Canyon in the Caballo Mountains. Paleomagnetic samples were collected at nearly uniform intervals from unweathered fine and medium sands from 16 sites across the two approximately 400-m-thick sections. The spacing between the 32 sites averaged 25 m and eight specimens were taken from each site. Sometimes weathered faces of beds were hammered to find fresh surfaces. About 5 sites had specimens drilled from within a one meter area; most other samples were taken across a 2-m-long horizon. Attitudes were determined from bedding orientation (Kieling, 1993). The Kneeling Nun Tuff and Vicks Peak Tuff were also sampled below the Thurman Formation at Apache Canyon to check for the possibility of block rotation about non-horizontal axes. The Thurman Formation was also sampled at two sites near the contact with the overlying Haynor Ranch Formation from an outcrop at another location along Apache Canyon.

Altogether about 300 paleomagnetic specimens were analyzed from the 32 sites. The cores were obtained using a hand-held battery-operated drill. The cores were 1.6 cm in diameter and 5-7 cm in length and were oriented by sun compass to an accuracy of

Figure 6 - Anomalous age spectrum indicative multiple age populations of sanidines in the Thurman Formation

about ± 2 degrees. Specimens were cut from the cores in lengths of 1.4 cm. Natural remanent magnetism (NRM) of specimens from each site was initially measured by a Schonstedt SSM-1 spinner magnetometer at the New Mexico Bureau of Mines and Mineral Resources but intensities (typically 10-20 mA/m) were too weak for accurate analysis by this instrument. Subsequent analyses were performed in the magnetic-field-shielded room at the University of New Mexico Paleomagnetism Laboratory. After remeasurement of NRM vectors, four specimens per site were thermally demagnetized in 9-11 steps and four specimens were demagnetized in progressive alternating fields of 2-60 mT in 11 steps measured by a 2-G Model 760R cryogenic magnetometer. Only three specimens were thermally demagnetized from site nm950. One pilot specimen from each site was thermally demagnetized to 660 °C in 17 steps, except for sites nm956, nm961-nm965, which were thermally demagnetized to 610 °C. Bulk susceptibility was measured after each heating increment by a Sapphire SI-2 induction coil to monitor changes in mineralogy. No significant changes were induced by heating, however, a slight increase at 350 °C may indicate that titanomaghemite formed from heating titanomagnetite in air (Figure 7). The lab-induced titanomaghemite should inherit the direction of the primary parent titanomagnetite (Gapeev and others, 1991). The slight increase in susceptibility at 350 °C may also reflect a minor amount of magnetite forming from alteration of clay minerals or oxidation of pyrite.

Most specimens were progressively AF demagnetized to 60 mT, however, by 40 mT the intensity remaining was often less than 10% of NRM. Results were analyzed using vector subtraction on orthogonal demagnetization diagrams (Zijderveld, 1967). The best estimate of the characteristic remanent magnetization (ChRM) direction for each specimen was obtained using principal component analysis (PCA; Kirschvink, 1980). Two to three components were commonly found at each site and site mean directions for the components were analyzed using Fisher (1953) statistics.

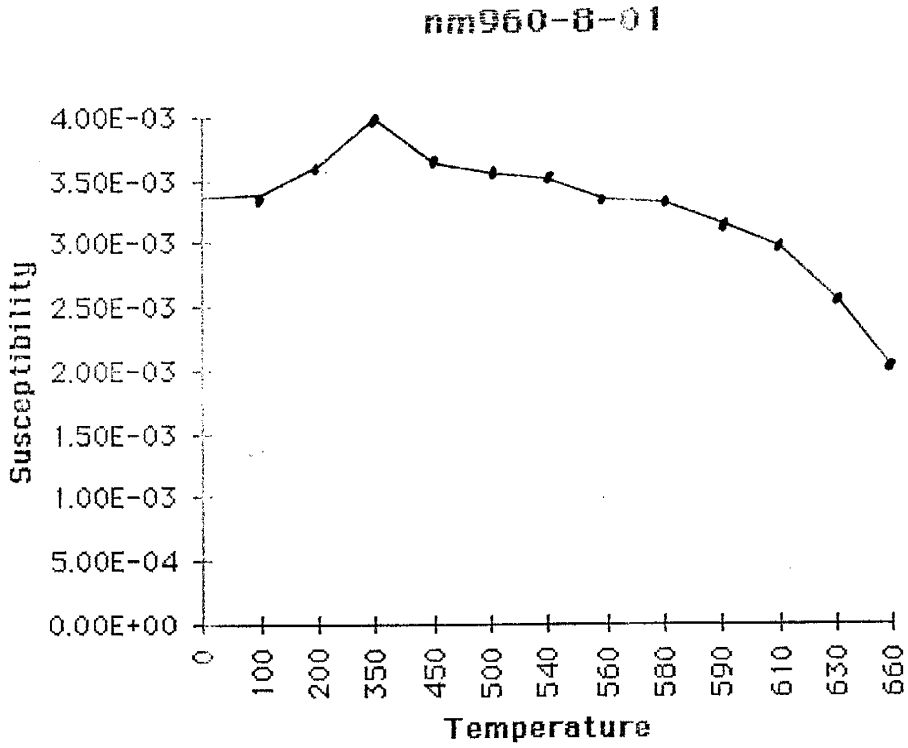

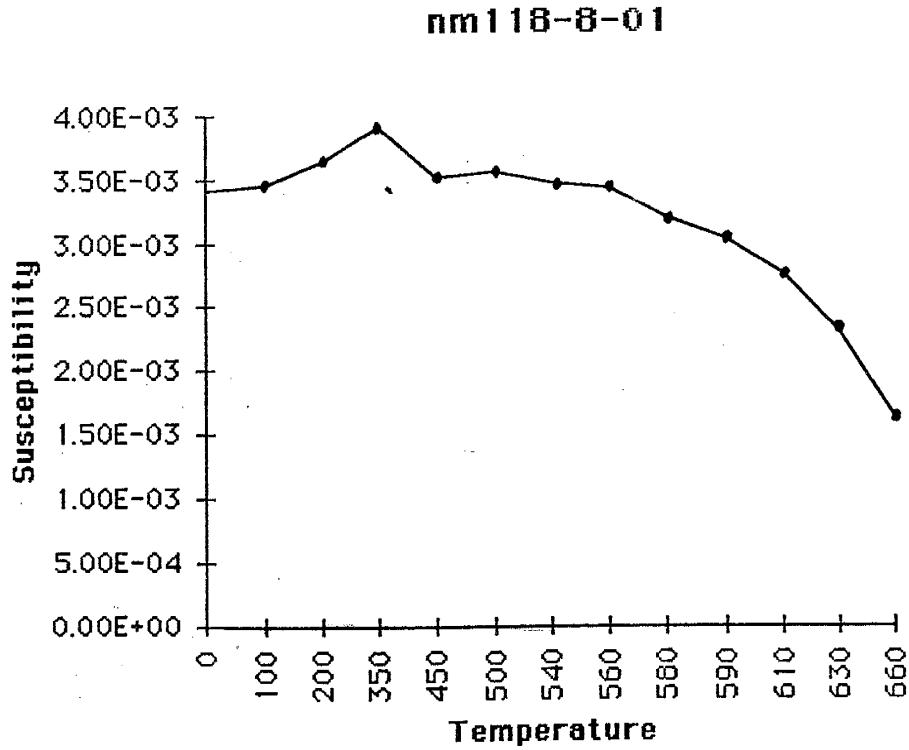

Figure 7 - Specimens displayed a slight increase in susceptibility at 350°C in sites from both localities.

Thin sections were made from rocks collected near and along the same stratigraphic horizon as the 32 paleomagnetic drill sites. Petrographic examination of the thin sections were used to recover the diagenetic history of the sands from deposition through burial, uplift, and tilting, to assess the depositional magnetic mineralogy, and to check for alteration that may have occurred during diagenetic changes and that may have affected the sanidines and the magnetic properties of the sands.

$^{40}Ar/^{39}Ar$ single-crystal laser fusion

Samples were taken in the field at 25 m intervals and were crushed and sieved and then chosen for mineral separation for $^{40}Ar/^{39}Ar$ geochronologic work. Based on the presence of sanidine, five horizons were chosen for dating in the Apache section and three horizons in the Johnson Spring section. The basal units of both sections were included although they contain multiple populations of fine-grained plagioclase and sparse sanidine. Detrital sanidines were separated from the samples using standard heavy liquid methods and the surrounding silicic glass was cleaned ultrasonically in distilled water and diluted HF. Most samples except those from the basal sands had identifiable populations of sanidine that could be hand picked on the basis of color and shape. Hand-picked grains were 0.4-0.8 mm in diameter from the Apache Canyon section and 0.25-0.4 mm from Johnson Spring. Two sub-populations of sanidines that varied in size or degree of abrasion were hand picked from samples from two horizons at Apache Canyon (nm1011, nm1016) to check for bias picking of sanidines. Approximately 3 mg samples of hand-picked sanidines were then wrapped in aluminum foil packets and were packaged in two quartz vials along with packets of 0.18-0.25 mm Fish Canyon Tuff sanidine (27.84 Ma) flux monitors positioned 3-7 mm apart. The flux monitors and samples were irradiated in the H-5 position at the University of Michigan Ford Reactor. Single grains of sanidines were placed in a copper sample holder and fused with an automated 4-W CO_2 laser through a ZnSe window and then analyzed by an automated MAP 215-50 mass

spectrometer. Blank gas was analyzed after every five samples. Total fusion and gas cleanup entailed less than one minute of laser heating and 10 minutes of gettering. The percentage of blank to sample gas remained low (<2%); the total ^{40}Ar system blank was typically less than 10^{-15} moles. The ages vs ^{39}Ar% released were plotted for each horizon and a mean age was calculated for 3 or more grains based on ^{39}Ar% released; sanidines that showed large variance from a mean age were excluded from calculation of the mean age (Figure 8). Crystals that showed low ^{39}Ar% released or low $^{40}Ar^*$ from incomplete fusion were rejected from further analyses. More accurate mean ages of sanidines for a horizon were then calculated and grouped by K/Ca. Uncertainties are quoted at the one sigma level.

Altogether 76 crystals were fused and analyzed; approximately eight crystals per horizon, five horizons from the Apache Canyon section and three horizons from Johnson Spring. The fine crystals from the basal units of the Apache Canyon section and Johnson Spring section (sites nm1004 and nm950) yielded anomalous data with low $^{40}Ar^*$ and low K/Ca which suggested that crystals other than sanidine were separated. Data from site nm1004 have been rejected from this study.

Results

Petrography

The fine to medium coarse sand beds of the Thurman Formation are generally massive, medium to medium-well sorted, and well cemented. A few crossbedded horizons (sites nm950, nm1011, nm1016) are well sorted. Pumice (typically 1-6 mm), andesitic and tuff fragments (1-2 mm), and feldspars and quartz (1-2 mm) are in a matrix of clayey volcanic rock fragments and feldspar. Grain contacts are tangential to longitudinal. Fractures along grains are largely nonexistent.

The detrital grains are angular to subrounded volcanic rock fragments (55-70%), plagioclase (10-15%), sanidine (15-25%), quartz (5-10%), and a trace other minerals

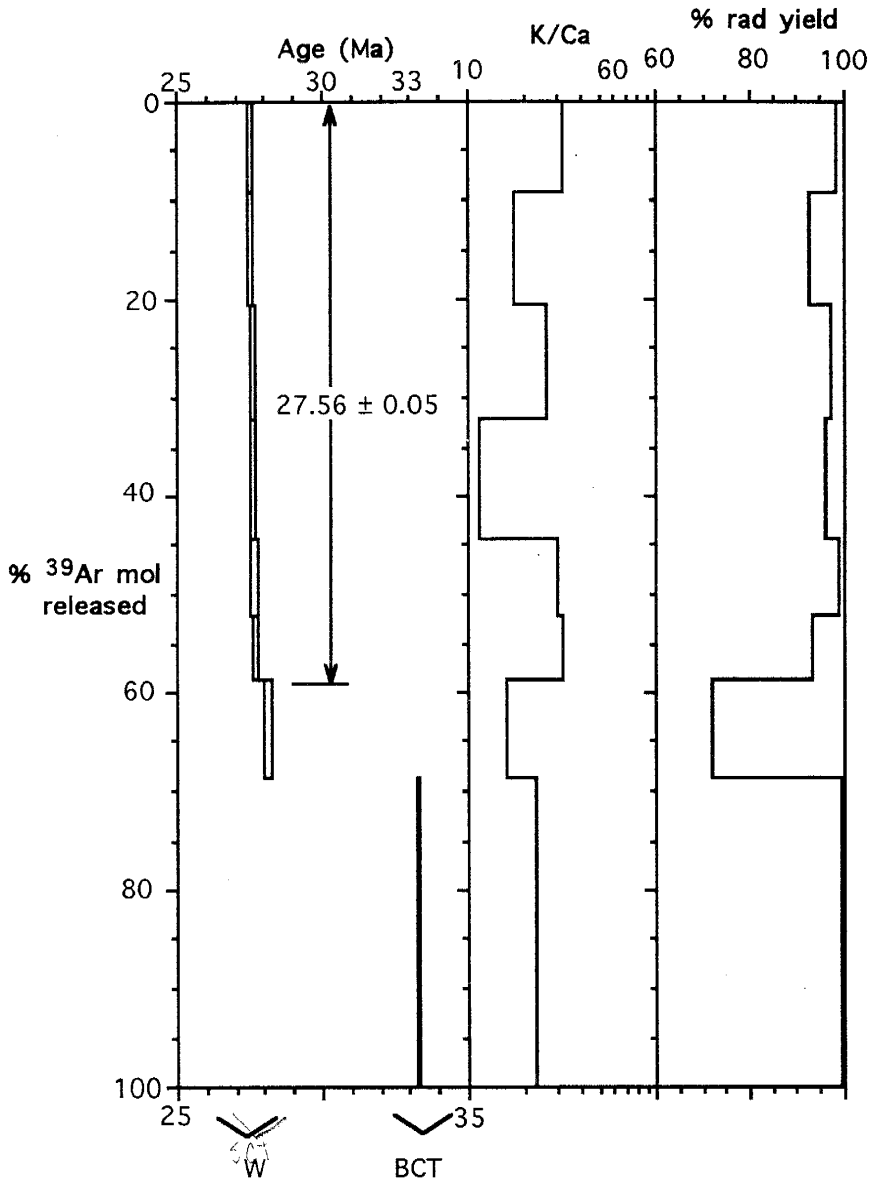

nm954, Johnson Spring, 122 m, sanidines, 0.25-0.4 mm

Figure 8. Preliminary $^{40}Ar/^{39}Ar$ total fusion spectrum showing age, K/Ca, and radiogenic yield for individual sanidine grains

including biotite. The volcanic rock fragments are predominantly relict pumice, welded and nonwelded tuff, and andesite (Figure 9). Delicate relict glass shards are also present (Figure 10), but their abundance is difficult to estimate because they are so easily altered from cristobalite and feldspar to clay and zeolite. The opaque minerals in andesitic fragments include pyrite, ilmenite with trellis structure, magnetite, titanomagnetite, and hematite that range in size from 0.6 to 5 μ. The opaque minerals in pumice and tuff fragments include magnetite and titanomagnetite that are generally smaller in size. Abundances of detrital grains change nonsystematically upsection, but no major change in mineralogy was noted (Figures 9,10). A few detrital grains of plagioclase have completely altered to calcite at certain horizons or have been partially to completely dissolved away, yet their relict morphology has been preserved.

Clay is strikingly prevalent throughout both sections of the Thurman Formation. Clay coats grain rims, lines pores, and delicately infills relict pumice. Some grains and volcanic rock fragments have meniscus coatings of clay on one side. Clay is generally absent at primary grain-to-grain contacts, yet is found infilling rare fractures in sanidines and plagioclases. The interior intergranular clay within relict pumice fragments is delicate and wispy and formed soon after deposition. The clay was largely derived by intrastratal alteration of silicic glass and feldspar in the surrounding pore water.

Two zeolites line relict pumice and glass shards and infill pores of the Thurman Formation. A tabular zeolite used the clay linings of pores, grain rims, and intergranular material as a substrate for nucleation throughout the section at Apache Canyon (Figure 10). A tabular zeolite and a zeolite with a more fibrous habit are prevalent throughout the section at Johnson Spring. The fibrous zeolite found only in the Johnson Spring section uses the older tabular zeolite as a substrate for nucleation and may have formed in response to a change in pore fluid chemistry in the Johnson Spring area.

Calcite is common as an authigenic cement only within 3 m of the top of the Thurman at both sections (sites nm965, nm1019, nm1021). A few calcite grains are

A

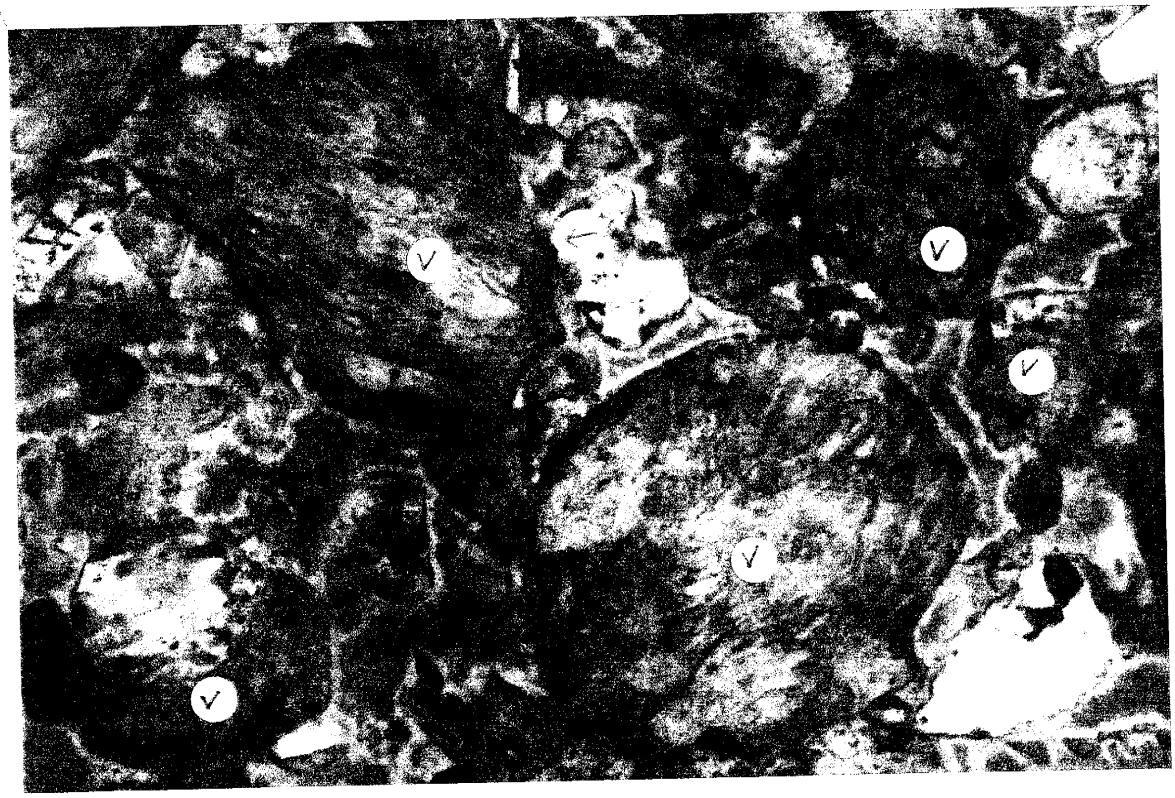

B

Figure 9 - Relict pumice fragments [illegible]
B) plane light, arrow points to [illegible]
[illegible] Site nm1007, 70m, Apache Canyon

A

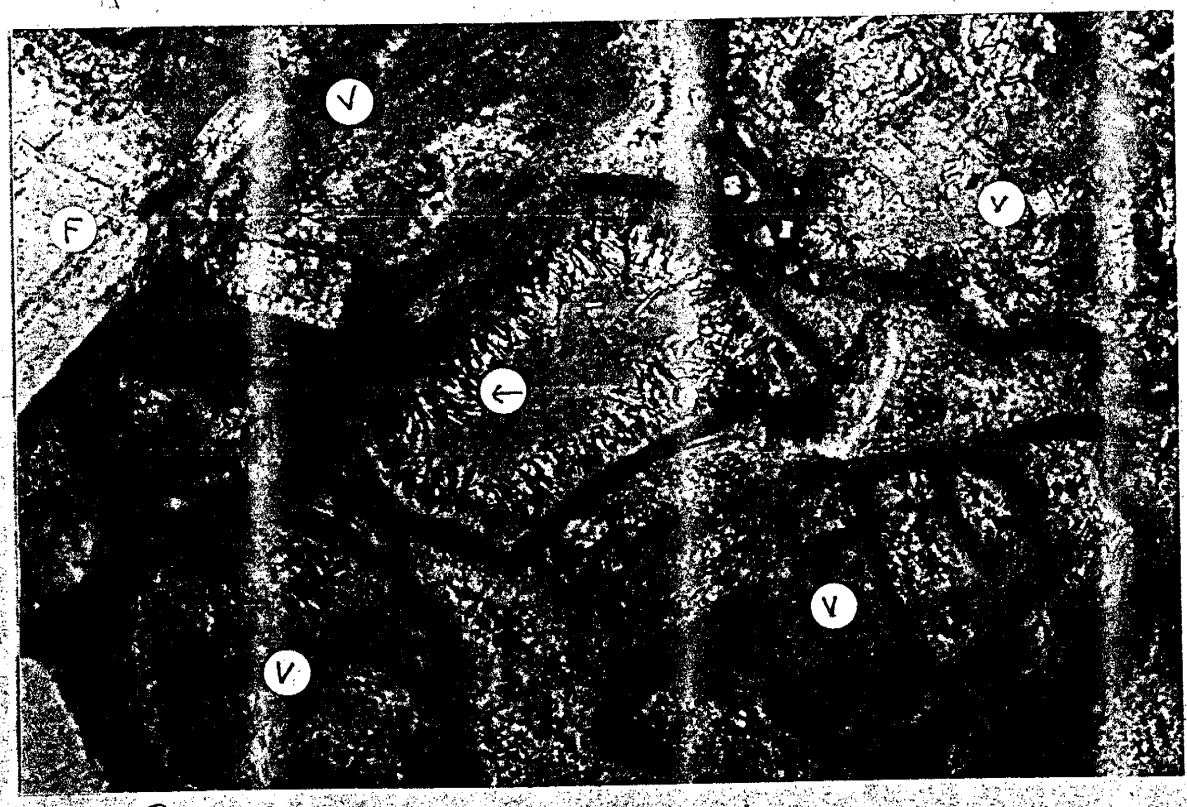

B

Figure 10 - Texture of tuffaceous sandstones: A) relict texture of delicate glass shard preserved, nm 952. B) dissolved, tangential volcanic rock fragments with clay rims preserving morphology of grains. Note tabular zeolite (clinoptilolite) growing toward pore center, nm 950. Length of photo = 1 mm, Johnson Spring, 9.5m.

disseminated in half of the other 30 thin sections of sites, except at another horizon (sites nm1006, 1007, 1008) near and above a clastic dike, where calcite grains are poikolotopic and partially replace plagioclases or infill pores within 5 μ of partially dissolved plagioclases.

Throughout both sections amorphous hydroxides coat andesitic rock fragments or fill nearby pores in splotches up to .05 mm wide (Figure 11). They are found crosscutting zeolites and calcite. These hydroxides may be lepidocrocite or goethite.

$^{40}Ar/^{39}Ar$ single-crystal laser fusion

The results of $^{40}Ar/^{39}Ar$ laser fusion on single grains from the Thurman Formation are shown in Table 1. The one-sigma analytical errors of single ages are listed; the J value represents the calculated analytical uncertainty of 0.25-0.33%. The dates were grouped in terms of K/Ca and then mean ages were computed. The K/Ca of sanidines from sandstone horizons at 205 m and 310 m (sites nm1011 and 1016) are relatively high for sanidines from ignimbrites from the Mogollon-Datil volcanic field and the Boot Heel volcanic field. These horizons also have abraded and blocky euhedral grains with lower radiogenic yields of 77-94%. Most sanidines from each horizon have radiogenic yields between 95 and 99%. Plagioclases with low K/Ca from site nm950 near the base of the Thurman Formation have low radiogenic yields of 56-90%.

The degree of abrasion had little to no effect on the results of dates from the sanidines in the Thurman Formation. Sites nm950, nm965, and nm1019 from sandstones and debris flows at the base and tops of both sections have sand-size sanidines that have been slightly abraded through mechanical abrasion during transport or chemical corrosion. Sites nm1011 and nm1016 from sandstones near the middle of the Apache Canyon section have abraded 0.4-0.8 mm sanidines and blocky euhedral 0.4-0.6 mm sanidines that show little to no abrasion, and yet the dates of the abraded and blocky euhedral sanidines from sites nm1011 and nm1016 are similar. Six abraded sanidines

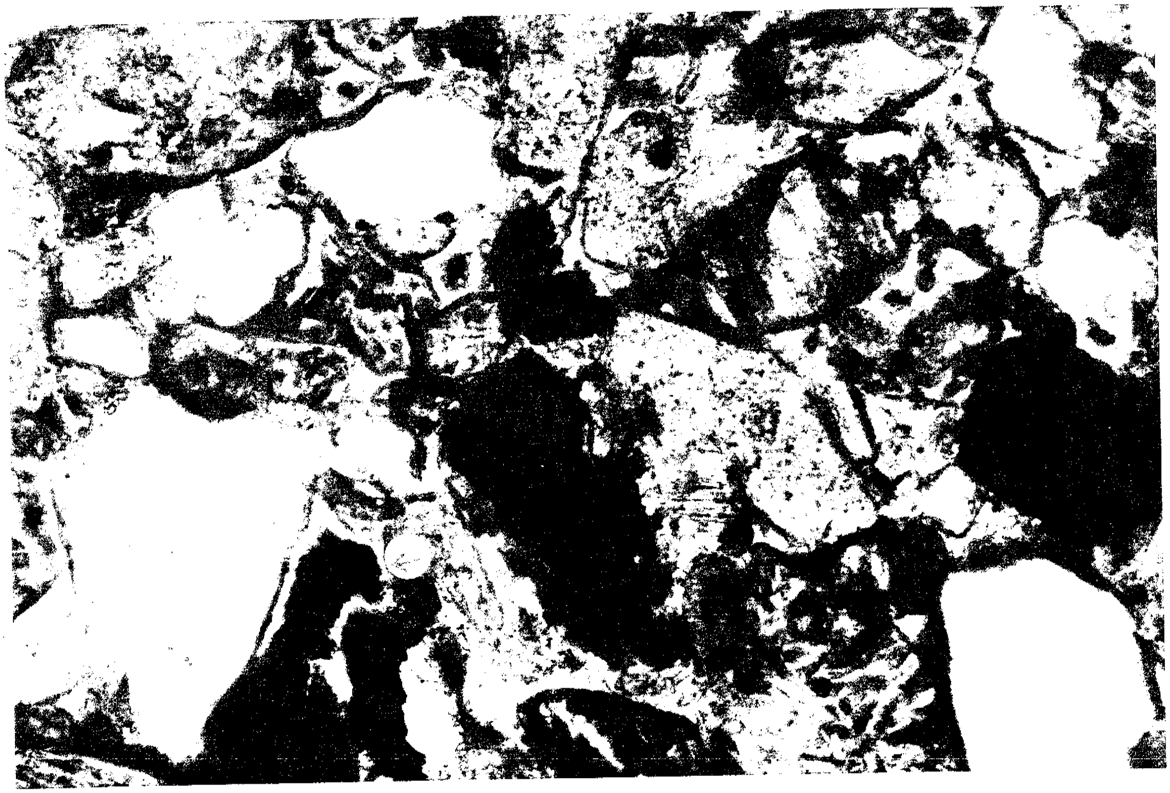

A

B

Figure 11 - Oxidized ... limestone ... Length of photos, 1 mm. ...

Table 1--40Ar/39Ar Provenance Ages of the Thurman Formation.

Lab#	40/39	37/39	36/39	39K moles	K/Ca	± Err	%40*	Age	± Err	SEM
nm1008, Apache Canyon, 98 m, sanidine, 0.6-0.8 mm, J=0.004287+0.00001										
211-86A	3.65	8.28E-03	3.64E-04	1.0E-14	61.6	5.2	97.1	27.057	0.065	
211-87A	3.64	7.54E-03	3.11E-04	2.9E-15	67.7	25.1	97.5	27.096	0.175	
211-83A	3.59	3.42E-03	9.05E-05	3.9E-15	149.2	70.7	99.3	27.215	0.115	
211-84A	3.71	7.94E-03	4.48E-04	5.8E-15	64.3	6.7	96.4	27.361	0.102	
211-82A	3.78	1.10E-02	6.38E-04	1.7E-14	46.4	1.1	95.0	27.439	0.063	
211-90A	3.79	1.03E-02	6.59E-04	3.1E-14	49.5	1.5	94.9	27.445	0.061	
211-81A	3.94	1.26E-02	1.17E-03	3.3E-14	40.5	0.8	91.2	27.455	0.070	
211-85A	4.00	6.08E-03	1.27E-03	6.0E-15	*83.9*	*97.8*	90.6	27.702	0.107	
mean of 1 to 8				n=8	68.448	36.989		27.346	0.214	0.076
nm1011, Apache Canyon, 205 m, sanidine, 0.4-0.6 mm, J=0.004312+0.00001										
211-96A	3.67	6.90E-03	3.11E-04	4.7E-15	73.9	14.0	97.5	27.467	0.102	
211-97A	4.59	1.38E-02	3.41E-03	1.8E-14	37.0	1.1	78.0	27.525	0.107	
211-95A	4.18	2.24E-03	2.02E-03	1.1E-14	227.8	37.8	85.7	27.538	0.090	
211-91A	3.63	2.42E-03	9.72E-05	1.3E-14	210.8	38.6	99.2	27.683	0.061	
211-94A	3.63	1.70E-03	8.90E-05	1.2E-14	300.1	70.5	99.3	27.692	0.067	
211-93A	4.13	2.03E-03	1.78E-03	1.1E-14	251.3	84.7	87.2	27.715	0.085	
211-92A	3.66	2.65E-03	1.68E-04	7.5E-15	192.5	50.4	98.6	27.745	0.082	
211-98A	4.60	7.07E-03	1.95E-04	8.0E-15	72.2	10.4	98.8	34.859	0.089	
mean of 1 to 2				n=2	55.5 n<3			27.496 n<3		
mean of 3 to 7				n=5	236.5	41.6		27.675	0.080	0.036
mean of 8				n=1	72.2 n<3			34.859 n<3		
nm1011a, Apache Canyon, 205 m, sanidine (abraded), 0.4-0.6 mm, J=0.004332+0.00001										
211-104A	4.01	9.89E-04	1.69E-03	7.4E-15	*515.9*	612.3	87.5	27.132	0.103	
211-105A	3.94	2.13E-03	1.21E-03	7.1E-15	239.1	104.0	90.9	27.633	0.091	
211-103A	3.62	3.03E-03	1.31E-04	1.2E-14	168.3	32.6	98.9	27.636	0.114	
211-101A	3.64	1.86E-03	1.83E-04	1.6E-14	274.0	45.8	98.5	27.693	0.065	
211-99A	3.63	1.88E-03	1.34E-04	1.6E-14	270.8	61.2	98.9	27.730	0.061	
211-100A	3.61	2.88E-04	3.26E-06	8.0E-15	*1769.1*	2577.7	100.0	27.857	0.066	
211-102A	4.62	9.46E-03	3.60E-03	2.0E-14	53.9	2.3	76.9	27.443	0.091	
mean of 1 to 6				n=6	238.0	49.1		27.614	0.250	0.102
mean of 7				n=1	53.9 n<3			27.443 n<3		

Table 1--40Ar/39Ar Provenance Ages of the Thurman Formation (continued).

Lab#	40/39	37/39	36/39	39K moles	K/Ca	± Err	%40*	Age	± Err	SEM
nm1016, Apache Canyon, 310 m, sanidine, 0.4-0.6 mm, J=0.004345+0.00001										
211-37A	3.64	2.29E-03	3.24E-04	2.8E-14	223.0	24.3	97.4	27.425	0.057	
211-24A	3.69	2.31E-03	4.29E-04	2.8E-14	220.9	17.2	96.6	27.612	0.055	
211-25A	4.54	1.41E-03	3.28E-03	2.4E-14	362.1	52.5	78.5	27.632	0.093	
211-38A	3.73	3.51E-03	5.26E-04	1.5E-14	145.6	22.4	95.8	27.682	0.076	
211-23A	4.04	2.98E-03	1.54E-03	1.6E-14	171.4	21.8	88.7	27.719	0.080	
211-36A	3.60	2.65E-03	6.77E-05	2.6E-14	192.6	23.9	99.4	27.726	0.059	
211-51A	3.85	2.66E-03	8.83E-04	3.5E-14	192.0	12.5	93.2	27.765	0.060	
211-49A	3.87	2.96E-03	9.51E-04	2.2E-14	172.4	16.0	92.7	27.770	0.065	
211-50A	3.64	2.14E-03	1.36E-04	2.8E-14	238.8	28.2	98.9	27.842	0.057	
mean of 1 to 9			n=9		213.2	63.1		27.686	0.121	0.040
nm1016a, Apache Canyon, 310 m, sanidine (abraded), 0.6-0.8 mm, J=0.004338+0.00001										
211-40A	4.14	2.80E-03	2.05E-03	4.4E-14	182.4	14.8	85.3	27.329	0.065	
211-53A	4.60	2.68E-03	3.55E-03	3.5E-14	190.1	20.0	77.1	27.444	0.087	
211-79A	3.98	1.37E-03	1.45E-03	3.7E-14	371.2	49.4	89.2	27.448	0.066	
211-14A	3.68	2.67E-03	3.81E-04	2.6E-14	191.2	21.8	96.9	27.560	0.067	
211-01A	3.61	2.51E-03	9.66E-05	3.8E-14	203.0	21.7	99.2	27.686	0.052	
211-66A	3.65	2.96E-03	1.96E-04	5.7E-14	172.4	7.8	98.4	27.764	0.053	
211-27A	3.91	3.06E-03	1.08E-03	2.8E-14	166.8	11.0	91.8	27.774	0.070	
mean of 1 to 7			n=7		211.0	71.7		27.572	0.174	0.066
nm1019a, Apache Canyon, 362 m, sanidine (abraded), 0.4-0.6 mm, J=0.004371+0.000014										
211-47A	3.61	4.39E-03	2.22E-04	8.4E-15	116.1	16.8	98.2	27.617	0.075	
211-42A	3.63	1.68E-03	2.25E-04	1.5E-14	304.6	47.5	98.2	27.710	0.061	
211-43A	5.39	1.96E-03	6.10E-03	1.2E-14	260.5	68.2	66.4	27.886	0.141	
211-41A	3.67	2.33E-02	3.16E-04	1.2E-14	21.9	0.5	97.5	27.852	0.071	
211-45A	4.31	1.34E-02	9.59E-05	1.6E-14	37.9	1.8	99.4	33.305	0.069	
211-48A	4.34	1.03E-02	2.01E-04	2.0E-14	49.4	2.3	98.6	33.319	0.066	
211-46A	4.33	1.55E-02	1.40E-04	1.3E-14	33.0	1.7	99.1	33.365	0.073	
211-44A	4.70	8.32E-03	8.09E-04	2.4E-14	61.4	1.6	94.9	34.671	0.070	
mean of 1 to 3			n=3		227.1	98.6		27.738	0.137	0.079
mean of 4			n=1		21.9 n<3			27.852 n<3		
mean of 5 to 7			n=3		40.1	8.4		33.330	0.032	0.018
mean of 8			n=1		61.4 n<3			34.671 n<3		

Table 1--40Ar/39Ar Provenance Ages of the Thurman Formation (continued).

Lab#	40/39	37/39	36/39	39K moles	K/Ca	± Err	%40*	Age	± Err	SEM
nm950a, Johnson Spring, 9.5 m, sanidine & plagioclase (abraded), 0.25-0.4 mm, J=0.004349+0.000014										
211-35A	4.33	6.71E+00	6.15E-03	2.3E-16	0.1	0.0	69.9	23.593	1.823	
211-29A	4.36	2.50E+00	3.36E-03	5.1E-16	0.2	0.0	81.5	27.633	0.886	
211-28A	4.00	2.69E+00	2.02E-03	6.6E-16	0.2	0.0	90.2	28.013	0.676	
211-31A	6.64	3.97E+00	1.09E-02	6.7E-16	0.1	0.0	56.0	28.953	0.819	
211-33A	4.08	4.62E+00	1.68E-03	3.7E-16	0.1	0.0	96.5	30.606	1.045	
211-32A	8.21	6.27E+00	1.01E-02	2.3E-16	0.1	0.0	69.5	44.299	2.149	
211-30A	4.46	9.66E-03	4.57E-04	5.0E-15	52.8	6.2	97.0	33.452	0.111	
plagioclase	mean of 1 to 5		n=5		0.1	0.1		27.760	2.597	1.161
plagioclase	mean of 6		n=1		0.1 n<3			44.299 n<3		
sanidine	mean of 7		n=1		52.8 n<3			33.452 n<3		
nm954, Johnson Spring, 122 m, sanidine, 0.25-0.4 mm, J=0.004325+0.00001										
211-64A	3.63	1.63E-02	2.22E-04	6.1E-15	31.2	2.5	98.2	27.461	0.094	
211-62A	3.85	2.92E-02	9.55E-04	7.7E-15	17.5	0.8	92.7	27.486	0.091	
211-88A	3.67	1.97E-02	3.38E-04	7.9E-15	25.9	1.7	97.3	27.548	0.092	
211-75A	3.74	4.43E-02	5.33E-04	8.2E-15	11.5	0.5	95.9	27.604	0.088	
211-89A	3.62	1.71E-02	1.17E-04	5.2E-15	29.8	3.0	99.1	27.639	0.114	
211-77A	3.85	1.63E-02	8.72E-04	4.4E-15	31.4	2.8	93.3	27.685	0.137	
211-76A	5.04	3.19E-02	4.74E-03	6.6E-15	16.0	0.5	72.2	28.062	0.143	
211-63A	4.36	2.27E-02	1.12E-04	2.1E-14	22.5	0.6	99.3	33.293	0.068	
mean of 1 to 6			n=6		24.6	8.3		27.571	0.088	0.036
mean of 7			n=1		16.0 n<3			28.062 n<3		
mean of 8			n=1		22.5 n<3			33.293 n<3		
nm965a, Johnson Spring, 362 m, sanidine (abraded), 0.25-0.4 mm, J=0.004378+0.000014										
211-70A	4.30	1.04E-02	6.33E-05	1.3E-14	49.0	2.4	99.6	33.371	0.081	
211-74A	4.31	1.49E-02	7.04E-05	6.4E-15	34.2	2.3	99.5	33.418	0.094	
211-67A	4.40	9.98E-03	3.60E-04	5.7E-15	51.1	7.2	97.6	33.433	0.120	
211-72A	4.31	1.09E-02	5.50E-05	8.1E-15	47.0	4.0	99.6	33.461	0.083	
211-68A	4.45	1.28E-02	4.89E-04	6.7E-15	39.8	3.7	96.8	33.571	0.100	
211-73A	4.47	8.77E-03	5.44E-05	5.4E-15	58.2	9.1	99.7	34.722	0.111	
211-69A	4.50	1.32E-02	1.41E-04	6.2E-15	38.6	2.7	99.1	34.748	0.109	
mean of 1 to 5			n=5		44.2	7.0		33.451	0.075	0.033
mean of 6 to 7			n=2		38.6 n<3			34.735 n<3		

		± Err
D=	1.00810	0.0015000
Ca 39/37=	0.00067	0.0000037
Ca 36/37=	0.00026	0.0000017
K 38/39=	0.01190	
K 40/39=	0.01800	0.0010000

from site nm1011 have an age of 27.61 ± .25 Ma and a K/Ca of 238 and five blocky euhedral sanidines have an age of 27.67 ± .08 Ma and a K/Ca of 237. Site nm1011 also has two blocky euhedral sanidines and one abraded sanidine dated at 27.47 ± .10 Ma, 27.52 ± .11 Ma, and 27.44 ± .09 Ma with a mean K/Ca of 55 and one blocky euhedral sanidine dated at 34.86 ± .09 Ma with a K/Ca of 72. Site nm1016 has seven abraded sanidines with an age of 27.57 ± .17 Ma and a K/Ca of 211 and nine blocky euhedral sanidines with an age of 27.69 ± .12 Ma and a K/Ca of 213. The abraded sanidines from site nm1016 were 1.5 to 2 times larger than the sanidines with uneroded surfaces yet the ages and K/Ca values are similar for both sizes of grains. Radiogenic yields, however, were slightly lower for the abraded sanidines from sites nm1011 and nm1016. They ranged from 76.9 and 77.1 to 99%, whereas the blocky euhedral sanidines have radiogenic yields from 78.0 and 78.5 to 99%. The effect of abrasion on the sanidines appears to have only slightly increased the error of the ages of grains. It is important to note that the source of the sanidines cannot be distinguished by degree of abrasion or size of grain. At 205 m and 310 m the source of sanidines in the Thurman Formation is similar: sanidines with an age of 27.64 ± .15 Ma and mean K/Ca of 222 ± 58. At 205 m there are two other minor sources of sanidines with an age of 27.48 ±.05 Ma and a K/Ca of 55 ± 19 and an age of 34.86 ± .09 Ma with a K/Ca of 72 ± 10.

Although the sparse sanidines at the base of the Apache Canyon section could not be adequately separated and dated, sanidines were dated from 1.5-2 cm pumice in a debris flow from site nm1008 at 98 m from the base of the Apache Canyon section. The eight blocky euhedral 0.6-0.8 mm sanidines have an age of 27.35 ± .21 Ma and a K/Ca of 68 ± 37. In contrast, abraded 0.4-0.6 sanidines dated from a debris flow at the top of the Apache Canyon section (site nm1019) vary in age from 27.74 ± .14 Ma to 34.67 ± .07 Ma. Three sanidines have an age of 27.74 ± .14 Ma and a K/Ca of 227 ± 99, one sanidine has an age of 27.85 ± .07 and a K/Ca of 22 ± 1, three sanidines have an age of 33.33 ± .03 Ma and a K/Ca of 40 ± 8, and one sanidine has an age of 34.67 ± .07 Ma and

a K/Ca of 61 ± 2. The delicate pumice collected at the 98 m horizon of the Apache Canyon section appear to have been derived from the same fall unit yet the abraded sanidines at 362 m have been reworked and eroded from four different ash-flow tuffs or fall units.

Horizons at 9.5 m, 122 m, and 362 m from the base of the Johnson Spring section have 0.25-0.4 mm sanidines that range in age from 27.57 ± .09 Ma to 34.74 ± .11 Ma. Five plagioclases from site nm950 at 9.5 m from the base of the Thurman Formation have an age of 27.76 ± 2.6 Ma and another plagioclase is as old as 44.3 ± 2.15 Ma. The only sanidine date from this basal horizon is from a sanidine with a K/Ca of 53 ± 6 and an age of 33.45 ± .11 Ma. The mean age of six sanidines from site nm954 is 27.57 ± .09 Ma and the ages of the other sanidines are 28.06 ± .14 Ma and 33.29 ± .17 Ma. The grain dated at 28.06 ± .14 Ma showed a relatively low radiogenic yield of 72.2%. The mean age of five sanidines from site nm965 is 33.45 ± .08 Ma. The ages of two other sanidines from this horizon at the top of the Thurman are 34.72 ± .11 Ma and 34.75 ± .11 Ma.

Demagnetization Behavior

AF demagnetization successfully isolated the characteristic remanent magnetism (ChRM) in the Kneeling Nun Tuff and Vicks Peak Tuff at the Apache Canyon locality and the site mean directions are in agreement with previously established magnetic directions for these tuffs (McIntosh, 1991; Figures 12, 13). The similarity in directions indicates that the ChRM in these ignimbrites is thermal remanent magnetism (TRM) in origin and that the fault block that comprises the Thurman Formation in the Caballo Mountains has not been rotated about non-horizontal axes. The site-mean directions for the Thurman Formation at the Apache Canyon section should reflect directions of the paleomagnetic field soon after deposition of the Thurman Formation if the isolated ChRM is detrital remanent magnetism (DRM) in origin.

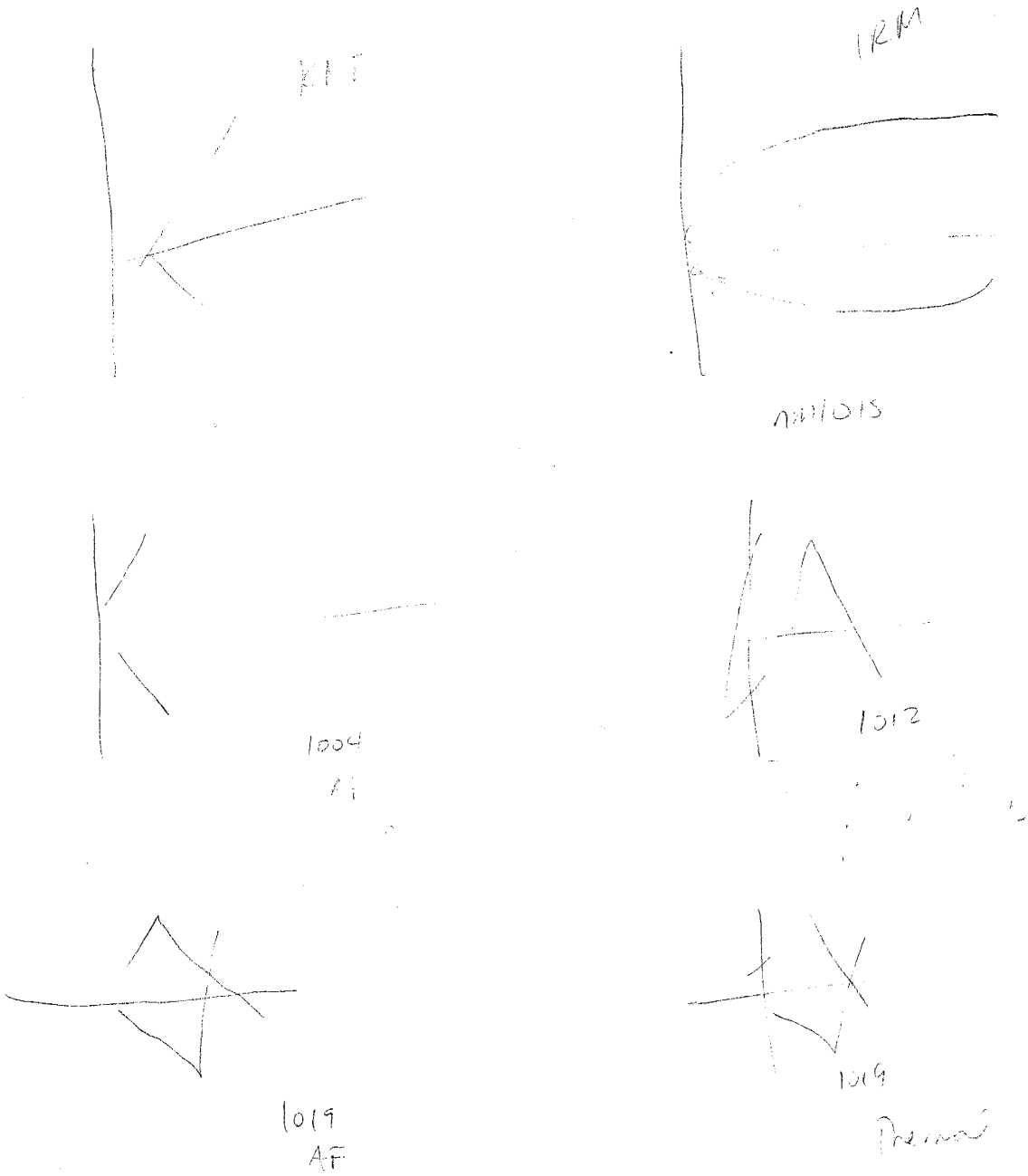

Figure 12 - Demagnetization behavior of specimens from The Apache Canyon section

Path: D:\JENNY\APACHE\JAN
File: NM104-3 .DU 1,040 .a.. 1-09-93 9:22:34 pm Page 1

nm104-3-01	0mT	21.0	61.8	53.7	329.8	2.070E-02	25.0	13.0	64.3	9.4
nm104-3-01	2mT	21.0	61.8	54.1	338.6	1.980E-02	25.0	13.0	61.0	18.1
nm104-3-01	5mT	21.0	61.8	52.6	339.9	1.900E-02	25.0	13.0	59.4	17.0
nm104-3-01	8mT	21.0	61.8	52.0	338.9	1.810E-02	25.0	13.0	59.3	15.3
nm104-3-01	10mT	21.0	61.8	51.2	338.9	1.730E-02	25.0	13.0	58.7	14.2
nm104-3-01	15mT	21.0	61.8	51.2	337.8	1.560E-02	25.0	13.0	59.2	13.3
nm104-3-01	20mT	21.0	61.8	50.8	337.4	1.380E-02	25.0	13.0	59.1	12.4
nm104-3-01	25mT	21.0	61.8	49.6	336.1	1.220E-02	25.0	13.0	59.7	11.6
nm104-3-01	30mT	21.0	61.8	49.5	335.9	1.070E-02	25.0	13.0	59.8	9.3
nm104-3-01	35mT	21.0	61.8	49.7	335.3	9.310E-03	25.0	13.0	59.2	11.0
nm104-3-01	40mT	21.0	61.8	49.1	336.3	8.450E-03	25.0	13.0	59.1	8.2
nm104-3-01	50mT	21.0	61.8	51.5	330.3	7.080E-03	25.0	13.0	62.6	6.5
nm104-3-01	60mT	21.0	61.8	48.8	330.8	6.490E-03	25.0	13.0	60.4	3.3

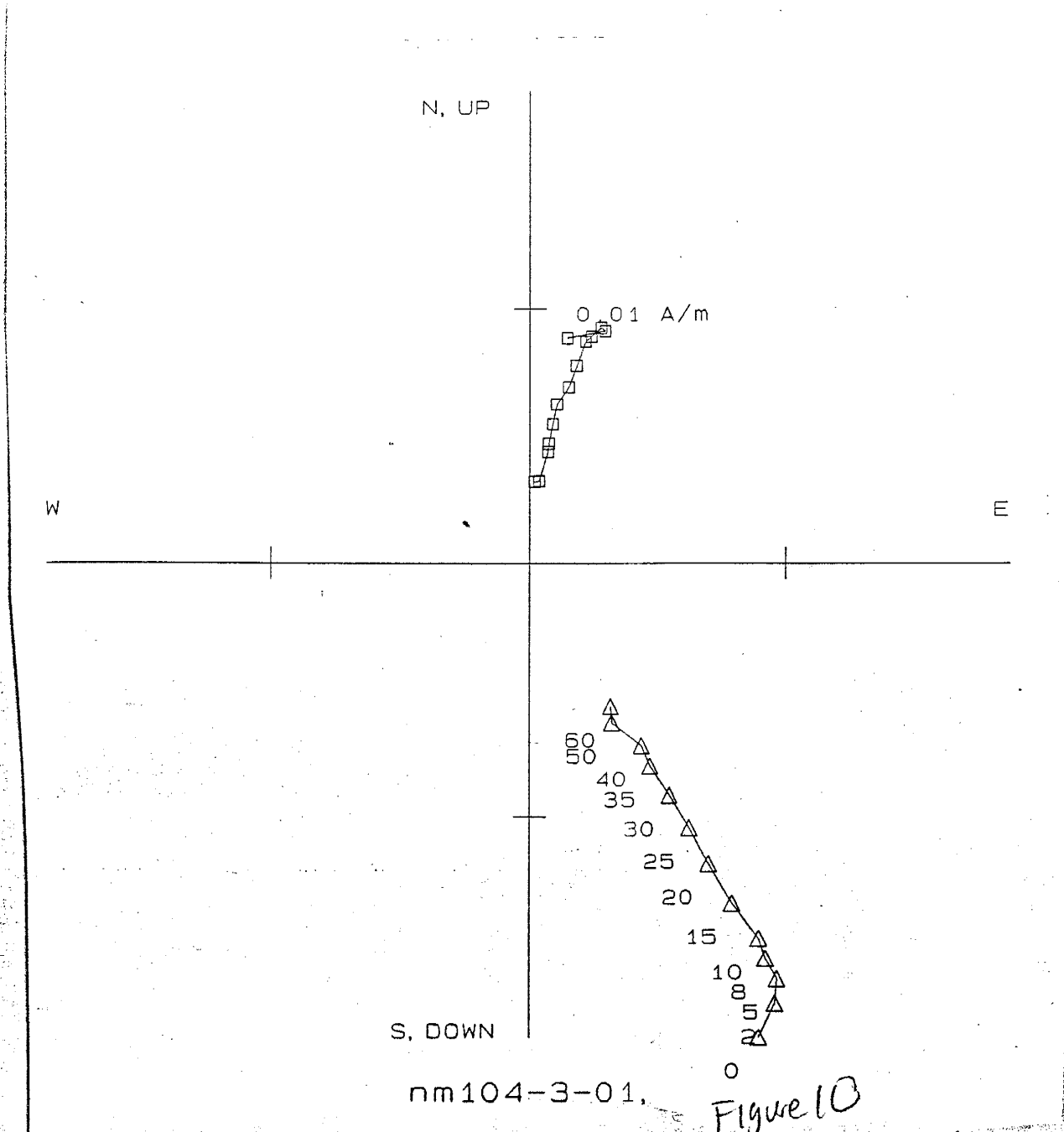

nm104-3-01, Figure 10

Path: D:\JENNY\APACHE\FEB
File: NM112-3A.DU 800 .a.. 2-21-93 12:39:12 pm Page 1

m112-3-02	0 C	40.0	25.4	37.7	344.2	1.520E-02	25.0	13.0	45.7	5.8
112-3-02	100 C	40.0	25.4	38.6	349.2	1.260E-02	25.0	13.0	44.3	11.2
m112-3-02	200 C	40.0	25.4	-72.1	147.0	1.250E-02	25.0	13.0	-72.9	236.2
m112-3-02	300 C	40.0	25.4	-58.1	144.8	1.100E-02	25.0	13.0	-69.4	193.3
m112-3-02	375 C	40.0	25.4	-48.9	132.5	7.110E-03	25.0	13.0	-67.6	161.3
m112-3-02	450 C	40.0	25.4	-48.7	130.9	4.020E-03	25.0	13.0	-68.0	158.6
m112-3-02	500 C	40.0	25.4	-56.0	163.1	3.400E-03	25.0	13.0	-60.4	204.4
m112-3-02	525 C	40.0	25.4	-69.2	61.8	2.940E-03	25.0	13.0	-73.8	339.9
m112-3-02	540 C	40.0	25.4	-75.0	150.7	3.090E-03	25.0	13.0	-71.6	245.5
m112-3-02	560 C	40.0	25.4	5.1	125.4	3.500E-03	25.0	13.0	-17.9	126.5

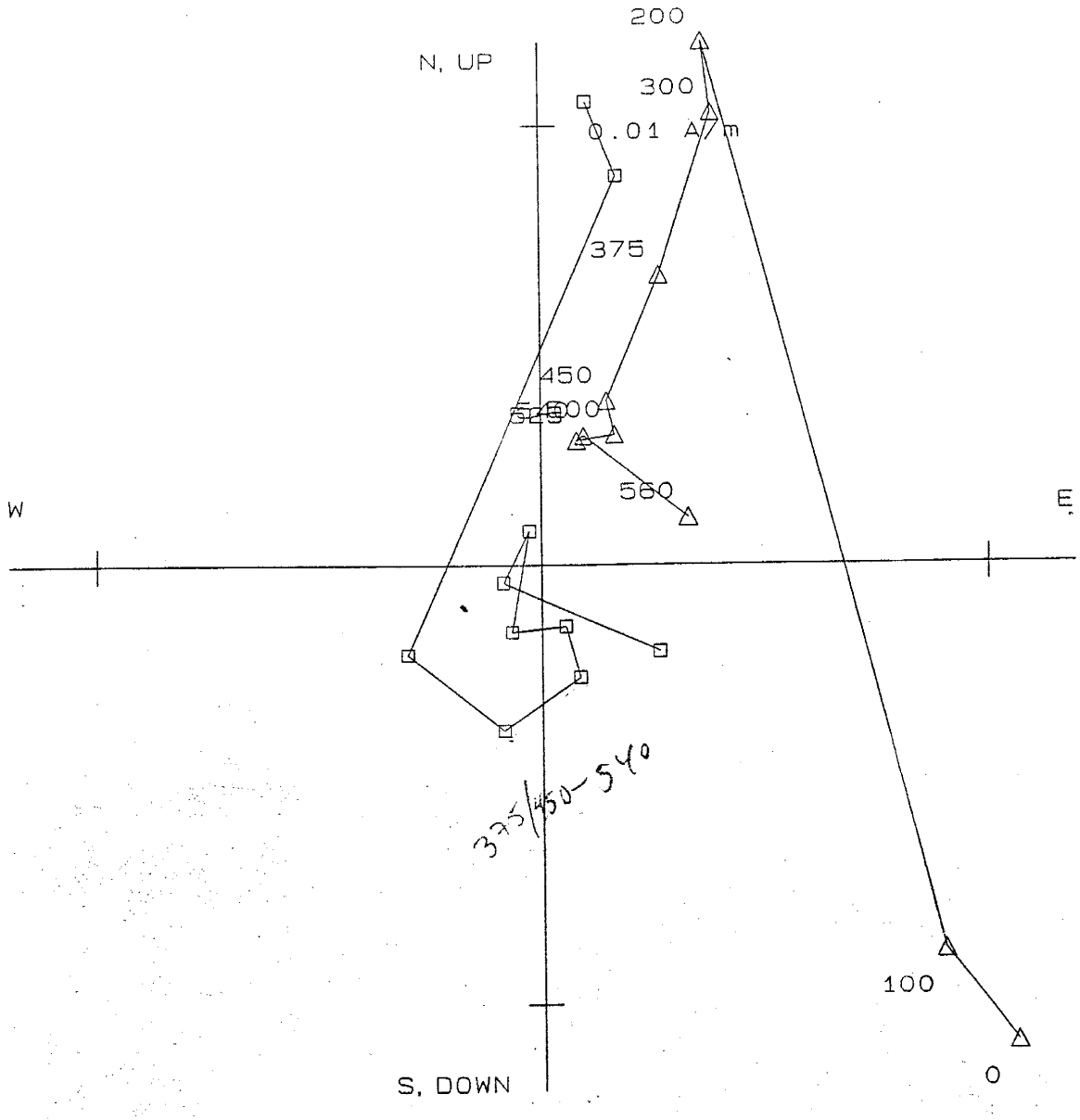

nm112-3-02.

Figure 11 — Thermal demagnetization isolates a ChRM with a southerly direction and negative inclination. Yet AF demagnetization could not adequately isolate this component in 3 of 4 specimens from site nm 1012.

(24A)

Path: D:\JENNY\HP
File: NM119-7B.DU 880 .a.. 6-16-93 4:53:52 pm Page 1

nm119-7-01	0mT	22.0	105.5	20.7	74.7	1.187E-02	25.0	13.0	-1.6	76.7
nm119-7-01	100mT	22.0	105.5	-0.2	94.6	1.111E-02	25.0	13.0	-24.9	93.8
nm119-7-01	200mT	22.0	105.5	-33.8	130.5	1.529E-02	25.0	13.0	-54.7	144.6
nm119-7-01	300mT	22.0	105.5	-34.7	128.7	1.691E-02	25.0	13.0	-56.0	142.6
nm119-7-01	450mT	22.0	105.5	-34.7	137.7	6.564E-03	25.0	13.0	-53.3	154.5
nm119-7-01	500mT	22.0	105.5	-27.5	150.7	8.208E-03	25.0	13.0	-42.1	165.2
nm119-7-01	540mT	22.0	105.5	-41.3	149.2	8.645E-03	25.0	13.0	-54.9	173.5
nm119-7-01	560mT	22.0	105.5	-39.5	140.2	1.007E-02	25.0	13.0	-50.7	161.2
nm119-7-01	580mT	22.0	105.5	-42.8	154.0	6.811E-03	25.0	13.0	-54.2	180.0
nm119-7-01	590mT	22.0	105.5	-34.8	140.8	5.082E-03	25.0	13.0	-53.1	171.5
nm119-7-01	610mT	22.0	105.5	-5.4	226.4	1.130E-03	25.0	13.0	3.5	207.7

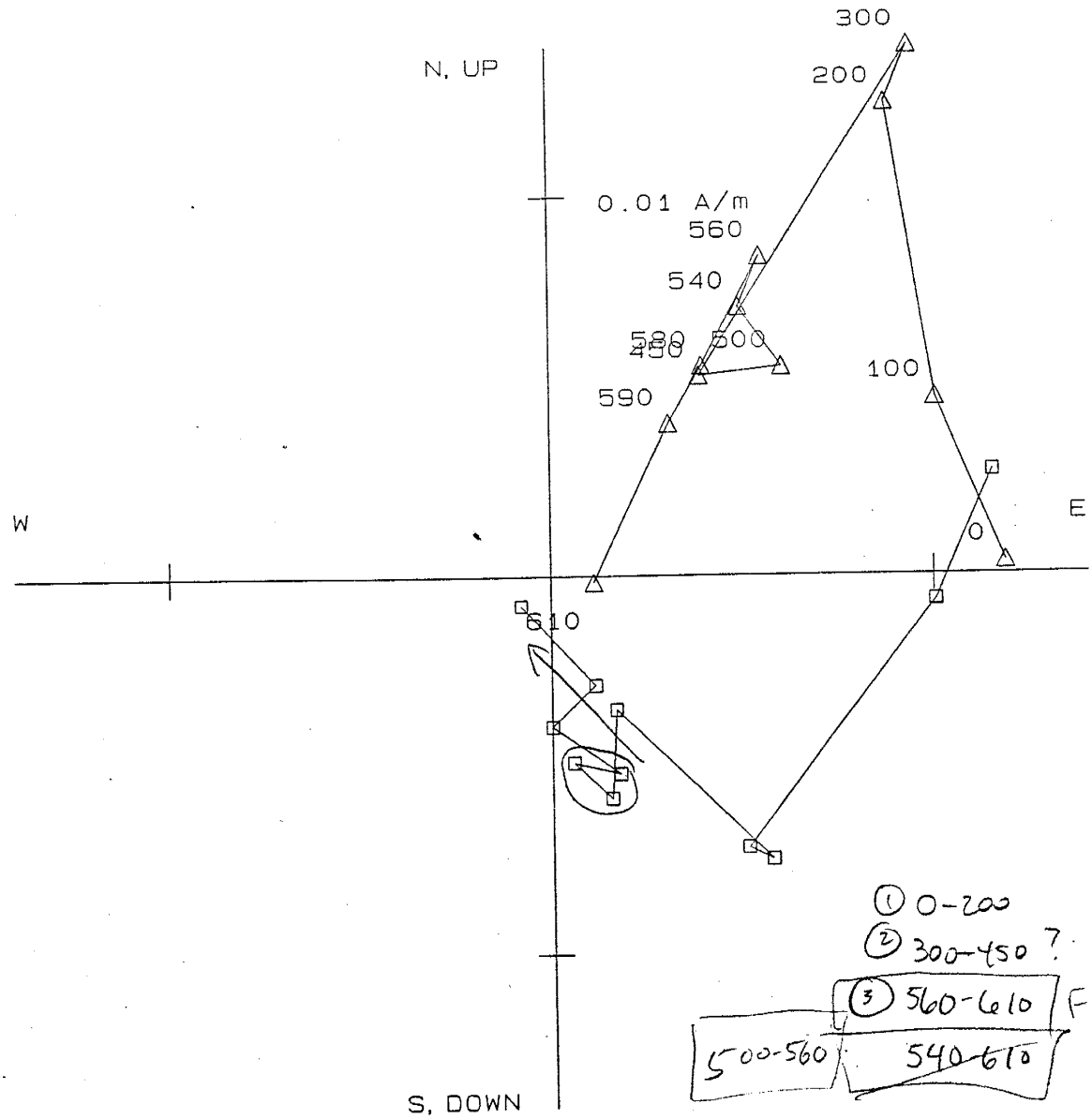

nm119-7-01.

Figure 12- AF and thermal demagnetization isolate a chRM with a southerly direction and negative inclin

Path: D:\JENNY\APACHE\JAN
File: NM119-3 .DU 1,040 .a.. 2-09-93 9:46:46 pm Page 1

m119-3-01	0mT	11.0	103.7	16.6	53.8	1.290E-02	25.0	13.0	-0.3	56.5
am119-3-01	2mT	11.0	103.7	-0.6	82.5	1.210E-02	25.0	13.0	-24.0	80.5
am119-3-01	5mT	11.0	103.7	-19.6	97.3	1.180E-02	25.0	13.0	-44.5	95.5
am119-3-01	8mT	11.0	103.7	-26.3	102.5	1.230E-02	25.0	13.0	-51.3	102.3
am119-3-01	10mT	11.0	103.7	-29.0	104.9	1.220E-02	25.0	13.0	-54.0	105.9
am119-3-01	15mT	11.0	103.7	-31.9	101.9	1.240E-02	25.0	13.0	-56.9	101.2
am119-3-01	20mT	11.0	103.7	-30.4	97.3	1.090E-02	25.0	13.0	-55.2	94.4
am119-3-01	25mT	11.0	103.7	-20.9	93.2	9.080E-03	25.0	13.0	-44.4	90.0
am119-3-01	30mT	11.0	103.7	-20.0	74.1	7.810E-03	25.0	13.0	-41.1	65.9
am119-3-01	35mT	11.0	103.7	-1[illegible]	71.6	7.070E-03	25.0	13.0	-36.6	64.4
am119-3-01	40mT	11.0	103.7	-23.2	76.3	[illegible]-03	25.0	13.0	-40.0	69.2
am119-3-01	50mT	11.0	103.7	-24.6	60.7	5.130E-03	25.0	13.0	-41.4	48.3
am119-3-01	60mT	11.0	103.7	-19.9	49.7	6.720E-03	25.0	13.0	-33.1	38.9

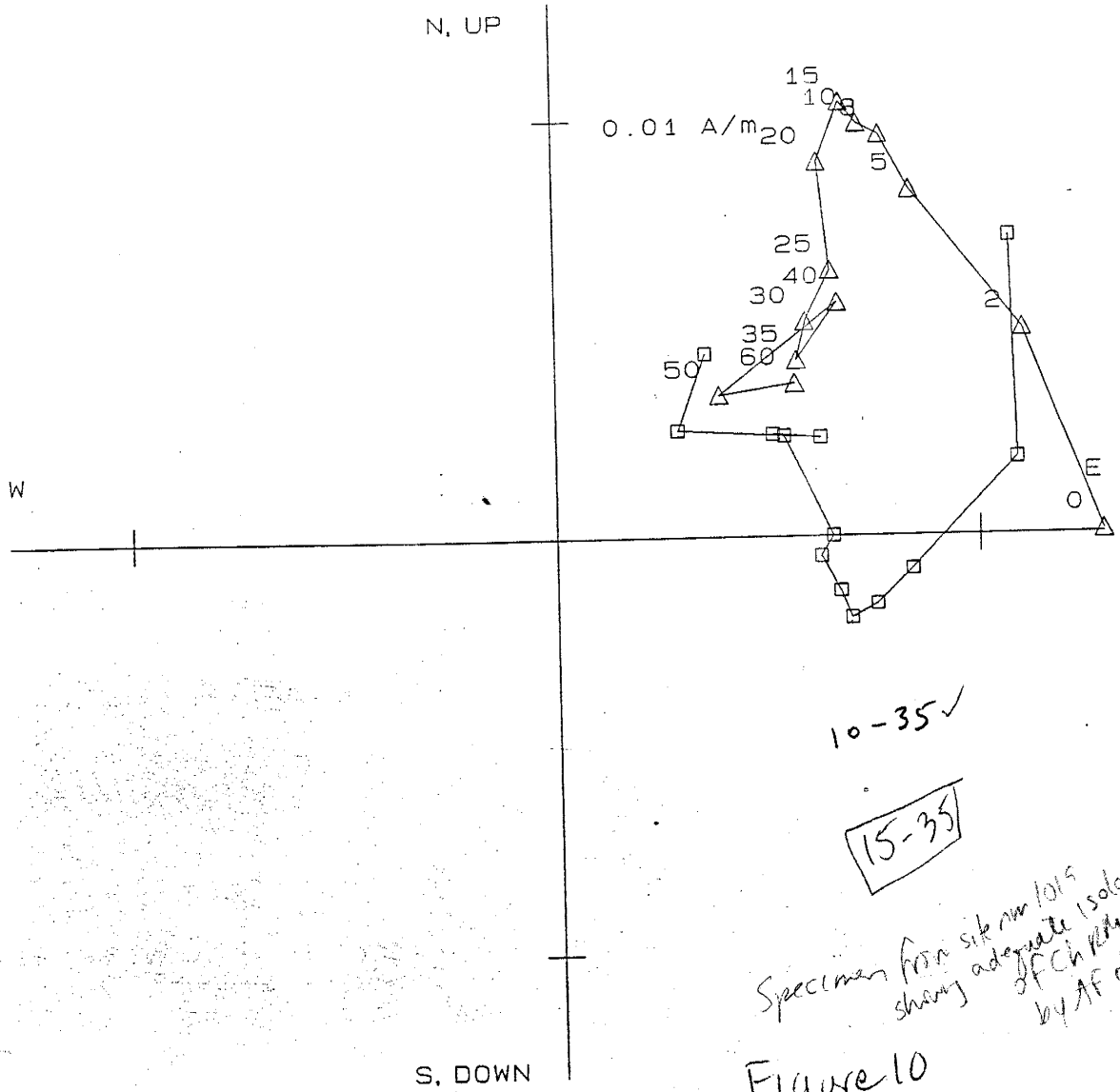

10-35 ✓

15-35

Specimen from site nm 1015 showing adequate isolation of ChRM and adequately by AF demag

Figure 10

nm119-3-01.

Apache Canyon

Figure 13- Site mean directions for Kneeling Nun Tuff and Vicks Peak Tuff on Apache Canyon, Sabaloli Mtns and established directions (McIntosh, 1991)

~~with low K/Ca from site BM850 near the base of the Thurman Formation have low~~

The Thurman Formation was sampled at two sites near the contact with the overlying Haynor Ranch Formation from an outcrop near the Apache Canyon section, however, the paleomagnetic data from the two ash units were spurious and were rejected from further analyses. [Previous $^{40}Ar/^{39}Ar$ geochronologic work on one of these ash units showed multiple age populations of sanidines (W. McIntosh, unpublished data, 1989).] Site nm1015 at the Apache Canyon section displayed a strong IRM component that could not be removed by AF or thermal demagnetization and also was rejected from further paleomagnetic study (Figure 12).

For the other 31 sites drilled, thermal demagnetization was more efficient than alternating field (AF) demagnetization in removing secondary magnetization components and in isolating ChRM directions (Figure 12). Many specimens showed spurious behaviour at peak alternating fields above 30 mT, and sufficient isolation of ChRM was in most cases not achieved by peak inductions <30 mT. ChRM directions were isolated by AF demagnetization in only one of the 16 sites from Johnson Spring and five of the 16 sites from Apache Canyon (nm956, nm1004, nm1005, nm1006, nm1008, nm1019). These sites displayed a low-coercivity viscous remanent magnetism (VRM) component and a medium-coercivity ChRM component. Directions were widely scattered for many sites yet a consistency in polarity was displayed from 15 to 35 mT for 2 or more specimens from 11 of the 16 sites from Apache Canyon.

Thermal demagnetization behavior for most specimens at Johnson Spring and Apache Canyon displayed remanences that unblocked by 590 °C with less than 20% NRM remaining (Figure 14). Four types of behavior during thermal demagnetization were observed (Table 2). Type A specimens (11%) showed a stable normal polarity magnetization that unblocked by 450 °C, above which no useful paleomagnetic data could be discerned. Type B specimens (30%) displayed a normal polarity component unblocked by 300 °C and a component of intermediate direction unblocked at higher temperatures. These anamolous specimens with remanences of overlapping coercivities

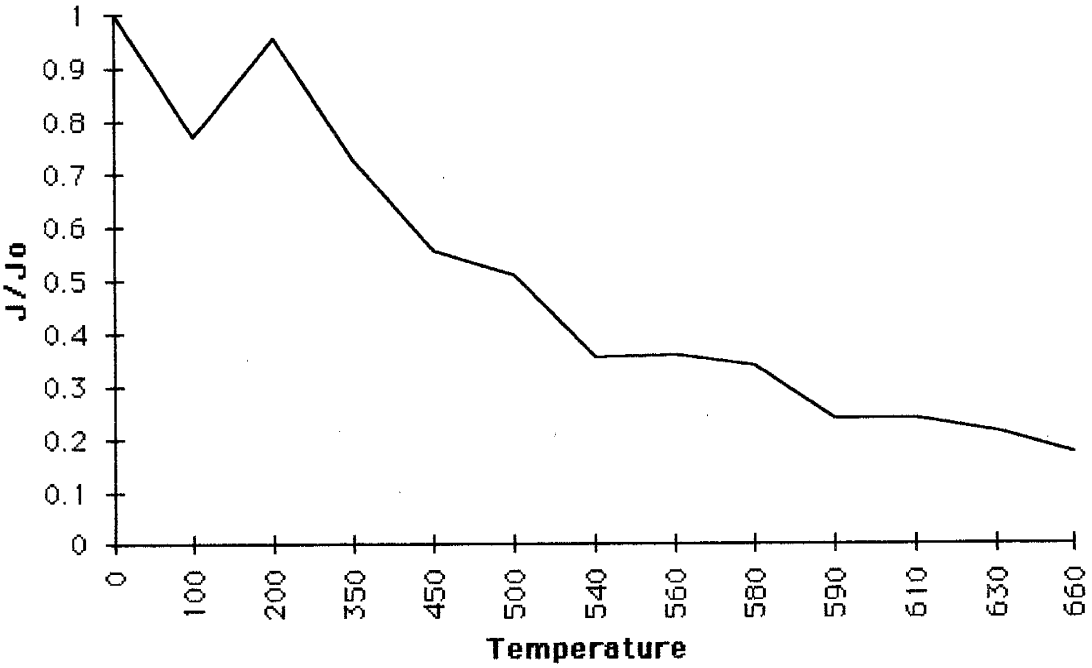

Figure 14 - Most specimens have remanences that unblock by 590°C with less than 20% NRM remaining.

Table 2--Types of thermal demagnetization behavior displayed by specimens. * = sites with specimens with NRM stable to 610-660 C

Specimens		Unblocking temperature	Polarity	Component	Unblocking temperature	Polarity	Component	Sites
		low temperature			high temperature			
Type A	11%	450 C	N					nm951,952,954,955,959, 960,965
Type B	30%	200-300 C	N	C1	500-590 C	Int		nm1006,1007,1009,1012 1014,1017,1018, 950, 952,953,955,957,958, 959,962,964
Type C	47%	200 C	N	C1	500-590 C (610-660)*	R	C2	nm1006,1008*,1011,1012*, 1013,1014,1016*,1017, 1018*,1019*,952,953*, 955,956*,958,961,962, 964,965*
Type D	12%	200-300 C	N	C1	500-610 C (610-660)*	N	C3	nm1004*,1005*,1010*,950 951,957,963

that were not isolated by thermal demagnetization may contain a secondary NRM component with medium to high unblocking temperatures and opposite polarity. Type C specimens (47%) displayed a normal polarity magnetization component removed below 300 °C and one or more components with a southerly direction and negative inclination unblocked at higher temperatures. Type D specimens displayed normal polarity components that remained stable at high temperatures.

Types A and B specimens are strongly overprinted by secondary components of magnetization. In type A specimens, the directions stable up to 450 °C were nearly parallel to the direction of the Earth's present field before tilt correction, although three specimens displayed intermediate directions that indicate overlapping low-temperature components of opposite polarity.

In type B specimens, the directions of the normal polarity low-temperature component uncorrected for tilt were parallel to the direction of the Earth's present field and to the low-temperature component of types C and D. This low-temperature normal polarity component (C1) was removed below 200 °C from specimens from Apache Canyon but the overprint persisted at higher demagnetization levels in specimens from Johnson Spring, where it was not removed until 300 °C (Table 2). Type C specimens displayed the low-temperature normal polarity component (C1) and a high-temperature reverse polarity component (C2). Type D specimens displayed insitu and tilt-corrected normal polarity components removed from 0 to 300 °C (C1) and from 300 to 500/525 °C, 500 to 560 °C, or 540 to 610 °C (C3), which were found in sites nm963, nm957, nm1010, and in the basal sandstones at both localities (sites nm950, nm951, nm1005, and nm1004).

Magnetic Mineralogy

The variations in paleomagnetic behavior are due to components that acquired variations in magnetic field directions at different times and to variations in magnetic

mineralogy or domain state. Altogether 13 type C and D specimens from Apache Canyon did not lose their natural remanent magnetism during thermal demagnetization until 610 to 660 °C (Table 2). One of these directions was intermediate (nm1004), one represented an insitu direction (nm1010), and nine of the 11 specimens displayed ChRM directions isolated by thermal demagnetization from 560 to 660 °C (nm1004, nm1005, nm1008, nm1012, nm1016, nm1018, nm1019).

Five specimens from sites nm1005 and nm1010 displayed stable insitu normal polarity magnetization up to 60 mT, one specimen from site nm1004 displayed tilt-corrected normal polarity up to 60 mT, and 3 specimens from sites nm1018 and nm1019 displayed tilt-corrected reverse polarity up to 60 mT. These rare high coercivity specimens from sites with specimens that also unblocked between 610 and 660 °C may carry hematite as a dominant magnetic mineral, however, only the AF demagnetization behavior of site nm1010 displayed sufficient isolation of a hematite component.

Most sites with type C specimens displayed medium-coercivity stable magnetizations and medium- to high-temperature stable magnetizations that unblocked between 525 and 590 °C (Figures 14, 15; Table 2). Sites from Johnson Spring with type C specimens displayed spurious low-coercivity magnetizations and medium- to high-temperature stable magnetizations that unblocked between 450 and 590 °C. Sites with medium-coercivity specimens and specimens that unblocked between 525 and 590 °C may carry impure magnetite as a dominant magnetic mineral. The range in unblocking temperatures may reflect the percentage of titanium in magnetite or the variation in domain state of the magnetite. Both localities showed only a slight variation in magnetic intensity and magnetic susceptibility with stratigraphic height (Figure 16). IRM acquisition and stepwise thermal demagnetization of IRM and SEM and electron microprobe work may more conclusively identify the domain state and magnetic mineralogy.

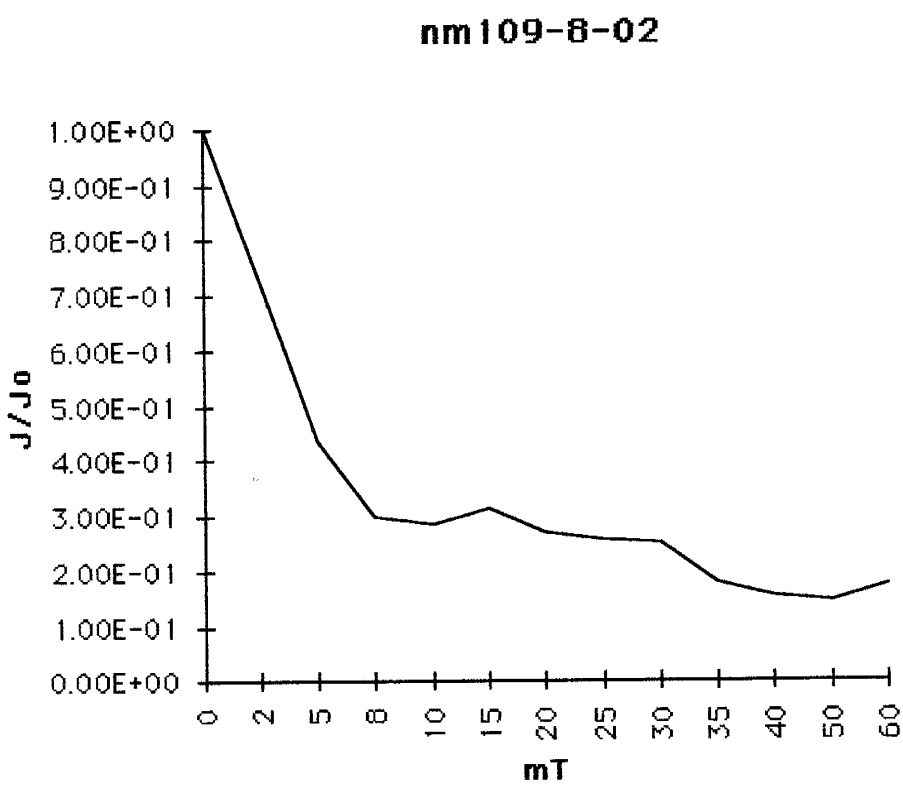

Figure 15 - Isolation of ChRM in most cases achieved by peak inductions to 40 mT. This AF demagnetization behavior indicates specimens contain minerals with low to medium coercivity.

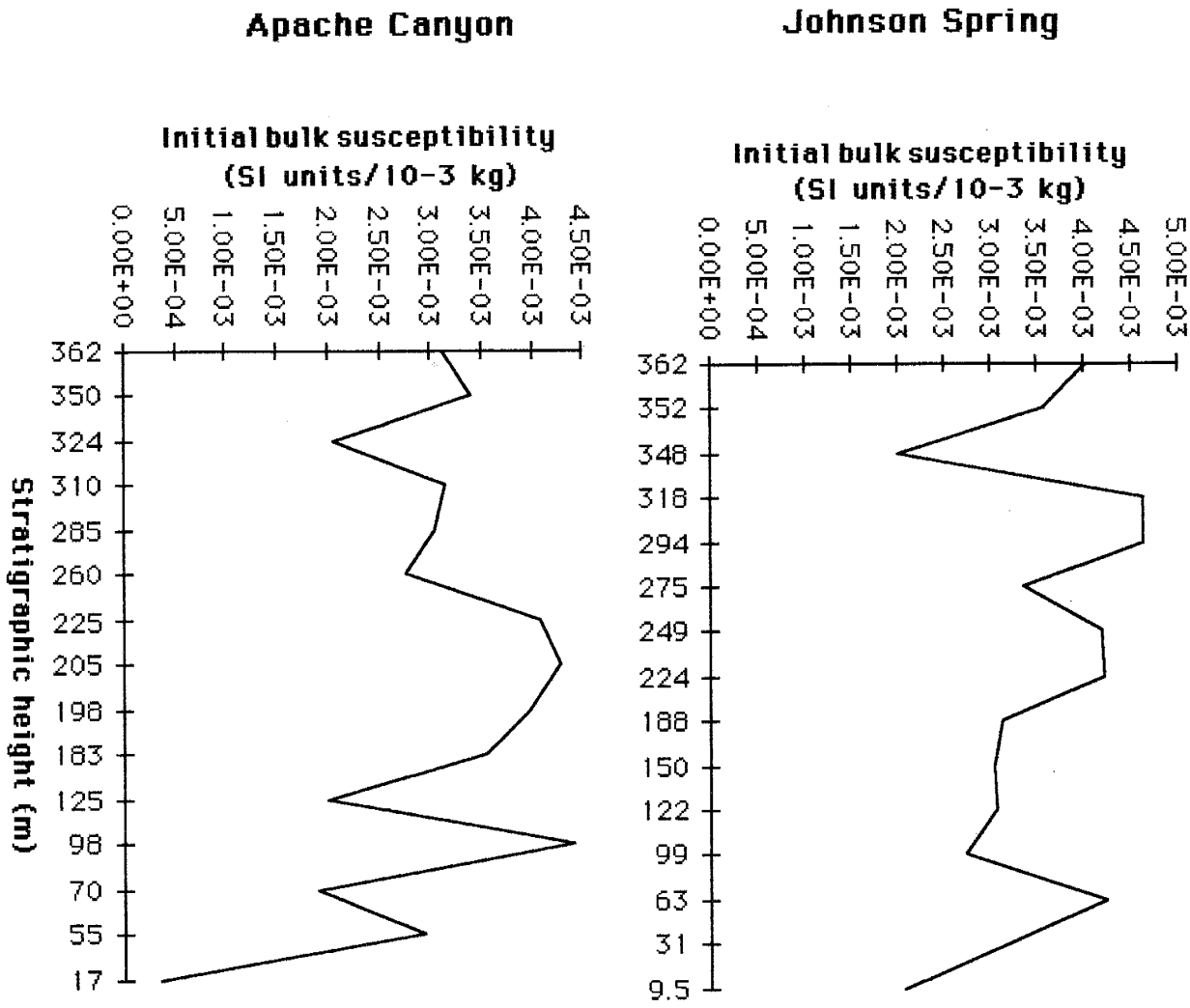

Figure 16 - Variations in initial bulk susceptibility with stratigraphic height.

Discussion

The resolutions of single-crystal provenance ages and magnetic polarity stratigraphy are limited by the inherent weaknesses of $^{40}Ar/^{39}Ar$ geochronology and paleomagnetism. Correlation of provenance ages of individual sanidines reported here with established ignimbrite ages of the Mogollon-Datil volcanic field is limited by the accuracy of the ages. Errors in ages are induced from variations in the neutron flux (J factor) and from the nature of the two $^{40}Ar/^{39}Ar$ methods used by the two different laboratories. The provenance ages of individual sanidines reported here have an error that is largely based on the J factor, calculated from laser fusion of single grains of Fish Canyon Tuff (27.84 Ma). Total laser fusion produces an age from one gas fraction for a sanidine that cannot be analyzed for possible contamination by inclusions or alteration as can plateau ages from multiple gas fractions of sanidines that are incrementally heated and analyzed using age spectra diagrams. The sanidines from Fish Canyon Tuff and the Thurman Formation are generally unaltered and inclusion free. This assumption is based not only on the appearance of sanidines under a binocular microscope, but also on the agreement of total gas ages with plateau ages reported for the Fish Canyon Tuff of the San Juan volcanic field and for most ignimbrites from the Mogollon-Datil volcanic field (McIntosh and others, 1990). Therefore, the total fusion ages and K/Ca of individual sanidines in the Thurman Formation can be correlated with confidence with the plateau ages and mean K/Ca of ignimbrites determined from incremental heating of bulk sanidine separates (McIntosh and others, 1991).

Disparity between ignimbrites erupted at intervals of 0.2 Ma or less (27.4 Ma vs. 27.6 Ma ages) and between K/Ca of 30-50 and 100-250 that are observed for ages of individual sanidine grains reported here, however, are not resolved by correlation with the established $^{40}Ar/^{39}Ar$ sanidine geochronology of McIntosh and others (1992), which is

based on dating bulk sanidine separates. It is difficult to estimate the effect of differences in ages and K/Ca of sanidines that may be represented by these established ages and the within-unit standard deviation of three to four bulk age determinations. In this study, Fish Canyon Tuff with an established age of 27.84 Ma (McIntosh, W., pers. comm. 1993) showed K/Ca values in individual sanidine grains that varied from 36 to 100.

Paleomagnetic methods are potentially sensitive as a geochronologic tool depending on the extent to which the detrital remanent magnetism of sedimentary units, which is 1000 times weaker than the thermal remanent magnetism of volcanic rocks (Stacey, 1958, 1962), has been disturbed by chemical and diagenetic processes (Khramov, 1958; Opdyke, 1972; Verosub, 1977; Johnson and others, 1975; Reynolds, 1979; Karlin, 1990). Sandstones and debris flows record directions of the geomagnetic field at a lower resolution than mudstones and siltstones due to postdepositional alignment errors at the time magnetic grains rotate and line up with the paleomagnetic field (Irving, 1957; Irving and Major, 1957; Collinson, 1965; Verosub, 1977). Magnetic grains in water-saturated ash often lie within larger glass shards and volcanic rock fragments and the attachment to these angular fragments restrict adjustment to the ambient field (Reynolds, 1979). The Thurman Formation represents a medial to distal alluvial fan sequence so bedding errors from deposition on a sloping surface are negligible.

The presence of authigenic minerals of clay, zeolites, calcite, and hydroxides indicate that chemical changes have affected the detrital grains and minerals of the Thurman Formation. Intrastratal alteration of unstable silicic glass produced one or two stages of clay and zeolite formation. Some grains and volcanic rock fragments were even partially to completely dissolved with only the relict morphology preserved by clay- and zeolite-coated rims. Plagioclases, which are sensitive to changes in pore-water chemistry, appear to have remained somewhat stable; some plagioclase show dissolution or replacement by calcite at certain horizons. Sanidines, however, appear to have remained

chemically and physically intact. Magnetic grains are especially sensitive to chemical changes and the late-stage formation of hydroxides evident in petrographic thin sections may have formed at the cost of preservation of primary remanent magnetism carried by magnetite and titanomagnetite. Late-stage genesis of hydroxides may be related to uplift and tilting of the Thurman Formation prior to deposition of the Camp Rice Formation.

Postdepositional DRM (detrital remanent magnetism) is the dominant process involved in the magnetization of sediments prior to diagenesis (Verosub, 1977). Successful paleomagnetic recovery of the DRM and its site-mean directions and polarity stratigraphy in the Thurman Formation at two localities in New Mexico requires the adequate isolation of the carriers of the NRM. Hillhouse and others (1977) reported their cautious approach to interpreting paleomagnetic polarity data from siltstones and sandstones in the Koobi Fora Formation in the East African rift. They concluded that some specimens acquire chemical remanence during periods of reversed polarity, but that most secondary components carry normal polarity. They developed a scheme on how to interpret scattered and intermediate directions of specimens taken from sandstones at a site along one stratigraphic horizon. The intermediate directions represent the superposition of primary and secondary magnetic components with opposite polarity. They rejected results from horizons where specimens yielded one or more intermediate and no reversed polarity and where only one short isolated normal zone occurred in a large reversed zone. This method was applied in determining the polarity profile for the Thurman Formation after isolation of the characteristic remanent magnetism (ChRM).

The ChRM in the Thurman Formation appears to be DRM in origion. The Thurman Formation is tuffaceous and white and does not appear to contain hematite which is often a red-staining diagenetic mineral in sandstones; the Thurman Formation appears to contain detrital magnetite that has escaped martitization or alteration to hematite. Detrital magnetite and titanomagnetite can survive diagenesis and dissolution in terrigenous red beds and pelagic marine sandstones but their abundance is minor and

often contributes little to the overall remanence of a sediment (Walker and others, 1982; Karlin, 1990; Roberts and Pillans, 1993; Roberts and Turner, 1993). The record of the paleomagnetic field is disrupted by nonfield effects on the DRM, such as variation in mineralogy, grain size, and concentration, and by chemical changes during diagenesis. The presence of detrital magnetite as a stable remanence carrier in the Apache Canyon section of the Thurman Formation suggests that the isolated ChRM is detrital in origin and that the site-mean directions and magnetic polarity stratigraphy represent the paleomagnetic field soon after deposition. The wide dispersions of site-mean directions reported here reflect the effect of the size of magnetic minerals in angular volcanic fragments (Irving and Major, 1957; Reynolds, 1979).

The difficulty in matching the magnetic polarity stratigraphy of the Thurman Formation with the Geomagnetic Polarity Time Scale is twofold: 1) the pattern must be ambiguous and the more the reversed and normal polarity zones the easier the fit and 2) late Oligocene-early Miocene ages are being calibrated.

Sanidine Provenance Ages and Correlation with Oligocene Ignimbrites

The Thurman Formation is filled with silicic and andesitic detritus shed from the Mogollon-Datil volcanic field. The sandstones are largely derived from cinder and the eroded rubbly tops of local andesite to basaltic andesite flows and from pumice and ash falls and nonwelded pumiceous rhyolitic and welded rhyodacitic ignimbrites shed from the Mogollon-Datil volcanic field. Provenance ages of individual sanidine grains help to determine which ignimbrites have been eroded and incorporated as detritus into the Thurman Formation. The sanidine age populations at different horizons of the Thurman Formation reflect the denudation and drainage of the eastern edge of the Mogollon-Datil volcanic field during the time of Thurman deposition.

The sanidine provenance ages are shown in Figure 17 along with established ages of correlative ignimbrites of the Mogollon-Datil volcanic field and Boot Heel volcanic

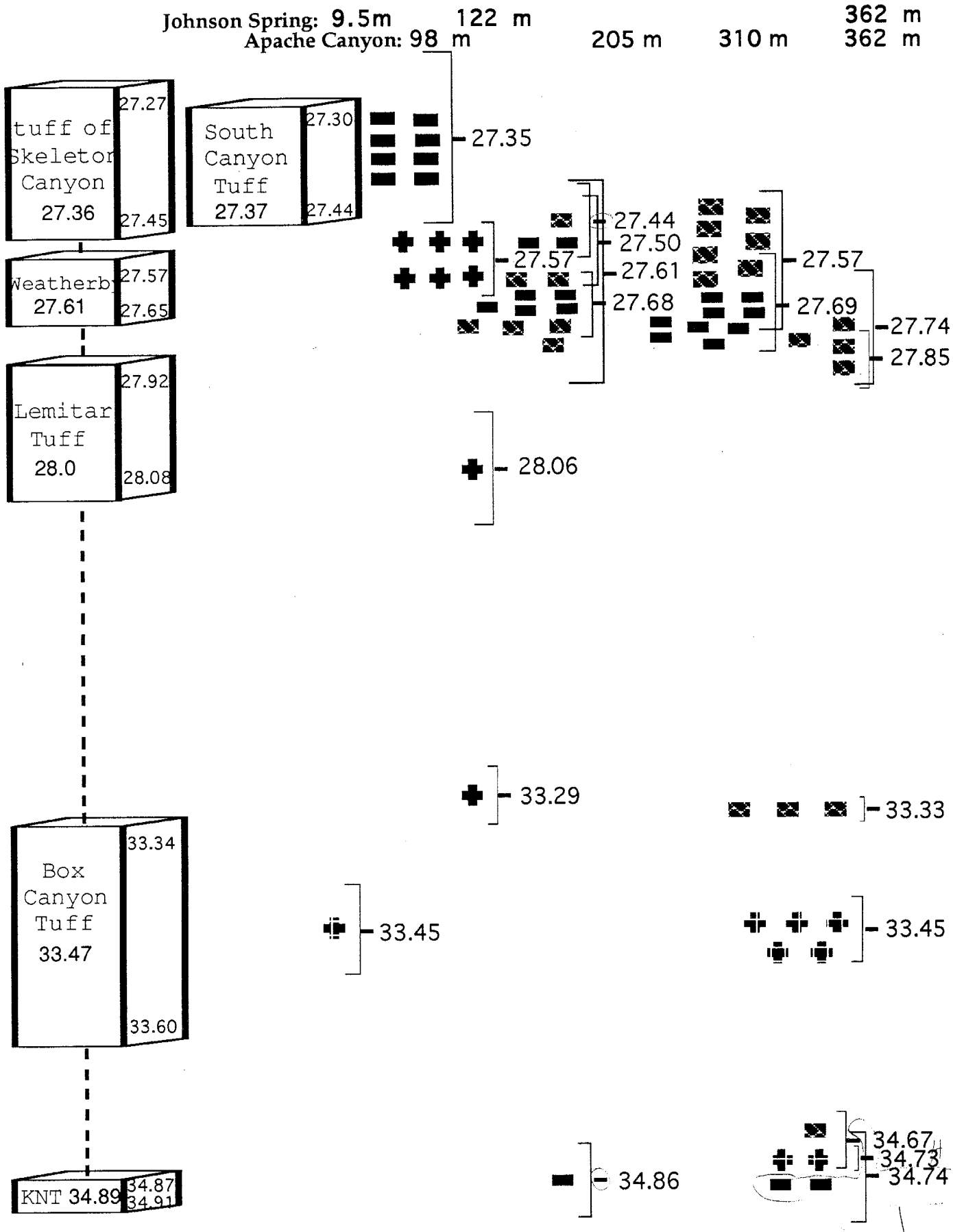

Figure 17 - Provenance of sanidines in the Thurman Formation

field that are similar in age and K/Ca (McIntosh and others, 1990, 1992b). The plateau ages of the ignimbrites are shown with their within-unit standard deviation of the mean from 3 to 7 bulk age determinations (McIntosh and others, 1990; 1992b). These standard deviations are identical with those from total gas ages for the Kneeling Nun Tuff and Lemitar Tuff. The total gas ages of the other ignimbrites vary, however; Box Canyon Tuff ranges from 33.4 to 33.7 Ma, South Canyon Tuff from 27.4 to 27.6 Ma, Weatherby Tuff from 27.4 to 27.8 Ma, and tuff of Skeleton Canyon from 26.3 to 27.7 Ma.

The oldest sanidines are 34.7 to 34.9 Ma and may correlate with Kneeling Nun Tuff (34.9 ± .03 Ma). An abraded detrital grain of 34.7 Ma was dated at the top of the Apache Canyon section, whereas two abraded grains of 34.7 Ma were dated at the top of the Johnson Spring section. The 34.7 Ma ages may reflect tuff of Lebya Well or Rock House Canyon Tuff, however, anomalous data for Rock House Canyon Tuff and uncertainty in the extent of the tuff of Lebya Well have been reported (McIntosh and others, 1992). Although the source calderas for both tuffs remain unknown, McIntosh and others (1992) suggested vent locations in the northern part of the Mogollon-Datil volcanic field, far from the site of deposition of the Thurman Formation. Midway through the Apache Canyon section a lone blocky euhedral sanidine dated at 34.9 Ma may be Kneeling Nun Tuff or Bell Top tuff 4, which were distributed to the north and west and within the study area. The Bell Top tuff 4 is slightly older than Kneeling Nun Tuff at 35.0 ± .04 Ma. The analytical error of 0.07-0.19 Ma for these four sanidines found in sandstones and debris flows at the top and middle of the Thurman Formation cannot exclude the strong possibility that all four sanidines were derived from Kneeling Nun Tuff.

Besides the oldest grains at the top of the Thurman, four prominent age groups are apparent and may reflect sanidines from Box Canyon Tuff (33.5 ± .13 Ma), the Lemitar Tuff (28.0 ± .08 Ma), the Weatherby Tuff (27.6 ± .04 Ma) of the Boot Heel volcanic field (now correlated with the tuff of Walking X Canyon, 27.6 ± .10 Ma; McIntosh, W., pers.

comm. 1994), and South Canyon Tuff (27.4 ± .07 Ma). The two ignimbrites of the Weatherby Tuff and the tuff of Skeleton Canyon from the Boot Heel volcanic field are included as possible ignimbrite sources for the detrital sanidines. Although their source calderas and extent of outflow lie far to the southwest, ash fall distributed from their eruptions could have been blown as far north as the edge of the Mogollon-Datil volcanic field; the wind direction for the late Oligocene was from the southwest (Lambert, 1968; Ferguson, 1985).

The youngest sanidines of 27.4 Ma are found in fragile 1.5-2-cm-wide pumice 98 m from the base of the Apache Canyon section (nm1008; Figure 9) and as detrital grains in a sandstone at the 205 m horizon (nm1011). The 27.9 to 28.1 Ma sanidines found in debris flows at the 122 m horizon of the Johnson Spring section and at the top of the Apache Canyon section were probably derived from the Lemitar Tuff. The K/Ca for these two sanidines is 16-22, which matches well with the K/Ca measured from Lemitar Tuff sanidines (McIntosh and others, 1990). Although Bloodgood Canyon Tuff (28.1 ± .04 Ma) is similar in age to these sanidines, it has higher K/Ca of 40-50.

The 33.3-33.5 Ma and 27.6-27.8 Ma sanidines in sandstones and debris flows in the middle of both sections and the dominantly 33.3-33.5 Ma detritus found at the base and top of the Johnson Spring section may represent erosion of Box Canyon Tuff (33.5 ± .13 Ma) and the Weatherby Tuff (27.6 ± .04 Ma). The extent of preserved outflow sheets of Box Canyon Tuff, which erupted from the Schoolhouse Mountain caldera, lie as far east as the study area (Figure 18). No known outcrops of ash fall units from the Weatherby Tuff are preserved in the Mogollon-Datil volcanic field. However, the presence of these 27.6 Ma sanidines suggests a distal unconsolidated fall of Weatherby Tuff tephra may have been deposited locally north of the site of deposition of the Thurman Formation and then reworked and redeposited as fluvial detritus into the Thurman. The 27.6 Ma sanidines are found in sandstones that are crossbedded. The sanidines have been abraded and the abrasion probably occurred during wind transport

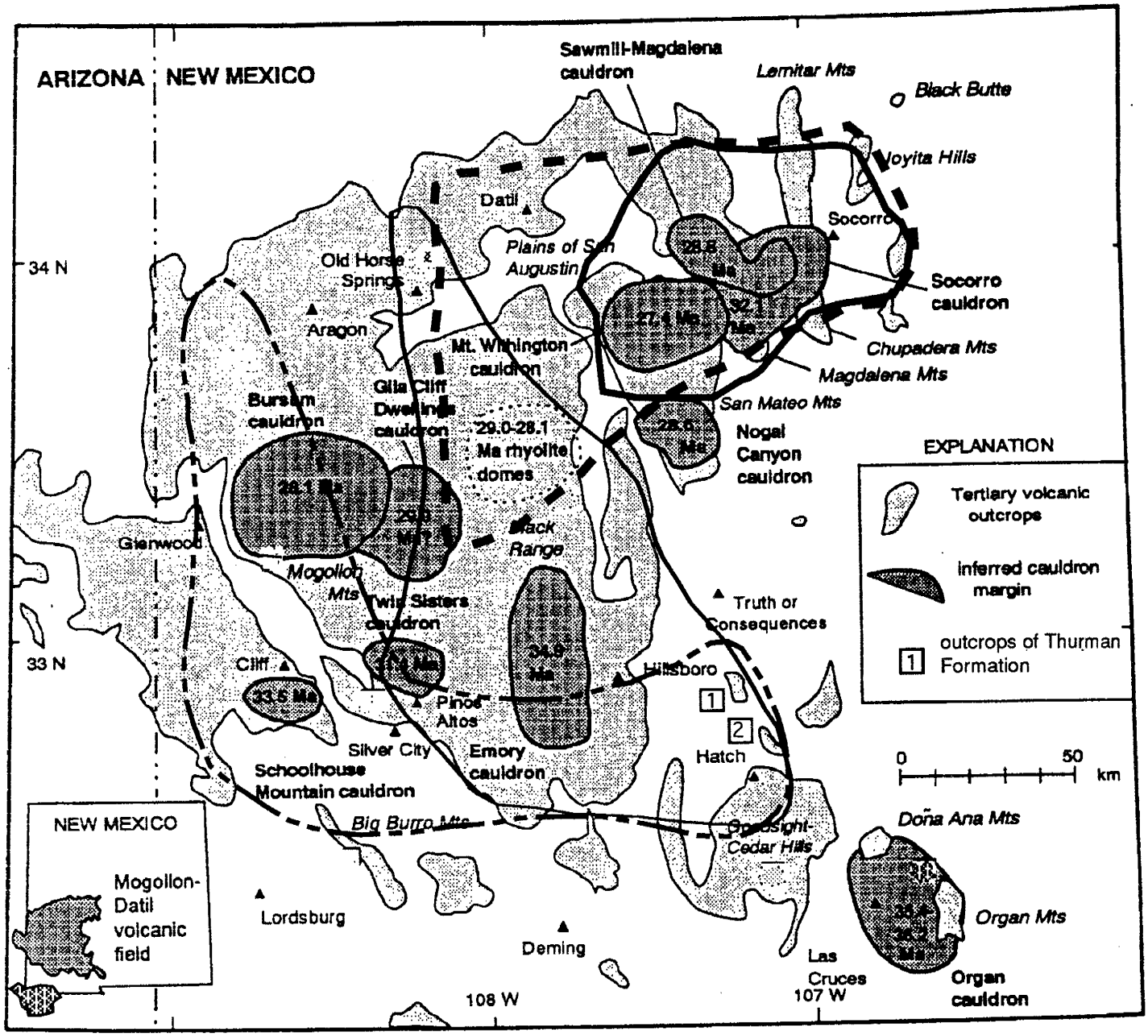

Boot Heel volcanic field

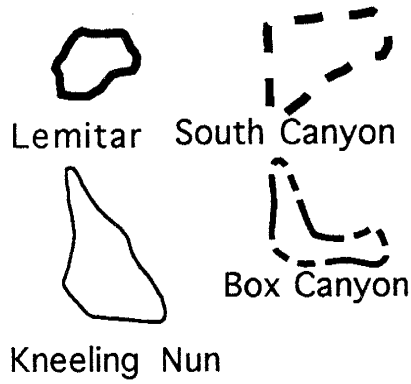

Figure 13-Extent of regional ash-flow tuffs (from McIntosh et al., 1992).

prior to fluvial deposition. The high K/Ca of the 27.6 Ma sanidines, however, does not match the K/Ca of the sanidines measured from Weatherby Tuff sanidines (McIntosh, W., pers. comm. 1994). The K/Ca values are 100-300 compared to 17-33 measured from the Weatherby Tuff sanidines (Table 1). The range in total gas ages reported for the South Canyon Tuff (27.4-27.6 Ma; McIntosh and others, 1990) cannot exclude the strong possibility that these sanidines are from reworked fall material from the South Canyon Tuff. The K/Ca of South Canyon Tuff, however, is low at 19-39 (McIntosh and others, 1990).

The South Canyon Tuff has been described as a multiple flow, simple cooling unit (LaRoche, 1980). The poorly welded upper unit preserved as a distal fringe in the Gallinas Peak area is relatively pumiceous (2-5%) and crystal rich with 6-9% 0.5-2.5-mm-long sanidines, quartz, a trace of plagioclase and biotite, and sparse andesitic lithic fragments (LaRoche, 1980). The South Canyon Tuff erupted from Mount Withington cauldron, north of the localities of Thurman Formation outcrops (Figure 18), which may have also been the caldera site for the source of the Lemitar Tuff. Lithic fragments of Lemitar Tuff are found in outflow sheets of South Canyon Tuff close to the cauldron (Ferguson, 1985). It is possible that the detrital sanidines of 28.0 Ma from Lemitar Tuff and sanidines from 27.4 Ma pumice that are found in debris flows in the middle and top of the Thurman Formation are derived from reworked nonwelded tuff of South Canyon Tuff and pumice fall from its early plinian phase (Ferguson, 1985).

The ignimbrite sources for the sanidine provenance ages in the Thurman Formation are summarized in Figure 19. The detrital sanidines of 33.3-33.5 Ma and 34.7-34.9 Ma from sandstones and debris flows are from reworked tuff of Box Canyon Tuff and Kneeling Nun Tuff. The detrital sanidines of 27.6 Ma with anomalously high K/Ca from sandstones in the middle of the Thurman Formation and abraded sanidines of 27.6 Ma with high K/Ca in a debris flow at the top of the Thurman Formation are from an unknown reworked ash fall (possibly from South Canyon Tuff or the Weatherby Tuff).

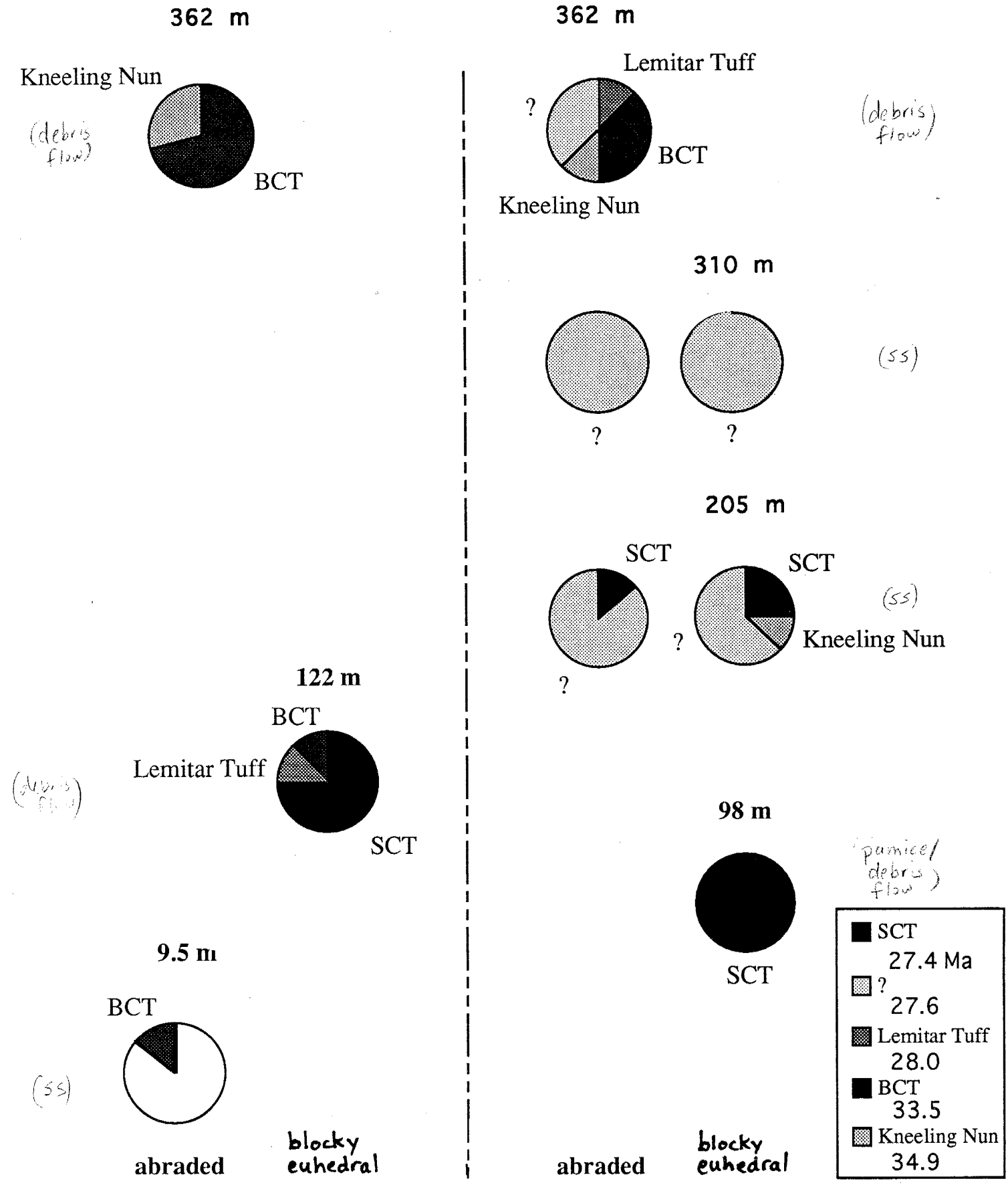

Johnson Spring, Rincon Hills

Apache Canyon, Caballo Mountains

Figure 19-Provenance of sanidines in the Thurman Formation

Because sanidines from an ash fall are often abraded during wind transport, the relatively high proportion of blocky euhedral sanidines of relatively large size from the 205 m and 310 m horizons (sites nm1011, nm1016) suggests sanidines from this ash fall may have not traveled very far before they were reworked and deposited in a debris flow. Sanidines collected from the Johnson Spring section, the southern locality of the Thurman Formation, were also slightly smaller than those from the Apache Canyon section. The questionable ignimbrite source for 27.6 Ma sanidines with high K/Ca may be South Canyon Tuff, which has total fusion ages of 27.6 Ma for multiple bulk sanidines (McIntosh and others, 1990). South Canyon Tuff is the source of delicate pumice in a pumiceous debris flow at the 98 m horizon in the Apache Canyon section and is the source of detrital grains in a pumiceous debris flow at the 122 m horizon in the Johnson Spring section. Petrographic thin sections of debris flows from these horizons and other units near these middle horizons show that the middle part of Thurman Formation is comprised mostly of South Canyon Tuff pumice fragments (Figure 9). Pumice and ash fall from South Canyon Tuff appear to be a dominant source for the volcaniclastic detritus shed into much of the Thurman Formation.

Detrital Remanent Magnetization and Dissolution

Petrographic examinations show that the lithology (mineral and volcanic rock fragment concentrations and sizes) in the Thurman Formation is similar at both localities. The samples contain a relatively large percentage of pyrite, clay, and hydroxides. Titanomagnetite, magnetite, hematite, and ilmenite as small as .06 μm were identified in volcanic rock fragments in thin section. AF and thermal demagnetization results indicate a mineral or minerals with a relatively soft component and an unblocking temperature of 300 °C is a dominant NRM carrier (component C1) at Johnson Spring, and is also present at a lower blocking temperature of 200 °C in most sites at Apache Canyon (Table 1). Sites with low- and high-temperature components (types C and D specimens) also

contain specimens with medium-coercivity components that were isolated from 15 to 35 mT. Sites with type C specimens contain a reversed-polarity medium-coercivity high-temperature C2 component with unblocking temperatures of 500-590 °C. Sites with type D specimens contain a normal-polarity medium-coercivity high-temperature C3 component with unblocking temperatures of 500-610 °C. The presence of a small percentage of high-coercivity minerals in some sites with types C and D specimens with maximum unblocking temperatures between 610 and 660 °C suggests a slight mixture of minerals with different coercivities. This variation in mineralogy and demagnetization behavior is expected for debris flows and fine to medium sandstones with angular volcanic fragments of variable size and composition.

Unblocking temperatures and peak induction fields together can indicate the dominant magnetic mineralogy that records the polarity and magnetic direction in a specimen. Ferrimagnetic iron sulphides (greigite and pyrrhotite) and iron oxides (titanomagnetite and titanomaghemite) display soft coercivities and thermal stability to 200-350 °C and 350-400 °C (Dekkers, 1989; Snowball, 1991). Goethite displays soft coercivities and thermal stability to 150 °C and then converts to hematite during laboratory heating to 300 °C (Butler, 1992). These minerals may comprise part of the C1 component of NRM in types B, C, and D specimens. The higher range of unblocking temperature of 500-610 °C observed in type C and D specimens (from sites with medium-coercivity ChRM components) indicates that the dominant ChRM carrier of the C2 and C3 components is impure magnetite. Hematite may be a significant remanence carrier in only about 5% of types C and D specimens (Table 1), however, its presence as a dominant remanence carrier is highly suspect. The hematite behavior displayed during thermal demagnetization in a few specimens may reflect hematite formed from oxidation of magnetite or dehydration of a minor component of a hydroxide (goethite?) during heating .

The dominant remanence of the high-temperature component in type B specimens may also be carried by impure magnetite. Intermediate directions recorded (northerly declinations and low positive or negative inclinations or southerly declinations and positive inclinations) in many specimens may reflect chemico-viscous remanence (CVRM; Dunlop and Ozdemir, 1990). Gapeev and others (1991) suggested that intermediate directions may reflect chemical remanent magnetism (CRM) forming parallel to direction of the initial remanence and viscous remanent magnetism (VRM) forming in the direction of the field applied during near-surface oxidation in the presence of groundwater. Thermal, not AF, demagnetization removes CVRM. Thermal demagnetization removes secondary NRM carried by grains of low relaxation time and low thermal blocking temperature. Intermediate directions that remain after thermal demagnetization in type B specimens may reflect composites of remanences with normal and reversed polarities with similar coercivity spectra or complications induced during laboratory heating.

ChRM could not be adequately isolated in many specimens from Johnson Spring. The low-coercivity low-temperature CVRM C1 component and medium-coercivity high-temperature ChRM C2 and C3 components were isolated by AF and thermal demagnetization in most sites at Apache Canyon with types C and D specimens, but were only isolated by thermal demagnetization from sites with types A and B specimens that comprise most of the Johnson Spring section. The C2 and C3 components could not be adequately isolated by thermal demagnetization for many sites from Johnson Spring. The sands at certain horizons at this section may contain a strong CVRM or CRM component that was inherited during diagenesis. The relative paleomagnetic instability and weak remanence intensities in the Johnson Spring section may be caused by lower concentrations of impure magnetite that resulted from its preferred dissolution during diagenesis and during precipitation of the hydroxides.

The differences in demagnetization behavior of specimens from Johnson Spring can be explained by the mineralogy. Detrital magnetite can survive diagenetic dissolution and retain early magnetizations in marine sediments that have experienced reduction-oxidation reactions (Karlin, 1990; Roberts and Pillars, 1993). The more stable magnetization found at Apache Canyon reflects the diagenetic history and fluid composition of the Thurman Formation at this locality. Submicron to 1μm-size titanomagnetites have been observed as inclusions in volcanic glass and pumice and as phenocrysts in lithic clasts of ash and ash-flow tuffs (Heider and others, 1993; Schlinger and others, 1986; Geissman and others, 1983). Petrographic examination reveals that magnetite as small or smaller than 0.06 μm is present in the Thurman Formation. Preferential dissolution of these fine grains is expected during diagenesis (Roberts and Pillans, 1993) and pumice dissolution is well documented by petrographic examinations in many of the sites in the Thurman. The Johnson Spring section may contain slightly smaller pumice fragments (with grains of titanomagnetite) that were more susceptible to dissolution than those at the Apache Canyon section. (Smaller sanidines were recovered from the Johnson Spring section.) The Johnson Spring section also contains two different zeolites, whereas the Apache Canyon section has only one zeolite. Petrographic observations indicate that the sediment and porewater geochemical conditions played a part in the variations seen at the Johnson Spring section. The lithology of the sands at both localities are largely similar so magnetic remanent variations may reflect this difference in postdepositional diagenesis.

Walker and others (1978) reported dissolution of hornblende in the Haynor Ranch Formation. Mack and Grigsby (1985) reported that hematite rims formed earliest in the diagenetic history of the Haynor Ranch Formation at San Diego Mountain. Zielinski and others (1983) reported that heavy metals (Co, Cr, Cu, Fe, Mn, Ni, Pb, U, V, Zn) are often redistributed on an intergranular scale from detrital host to secondary iron oxides.

Magnetite is commonly altered during burial and diagenesis (Walker and others, 1978; Welty, 1988), which may explain why the primary remanence of detrital impure magnetite at Johnson Spring could not be successfully isolated in many specimens. Titanomagnetite and magnetite dissolution and precipitation of hydroxides compromise the fidelity of the DRM record.

At least three components comprise the NRM in the Thurman Formation. The C1 component has a consistent direction common throughout both sections of the Thurman Formation. It is nearly parallel to the Earth's present day magnetic field direction and formed since the time the beds were tilted. This component was effectively removed by AF demagnetization to 10 or 15 mT and by thermal demagnetization to 200 °C. The C2 and C3 components were isolated by AF and thermal demagnetization at higher thresholds. The normal-polarity C3 component is found near the base of the Apache Canyon and Johnson Spring sections. The reverse-polarity C2 component is prevalent throughout most of the Apache Canyon (Table 3). One site in the Apache Canyon section shows anamolous normal-polarity directions (nm1010) but the demagnetization behavior displayed may indicate a late-stage CRM carried by hematite or CRM formed during laboratory heating.

Carriers of NRM vary through each section. Carrier of the C1 component may be a late-stage hydroxide (goethite), a sulfide mineral (greigite or pyrrhotite) or impure magnetite (titanomagnetite). Carriers of the C2 and C3 components is dominantly impure magnetite in ash and detrital andesitic and pumice fragments.

In summary both sections contain hydroxides that carry VRM and impure magnetite that carries ChRM. Most of the ChRM in magnetic minerals in smaller volcanic rock fragments may have been removed by dissolution or obliterated by CRM-CVRM at the Johnson Spring section. The dissolution and chemical overprints may have been induced by the changing pore water chemistry represented by two different zeolites in the Johnson Spring section. Slight differences in the ChRM in sandstones and debris

Table 3--Polarity of ChRM isolated by AF and thermal demagnetization. AF=coercivity range; Temp=temperature range.

	Strat Height (m)	Polarity	No.	AF (mT)	Polarity	No.	Temp (C)
nm1019	362	R	7/9	15-30	R	3/4	450-610
		int	2/9	15-30	int	1/4	450-590
nm1018	350	R	4/5	15-35	R	2/4	500-610
					int	2/4	300-580
nm1017	324	R	1/5	10-30	R	3/4	300-590
					int	1/4	500-580
nm1016	310	R	2/5	15-30	R	3/5	500-560
					int	2/5	450-590
nm1014	260	int	3/5	35-60	R	2/5	200-560
					int	2/5	500-580
nm1013	225	R	2/4	15-40	R	4/4	200-660
		int	2/4	15-40			
nm1011	205	R	1/4	20-40	R	4/4	300-540
		int	3/4	25-40			
nm1012	198	R	1/4	15-25	R	2/4	375-660
		int	2/4	15-25			
nm1010	183	N	6/6	25-60	N	5/6	450-630
					int	1/6	450-590
nm1009	125	R	3/6	15-35	int	3/4	525-590
		int	3/6	15-35			
nm1008	98	R	9/9	15-35	R	4/4	450-660
nm1007	70	R	4/8	25-35	int	2/4	525-560
nm1006	55	R	6/7	15-35	R	2/4	300-560
					int	2/4	350-540
nm1005	25	N	3/4	8-40	N	4/4	540-610
		int	1/4	25-35			
nm1004	17	N	4/4	10-60	N	3/4	500-610

flows were documented during demagnetization. These differences survived diagenesis and allowed statistical derivation of ChRM directions at both localities. Although there are multiple carriers of NRM, a reliable polarity stratigraphy can be constructed for the Apache Canyon section and part of the Johnson Spring section.

Magnetic Polarity Stratigraphy

The polarity profile for the Apache Canyon section is shown in Figure 20 and is constructed from isolation of ChRM by AF and thermal demagnetization (Table 3). Polarity results from AF and thermal demagnetization methods are in agreement (Table 3); AF and thermal demagnetization successfully removed secondary viscous and chemical overprints and ChRM has been adequately isolated for all sites in the Apache Canyon section. Site- mean directions of tilt-corrected C2 and C3 ChRM components are shown in Table 4 and Figure 21. Six horizons from the Apache Canyon section displayed field directions of ChRM isolated by thermal demagnetization near the time-averaged Oligocene field direction (Table 4). A complete polarity profile through the section at Johnson Spring could not be produced, however two horizons give statistical directions that are near the time-averaged Oligocene field direction (nm950, nm956; Table 4). The mean directions are fair to poor. Inclination errors from a high sedimentation rate coupled with slight compaction and dispersion from variable grain size, angular volcanic rock fragments, and multiple carriers of ChRM explain the scatter. It is difficult to acquire a direction of high resolution ($k>30$; $a95<15$) from specimens drilled from sandstones and debris flows, and from averaging only 3 out of 4 specimens, rather than 7 out of 8 specimens.

The determination that the polarity of ChRM in the Apache Canyon section is DRM in origin is not unequivocal. The set of ChRM site-mean directions obtained from 400 to 590 °C in the Apache Canyon section could not be adequately tested by a tilt test because all the beds have the same strike and dip, however the proximity of the tilt-

Figure 20- Polarity of isolated characteristic remanent magnetism in the Thurman Formation

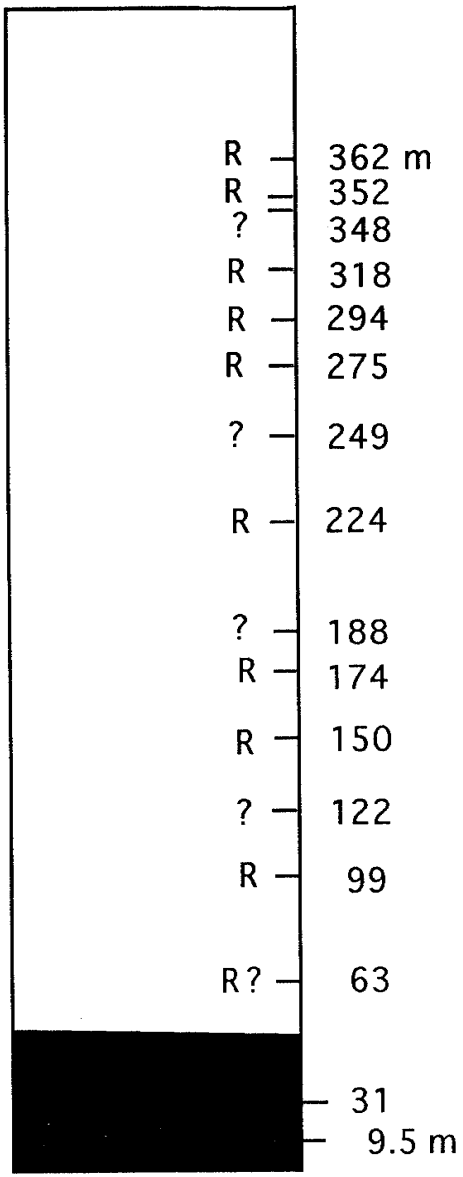

Johnson Spring, Rincon HIlls

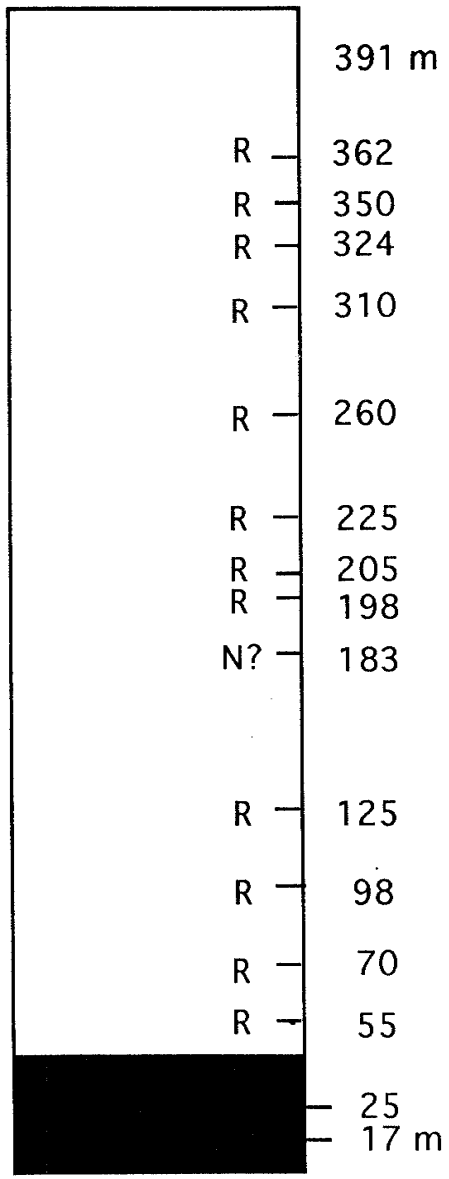

Apache Canyon, Caballo Mountains

Table 4--Site-mean directions of ChRM isolated by thermal and AF demagnetization.
*** = sandstone**

	Site	Strat height (m)	Pol	dm	n/t	inc	dec	k	a95
AF	**nm956**	174	R	15-40 mT	6/8	-27.9	179.8	14.7	18.07
	nm1004*	17	N	10-60 mT	4/4	52.2	3.3	92.8	9.5
	nm1005*	25	N	10-40 mT	3/4	50.4	5.5	278.3	7.4
	nm1006	55	R	15-35 mT	5/8	-25	155	8.1	28.6
	nm1008	98	R	15-35 mT	9/9	-44.5	141.6	61.6	6.61
	nm1009	125	R	10-35 mT	3/7	-31.9	128	4.9	62.7
	nm1018	350	R	15-35 mT	2/3	-66.8	136.2	21.1	57.4
	nm1019	362	R	10-35 mT	5/9	-54.6	171.5	25.3	15.5
Thermal	**nm950***	9.5	N	200-560 C	2/3	18.1	15.8	26.9	50.17
	nm956	174	R	300-610 C	3/4	-49.9	188.6	30.3	22.8
	nm961*	294	R	450-610 C	3/4	-33.9	211.9	10.3	40.53
	nm962	318	R	300-560 C	2/4	-51.2	144.5	5.4	17.72
	nm965	362	R	500-590 C	3/4	-43.7	210.6	6.9	51.14
	nm1004*	17	N	500-610 C	3/4	55	4.3	35.3	21.07
	nm1005*	25	N	540-610 C	4/4	47.7	353.2	32.6	16.33
	nm1008	98	R	400-580 C	4/4	-47.1	152.4	105	9.01
	nm1011*	205	R	200-560 C	3/4	-57.5	156	10.3	30
	nm1013	225	R	200-580 C	4/4	-54.4	167.5	35.3	15.6
	nm1016*	310	R	450-590 C	4/5	-33	195.2	14.6	24.8
	nm1017*	324	R	300-590 C	3/4	-39.7	139	5.9	56
	nm1019	362	R	450-610 C	3/4	-57.7	166.9	16.7	31.2

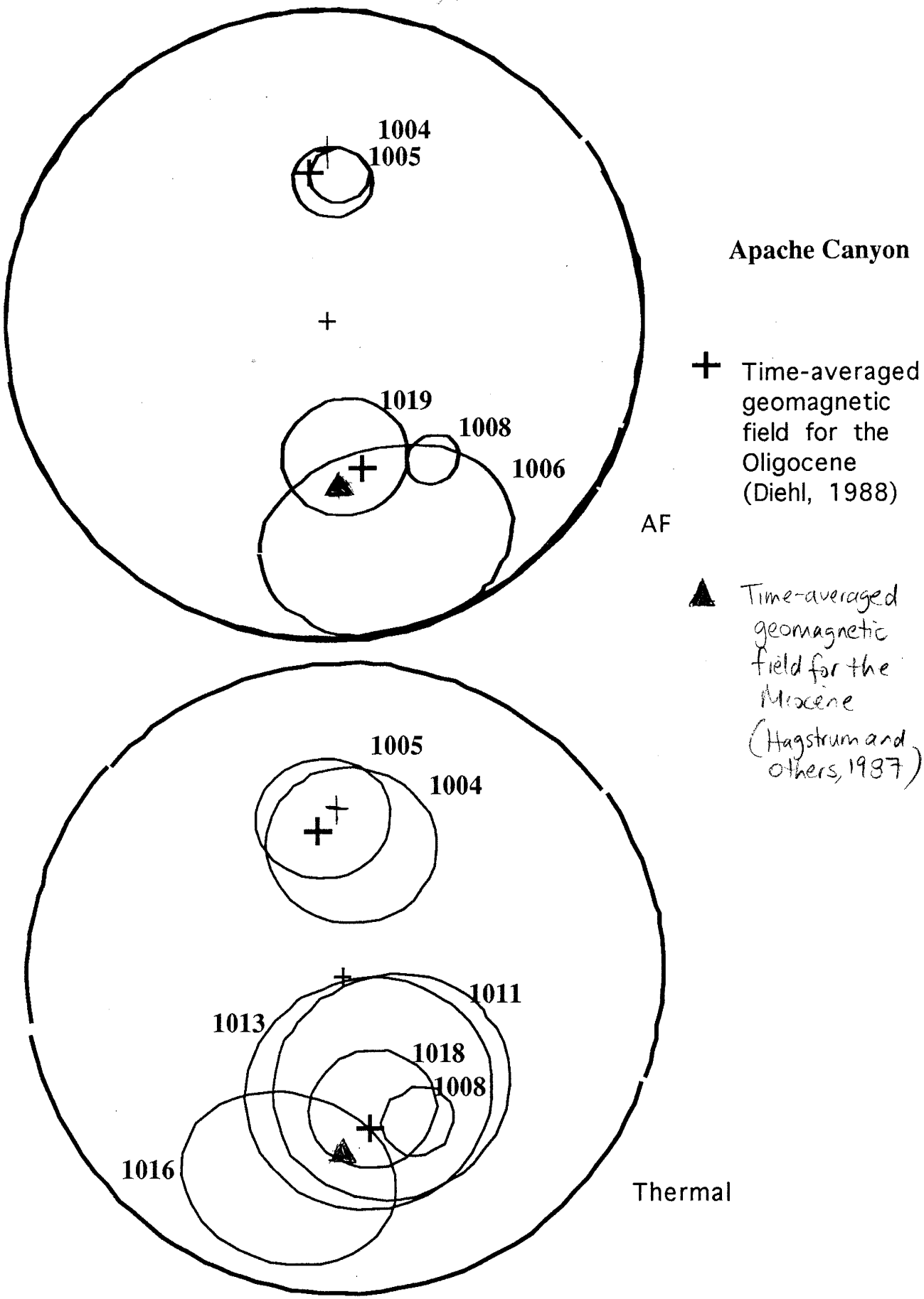

Figure21– Site mean directions of isolated ChRM components

corrected site-mean directions to the time-averaged Oligocene field direction suggests that the remanence isolated by thermal demagnetization formed prior to tilting. ChRM directions have been adequately isolated in the Apache Canyon section, but postdepositional DRM cannot be confirmed. Comparison with the calculated time-averaged field direction (dec=350.5, inc=50; Diehl and others, 1988) for the Oligocene shows that the site-mean directions of ChRM isolated by thermal demagnetization and corrected for tilt lie within a 12° arc of the time-averaged Oligocene field direction (Figure 22). The site-mean directions of ChRM isolated by AF demagnetization and their proximity to the time-averaged Oligocene field direction after correction for tilt is shown in Figure 23. Although the site-mean directions are closest to the time-averaged Oligocene field direction, they are also close to the time-averaged Miocene field direction (dec=355.4, inc=48; Hagstrum and others, 1987) calculated for this area (Figure 21). If ChRM is carried by impure magnetite, which should be detrital in origin, the direction and polarity should represent the magnetic field soon after deposition. Demagnetization behavior indicates ChRM in the Thurman Formation is carried by detrital magnetite. Therefore, the site-mean directions corrected for tilt and the polarity of ChRM in the Apache Canyon section are detrital in origin and the site-mean directions are close to the time-averaged field direction for the Oligocene.

In the Johnson Spring section the only site that responded adequately to AF demagnetization was the site drilled into a laminated sandstone interpreted as a sheetflood deposit (Kieling, 1993). The site-mean direction of site nm956 is dec=179.8 inc=-27.9 k=14.7 a95=18.07, n=6/8 , which is similar both to the mean direction of site nm956 determined by thermal demagnetization from 400 to 580 °C, dec=188.6, inc=-49.9, k=30.3, a95=22.8, n=3/4 and to the time-averaged field direction for the Oligocene, dec=170.5, inc=-50 (Diehl and others, 1988; Table 4). Results from thermal demagnetization of eleven of the 16 sites in the Johnson Spring section agree with the Apache Canyon polarity profile and a set of magnetic directions obtained from isolation

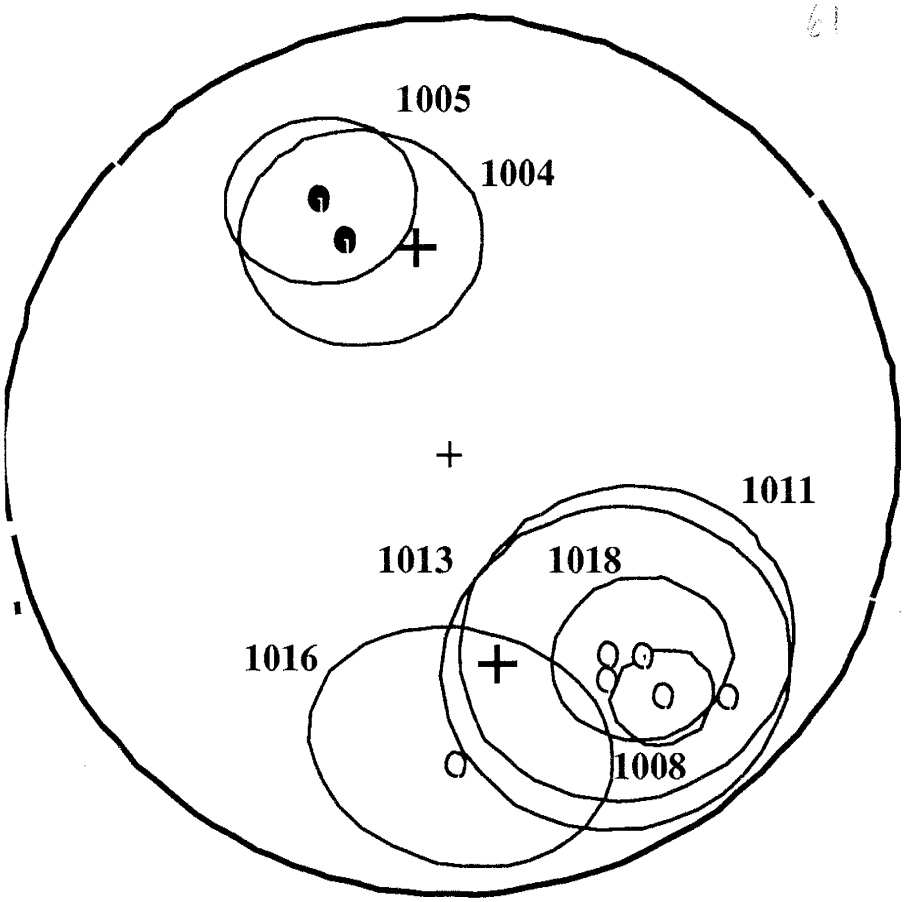

Apache Canyon

in situ

+ Time-averaged geomagnetic field for the Oligocene (Diehl, 1988)

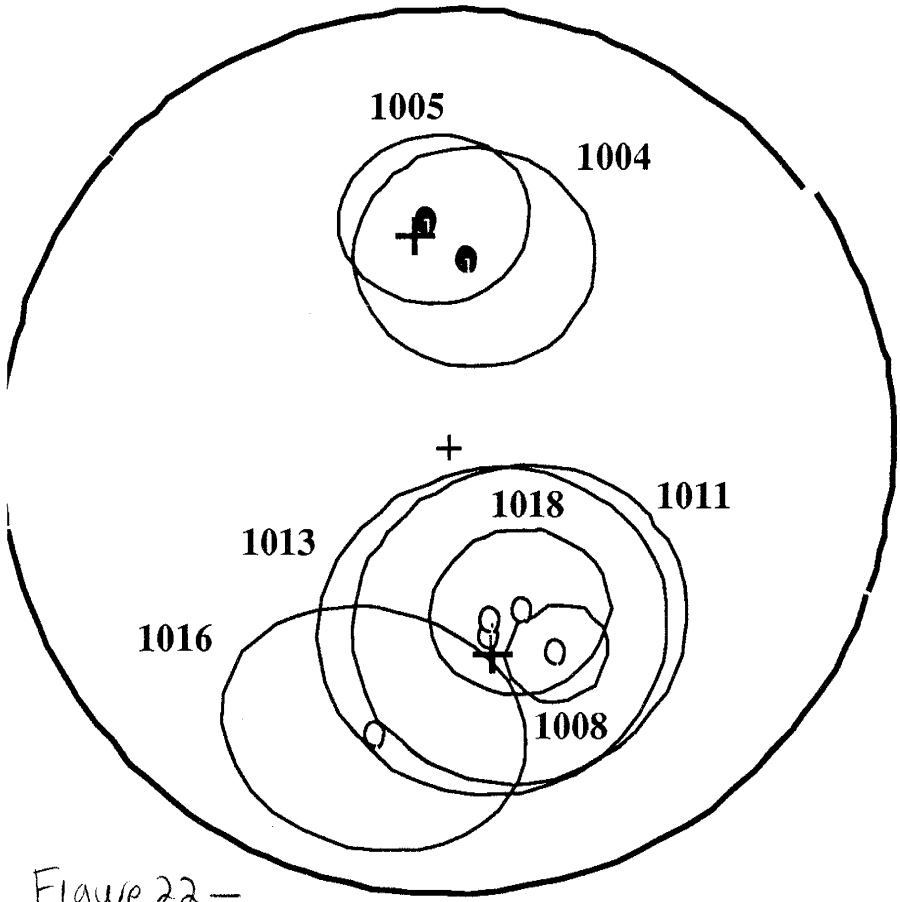

tilt corrected

Figure 22—

Site mean directions of isolated ChRM components from thermal demagnetization

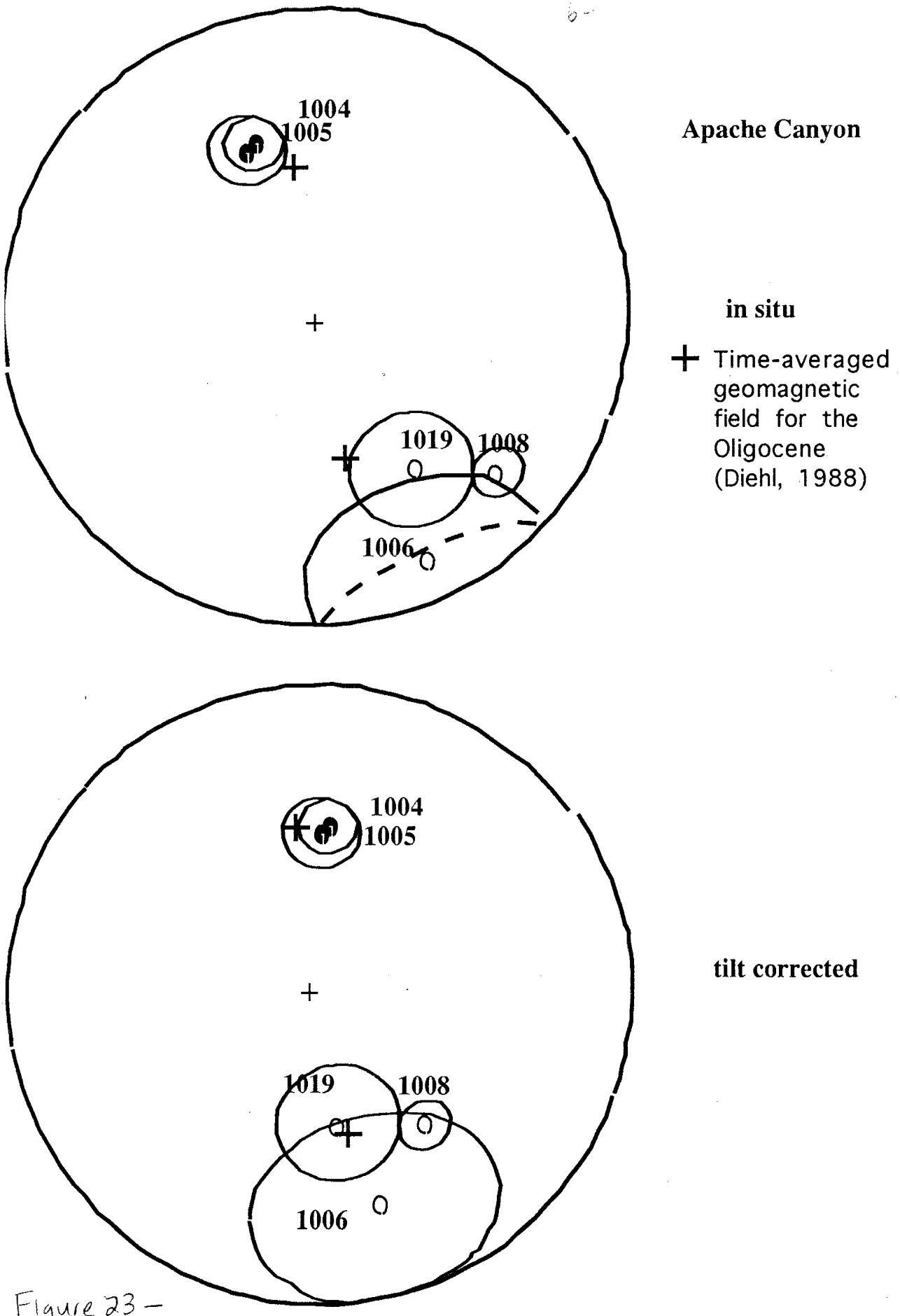

Figure 23 –

Site mean directions of isolated ChRM components from AF demagnetization

of component C2 at 400-590 C from 4 sites also clustered within a 12° arc of the time-averaged Oligocene field direction.

The time-averaged Miocene field direction calculated for the area is dec = 175.5 and inc=-48 (Hagstrum and others, 1983) so the fair to poor mean directions do not preclude the possibility that they represent the time-averaged field direction for the Miocene, not the Oligocene. During the Miocene, however, reversals occurred more often than in the Oligocene, and more than one reversal would be expected in a 400-m-thick sandstone unit. The polarity recovered from isolated ChRM from the horizon at 183 m (nm1010) in the Apache Canyon section suggests normal polarity, yet this normal polarity is carried by a high-temperature component with an unblocking temperature as high as 630°C and units drilled above and below it have reversed polarity. The horizon at 174 m in the Johnson Spring section has reversed polarity so this lone thin normal polarity zone recovered at 183 m may represent a very short polarity interval or may not be detrital in origin.

In summary, the site-mean directions corrected for tilt show that the polarity recovered and the isolated ChRM are detrital in origin and that the mean directions are close to the time-averaged field directions for the Oligocene. The magnetic polarity stratigraphy of the Thurman Formation and its correlation with the provenance ages of sanidines is shown in Figure 24. The base of the Thurman Formation has normal polarity and the middle and top have reversed polarity. The questionable normal-polarity horizon at about 183 m may be DRM in origin. The independent age control of 27.4 Ma sanidines of South Canyon Tuff pumice suggest that the reversal recorded in the Thurman Formation occurred at 27.4 Ma. The Geomagnetic Polarity Time Scale (GPTS; Cande and Kent, 1992) and the best match with the magnetic polarity stratigraphy in the Thurman Formation is shown in Figure 25. Although not shown in the GPTS of Figure 25, a normal polarity horizon has been recorded in marine magnetic profiles during the reversal that occurred at 27.4 Ma (9r-1; Cande and Kent, 1992). This short normal-

Figure 24 – Polarity and sanidine provenance in the Thurman Formation

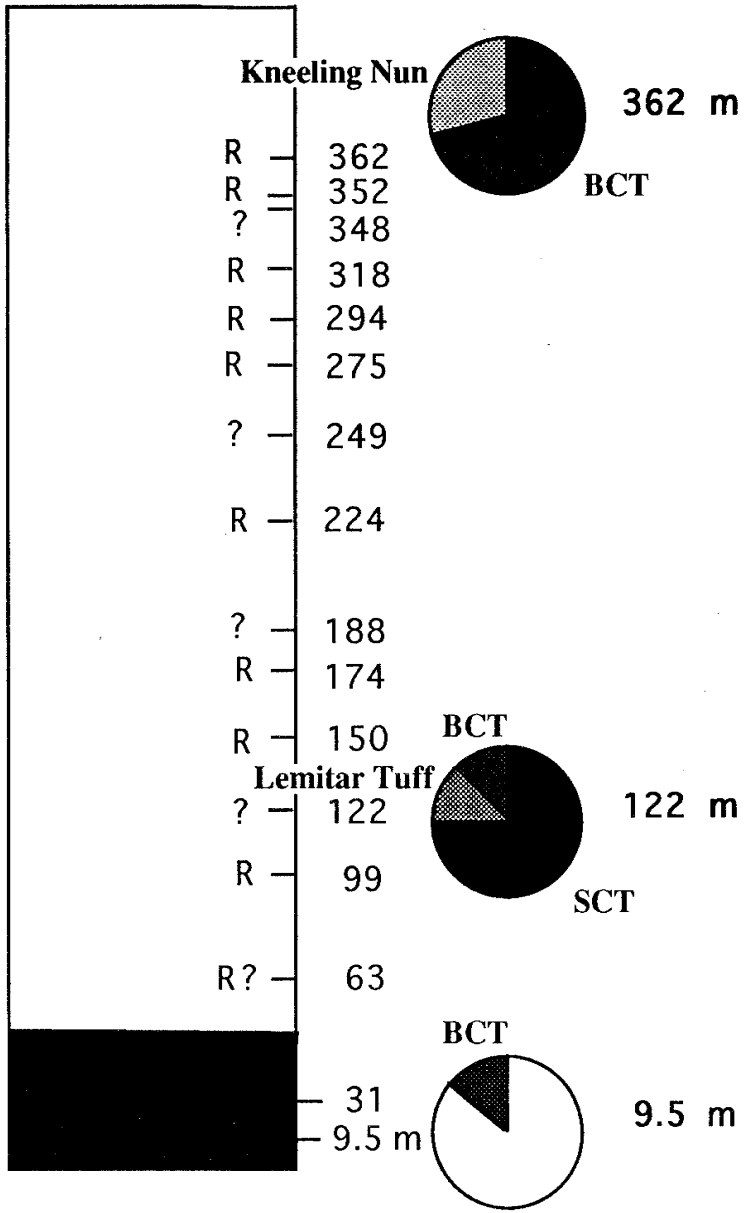

Johnson Spring, Rincon HIlls

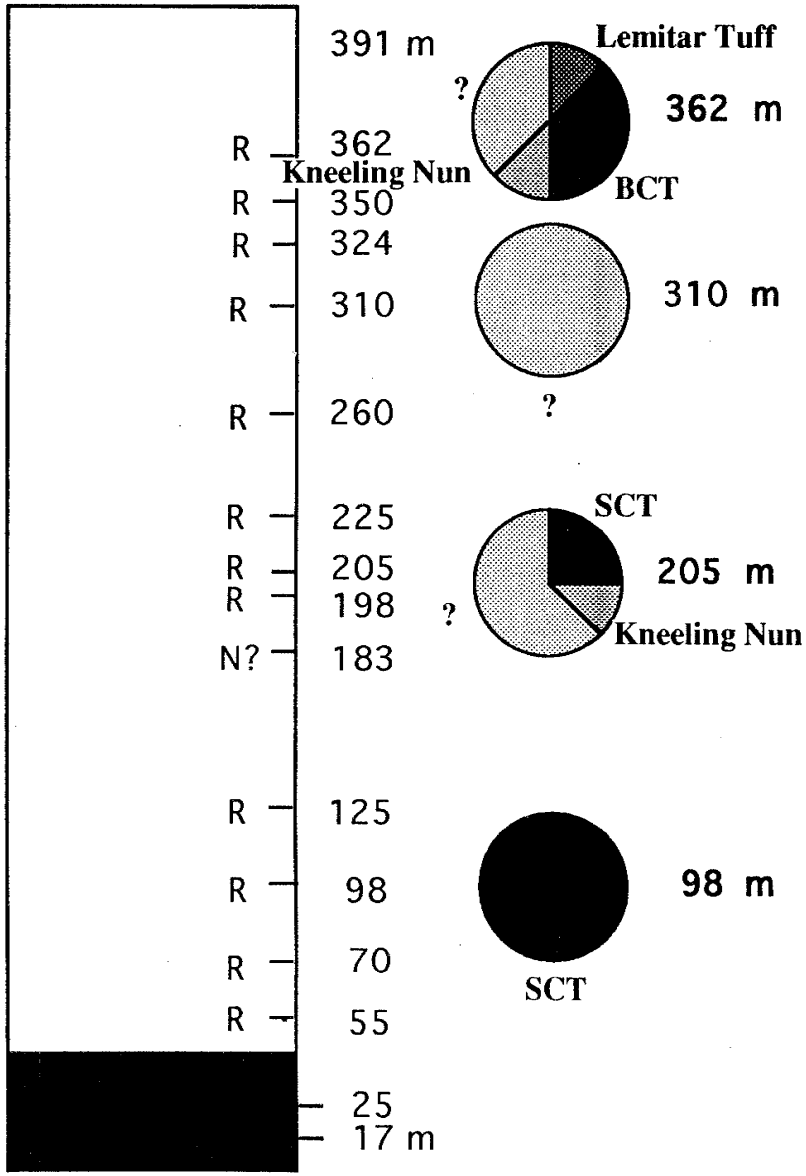

Apache Canyon, Caballo Mountains

49

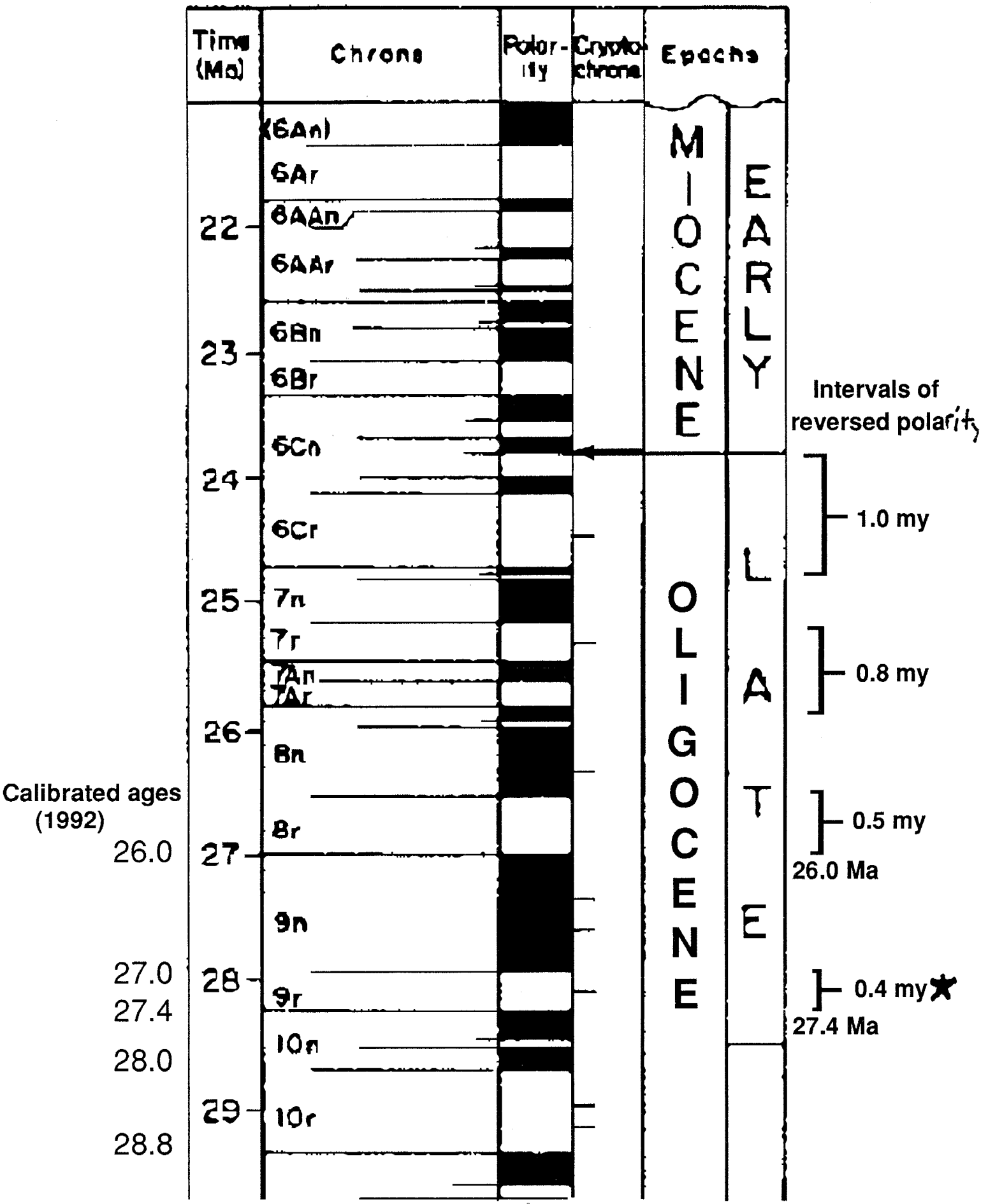

Figure 25 - GPTS (Cande and Kent, 1992).

polarity interval is less than 30 ky and may match the anomalous normal-polarity horizon at 183 m (site nm1010).

Faulting, volcanism, and deposition of the Thurman Formation along the Rio Grande rift

The Thurman Formation represents the distal facies of a volcaniclastic alluvial fan sequence that extended from the eastern margin of the Mogollon-Datil volcanic field and accumulated in an early rift basin of the Rio Grande rift. The sediments consist of andesitic and silicic pyroclastic and epiclastic material that was redistributed through gravity and stream-flow sedimentary processes. The sediments are largely pumiceous sandstones deposited as debris flows and sheet-flood deposits (Kieling, 1993). The debris flows and conglomeratic, crossbedded sandstones are comprised of pumice and tuff clasts, andesitic rock fragments, grains of sanidine, quartz, plagioclase and a trace of biotite in a matrix of finer ash that has been altered to clay, zeolites, and hydroxides. The debris flows and conglomeratic, crossbedded sandstones are largely derived from the eroded unwelded bottoms and tops of pumiceous rhyodacitic ignimbrites shed from the Mogollon-Datil volcanic field. Provenance ages of sanidines show that the Thurman Formation was also eroded in part from Box Canyon Tuff (33.5 Ma) and then Kneeling Nun Tuff (34.9 Ma), which are regional ignimbrites that extended to the eastern margins of the volcanic field. This epiclastic material shed from andesitic rocks, Box Canyon Tuff, and Kneeling Nun Tuff was deposited into a northwest-trending basin, where the Thurman Formation has been preserved. Independently established paleocurrent directions are southwestward (Kieling, 1993).

The Thurman Formation was deposited on tongues of Uvas Basaltic Andesite at the southern locality in the Rincon Hills and on the Vicks Peak Tuff (28.6 Ma) at the

northern locality in the Caballo Mountains. The Uvas Basaltic Andesite and the Vicks Peak Tuff extruded and erupted from their volcanic centers along a shallow-dipping shield. The sparse volcaniclastic rocks which were intercalated with these volcanic rocks and other 29.0-27.4 Ma SCORBA and rhyolitic ignimbrites indicate the Mogollon-Datil volcanic field was topographically low and formed a shallow-dipping plateau immediately prior to deposition of the Thurman Formation. The magnetic polarity stratigraphy recorded at the base of the Thurman Formation indicates that deposition of the Thurman Formation began during a normal polarity zone. Sanidine provenance ages show that Box Canyon Tuff was being eroded during this time.

The petrography and the sanidine provenance ages from the middle and top of the Thurman Formation indicate that andesitic volcanic rocks and the Box Canyon Tuff continued to be eroded and deposited as detritus throughout deposition of the Thurman Formation. Sanidine provenance ages from pumice at a 98 m horizon indicate that pumice fall from South Canyon Tuff was also incorporated into debris flows that fed into the medial to distal edges of the alluvial fan. Sanidines of South Canyon Tuff and the Lemitar Tuff were also dated at other middle to upper horizons of debris flows and sandstones in the Thurman Formation. The magnetic polarity stratigraphy recorded at these horizons indicate that a polarity reversal had occurred soon after the Thurman Formation first began to accumulate. This volcanic debris, which had been removed from rhyolitic volcanic centers to the north, were redeposited as volcaniclastic debris flows and sheet-flood deposits along the alluvial fan during a reversal of the geomagnetic field. Because the base of the Thurman Formation is relatively sparse in sanidines, lacks sanidines of South Canyon Tuff, and has normal polarity and because the South Canyon Tuff has reversed polarity and erupted soon after a polarity reversal (McIntosh and others, 1992), the age of the reversal recorded in the Thurman Formation appears to be the one at 27.4 Ma. The duration of this reverse-polarity zone is 0.4 my and indicates that volcaniclastic detritus was being deposited at an average rate greater than 1 mm/year.

The Thurman Formation records a change in the sedimentary system of the Mogollon-Datil volcanic field that coincided with the eruption of South Canyon Tuff from Mount Withington cauldron at 27.4 Ma.

Ferguson (1985) mapped the South Canyon Tuff (27.4 Ma) and located the southern margin of its cauldron from the distribution of co-ignimbrite lag-fall deposits along a structural depression. He also mapped at least 200 m of pumiceous and tuffaceous sandstones and debris flows in a basin to the south of the Mount Withington cauldron that formed after eruption of South Canyon Tuff and prior to the tuff of Turkey Springs (24.3 Ma). He described this unit of East Red Canyon as having rhyolitic and andesitic volanic rock fragments, burrows buried by ash, up to 15% pumice fragments 5 to 10 times larger than the median grain size, and clasts of rhyolite lava and tuff that decreased in size from the southeast to the northwest. A highland lay to the southeast of the Mount Withington cauldron during eruption of South Canyon Tuff and was blanketed by 20 m of pumice fall from South Canyon Tuff (Ferguson, 1985). The South Canyon Tuff is a multiple flow, simple cooling unit (Ferguson, 1985; LaRoche, 1981). A basal plinian deposit, a welded lower member, and an unwelded upper member that contains 6-9% pumice have been described near its source and the welded and unwelded members have been preserved as outflow (Ferguson, 1985; LaRoche, 1981). The South Canyon Tuff is a two-feldspar tuff that has a 3:2 proportion of sanidine to quartz and plagioclase and biotite present in trace amounts (Ferguson, 1985). Pumice fall at the base of the South Canyon Tuff is 20-70 m thick near the Mount Withington cauldron and its overall extent indicates that the prevailing wind was from the southwest (Ferguson, 1985). The late Oligocene prevailing wind direction recorded by these plinian deposits of South Canyon Tuff also parallels the direction recorded by eolian sandstones of the basin fill (Ferguson, 1985).

The prevailing wind during the late Oligocene was from the southwest (Ferguson, 1985). The pumice of South Canyon Tuff in the Thurman Formation could only have

been carried to its site of deposition by fluvial processes. Pumice fall of South Canyon Tuff or its unwelded tuff was reworked and deposited in debris flows and fluvial sandstones in an area along the eastern edge of the plateau of the Mogollon-Datil volcanic field, where the drainage pattern was to the south. The source of most of the volcaniclastic sandstone in the Thurman Formation was derived from a highland slightly southeast of the Mount Withington cauldron.

Volcaniclastic sediments of epiclastic, pyroclastic and autoclastic origin accumulate within 1 to 5 years after cataclysmic eruptions from stratovolcanoes, when more than half of fall material is removed (Swanson and others, 1982). Pyroclastic material usually ranges from sand to pebble size and when reworked can be deposited as what appears to be poorly sorted sand with larger buoyant pumice clasts (Smith, G., wr. comm. 1989). For shield-like volcanic centers, accumulation rates are far less for rhyolitic ash and pumice and andesitic cinder, as is documented by the sparse sediments accumulated from 34.9 and 32.1 to 27.4 Ma in the Mogollon-Datil volcanic field. The dramatic increase in sediment supply that began with the Thurman Formation and continued with the Haynor Ranch Formation of the Santa Fe Group was triggered by the sudden change in stress of the tectonic regime for southern New Mexico that coincided with the formation of the San Andreas transform fault 1000 miles to the west. The sanidine provenance ages and the magnetic polarity stratigraphy in the Thurman Formation show that this change in stress took place at about 27.4 Ma immediately prior to the catastrophic eruption of South Canyon Tuff (700 km^3) from Mount Withington caldera. The increase in sediment supply in grabens of the southern Rio Grande rift began with deposition of reworked pyroclastic fall of South Canyon Tuff and continued with faulting and deposition of the lower Santa Fe Group through the late Oligocene.

Conclusions

1) Although there are multiple carriers of NRM, a reliable polarity stratigraphy can be constructed for the Apache Canyon section and part of the Johnson Spring section and can be matched with the Geomagnetic Polarity Time Scale.

2) The magnetic polarity stratigraphy recorded at the base of the Thurman Formation indicates that deposition of the Thurman Formation began during a normal-polarity zone. Sanidine provenance ages show that Box Canyon Tuff was being eroded during this time.

3) A polarity reversal occurred soon after tuffaceous sandstones and pumiceous debris flows in the Thurman Formation first began to accumulate. Except for one short normal-polarity interval of <30 ky recorded at 183 m, the rest of the Thurman Formation records a reverse polarity.

4) Provenance ages indicate that pumice and ash fall from South Canyon Tuff appear to be a dominant source for the volcaniclastic detritus shed into much of the Thurman Formation.

5) The polarity stratigraphy, provenance ages, and the pumiceous lithology of the sandstones and debris flows indicate that the Thurman Formation was deposited near the reversal at 27.4 Ma that lasted 0.4 my. Volcaniclastic detritus was being accumulated at an average rate greater than 1 mm/year.

6) The Thurman Formation may correlate with the 200-m-thick pumiceous and tuffaceous sandstones and debris flows of the unit of East Red Canyon in a basin to the south of the Mount Withington cauldron that formed after eruption of South Canyon Tuff and prior to the tuff of Turkey Springs (24.3 Ma).

7) Most of the detritus in volcaniclastic sandstones and debris flows in the Thurman Formation was derived from a highland slightly southeast of the Mount Withington cauldron.

8) The Thurman Formation records a sudden change in the sedimentation pattern along the eastern edge of the Mogollon-Datil volcanic field that coincided with the eruption of South Canyon Tuff from Mount Withington cauldron at 27.4 Ma.

9) The depositional history of the Thurman Formation can be determined from the petrography, polarity stratigraphy, and provenance ages. In summary, a source area underwent rapid unroofing at a time that fresh pumice was incorporated as float into at least one debris flow (nm1008; 98 m horizon). The independent age control of the 27.4 Ma sanidines of South Canyon Tuff pumice suggest that the Thurman Formation is as old as 27.4 Ma. No sanidines this young were dated from the base of the Johnson Spring section. Only Box Canyon Tuff appears to have been eroded during the normal polarity zone recorded at the base of the Thurman Formation. A reversal that occurs at 27.4 Ma (McIntosh et al., 1992) matches well with the magnetic polarity stratigraphy at the Apache Canyon section.

Sanidine provenance ages indicate the sands of the Thurman were derived locally and from the north and west, where the caldera explosions and outflow distributions for the Lemitar Tuff and South Canyon Tuff are located. The ignimbrite detritus in the Thurman Formation is not derived solely from local outcrops because the extents of South Canyon Tuff and Lemitar Tuff end 20 km to the north of the Caballo Mountains. Local faulting, tectonic unroofing, and erosion of rhyolitic and andesitic volcanic rocks and mass wasting soon after a caldera explosion produced the thick assemblage of volcaniclastic rock fragments and minerals found in the Thurman Formation. Local faulting and a caldera explosion remobilized thick poorly consolidated 27.6-27.4 Ma ash fall, pumice, and tuff. At 27.4 Ma debris flows along a southward drainage pattern carried detritus of Lemitar Tuff and freshly erupted pumice and ash fall of South Canyon Tuff into a newly formed rift basin, where volcaniclastic detritus was deposited at an average rate of 1 mm/year.

The provenance age distributions and magnetic polarity stratigraphy support earlier conclusions that extensional faulting and basin subsidence associated with rifting and volcanism began along the Mogollon-Datil volcanic field around 28 to 27 Ma. The Thurman Formation represents the medial to distal edges of an alluvial fan in an area that was undergoing faulting at the time that the Mount Withington caldera erupted the 27.4 Ma South Canyon Tuff. The Thurman Formation documents the change in sedimentation along the edge of the Mogollon-Datil volcanic field that began at 27.4 Ma and continued with sedimentation of the lower Santa Fe Group through the late Oligocene.

References

Banerjee, S. K., 1987, Problems and current trends in rock magnetism and paleomagnetism: EOS Trans. Am. Geophys. Union, 68 (30), p. 650 and 662-663.

Barghoorn, S., 1981, Magnetic-polarity stratigraphy of the Miocene type Tesuque Formation, Santa Fe Group, in the Espanola Valley, New Mexico: GSA Bulletin, v. 92, p. 1027-1041.

Bogaard, P. V. D, Hall, C. M., Schmincke, H., York, D, 1987, 40Ar/39Ar laser dating of single grains: ages of Quaternary tephra from the East Eifel volcanic field, FRG: Geophysical Research Letters, v. 14, pp. 1211-1214.

Butler, R. F., 1992, Paleomagnetism: Blackwell Scientific Publications, Boston, 319 pp.

Cameron, K. L, Nimz, G. J., Kuentz, D., Niemeyer, S., and Gunn, S., 1989, Southern Cordilleran Basaltic Andeite suite, southern Chihuahua, Mexico--a link between Tertiary continental arc and flood basalt magmatism in North America: Journal of Geophysical Research, v. 94, pp. 7817-7840.

Cande, S. C., and Kent, D. V., 1992, A new geomagnetic polarity time scale for the Late Cretaceous and Cenozoic: Journal of Geophysical Research, v. 97, pp. 13,917-13,951.

Cather, S. M., and Chapin, C. E., 1989, Field guide to upper Eocene and lower Oligocene volcaniclastic rocks of the northern Mogollon-Datil volcanic field: NMBMMR Memoir 46, pp. 60-67.

Chamberlin, R. M., 1983, Cenozoic domino-style crustal extension in the Lemitar Mountains, New Mexico: A summary: NM Geological Society, Guidebook 34, p. 111-118.

Chapin, C. E., 1988, Axial basins of the northern and central Rio Grande rift; in Sloss, L. L. (ed.), Sedimentary cover--North American craton: US: GSA, The Geology of North America, v. D-2, p. 165-170.

Chapin, C. E., and Seager, W. R., 1975, Evolution of the Rio Grande rift in theSocorro and Las Cruces areas: NM Geological Society, Guidebook 26, p. 297-321.

Christianson, R. L., and Lipman, P. W., 1972, Cenozoic volcanism and plate tectonic evolution of the western United States, part II, Late Cenozoic: Philosophical Transactions of the Royal Society of London Series A, v. 271, pp. 249-284.

Clemons, R., 1975, Petrology of the Bell Top Formation: NMGS, Guidebook 26, p. 123-130.

Collinson, D. W., 1965, Depositional remanent magnetisation in sediments: Journal of Geophysical Research, v. 70, pp. 4663-4668.

Dalrymple, G. B, and Duffield, W. A., 1988, High-precision 40Ar/39Ar dating of Oligocene rhyolites from the Mogollon-Datil volcanic field using a continuous laser system: Geophysical Research Letters, v. 15, pp. 463-466.

Deino, A. L., 1989, Single-crystal 40Ar/39Ar dating as an aid in correlation of ash flows: examples from the Chimney Spring/New Pass Tuffs and the Nine Hill/Bates Mountain Tuffs of California and Nevada: (abstract) NMBMMR Bulletin 131, p. 70.

Deino, A. L., and Best, M. G., 1988, Use of high-precision single-crystal 40Ar/39Ar ages and TRM data in correlation of an ash-flow deposit in the Great Basin: (abstract) GSA Abstracts with Program, v. 20, p. 397.

Dekkers, M. J., 1989, Magnetic particles of natural pyrrhotite. II. High- and low-temperature behavior of Jrs and TRM as function of grain size: Physical Earth Planetary Inter., v. 57, pp. 266-283.

Diehl, J. F., McClannahan, K. M., and Bornhorst, T. J., 1988, Paleomagnetic results from the Mogollon-Datil volcanic field, southwestern New Mexico, and a refined mid-Tertiary reference pole for North America: Journal of Geophysical Research, v. 93, pp. 4869-4879.

Duffield, W. A., and Dalrymple, G. B., 1990, The Taylor Creek Rhyolite of New Mexico: a rapidly emplaced field of lava domes and flows: Bulletin of Volcanology, v. 52, pp. 475-487.

Dunlop, D. J., and Ozdemir, O., 1990, Alternating field stability of high-temperature viscous remanent magnetism: Physics of the Earth and Planetary Interiors, v. 65, pp. 188-196.

Ferguson, C. A., 1985, Geology of the east-central San Mateo Mountains, Socorro County, New Mexico: unpublished thesis, New Mexico Tech, 118 pp.

Fisher, R. A., 1953, Dispersion on a sphere: Proceedings of Royal Society of London, 217, p. 295-305.

Gapeev, A. K., Gribov, S. K., Dunlop, D. J., Ozdemir, O., and Shcherbakov, V. P., 1991, A direct comparison of the properties of CRM and VRM in the low-temperature oxidation of magnetite: Geophysical Journal International, v. 105, p. 407-418.

Hagstrum, J. T., Sawlan, M. G., Hausback, B. P., Smith, J. G., and Gromme, C. S., 1987, Miocene paleomagnetism and tectonic setting of the Baja California peninsula, Mexico: Journal of Geophysical Research, v. 92, pp. 2627-2640.

Harrison, R. W., 1990, Cenozoic stratigraphy, structure, and epithermal mineralization of the north-central Black Range, New Mexico, in the regional geologic framework of south-central New Mexico: unpublished dissertation, New Mexico Tech, 960 pp.

Harrison, T. M., and Burke, K., 1989, 40Ar/39Ar thermochronology of sedimentary basins using detrital K-feldspar: Examples from the San Joaquin Valley, California, Rio Grande Rift, New Mexico and North Sea; in Naeser, N., and McCulloh, T., Thermal Histories of Sedimentary Basins: Springer Verlag, pp. 141-155.

Heider, F., and Dunlop, D. J., 1987, Two types of chemical remanent magnetism during the oxidation of magnetite: Physics of the Earth and Planetary Interiors, v. 46, pp. 24-45.

Heizler, M. T., and Harrison, T. M., 1991, The heating duration and provenance age of rocks in the Salton Sea geothermal field, southern California: Journal of Volcanology and Geothermal Research, v. 46, pp. 73-97.

Hillhouse, J. W., Ndombi, J. W. M., Cox, A., Brock, A., 1977, Additional results on palaeomagnetic stratigraphy of the Koobi Fora Formation, east of Lake Turkana (Lake Rudolf), Kenya: Nature, v. 265, p. 411-415.

Irving, E., 1957, Origin of the paleomagnetism of the Torridonian sandstones of north-west Scotland, Philosophical Transactions of the Royal Society of London, v. 250, pp. 100-110.

Irving, E., and Major, A., 1964, Post-depositional detrital remanent magnetism in a synthetic sediment: Sedimentology, v. 3, pp. 135-143.

Johnson, N. M., Officer, C. B., Opdyke, N. D., Woodard, G. D., Zeitler, P. K., Lindsay, E. H., 1983, Rates of late Cenozoic tectonism in the Vallecito-Fish Creek basin, western Imperial Valley, California: Geology, v. 11, pp. 664-667.

Johnson, N. M., Sheikh, K. A., Dawson-Saunders, E., McRae, L. E., 1988, The use of magnetic-reversal time lines in stratigraphic analysis: a case study in measuring variability in sedimentation rates; in New perspectives in basin analysis, Kleinspehn, K. L., and Paola, C. (eds.): Springer Verlag, New York, p. 189-200.

Johnson, N. M., Stix, J., Tauxe, L., Cerveny, P. F., and Tahirkheli, R. A. K., 1985, Paleomagnetic chronology, fluvial process and implications of the Siwalik deposits near Chinji Village, Pakistan: Journal of Geology, v. 93, pp. 27-40.

Johnson, N. M., and McGee, V. E., 1983, Magnetic polarity stratigraphy: Stochastic properties of data, sampling problems, and the evaluation of interpretations: Journal of Geophysical Research, v. 88, no. B2, p. 1213-1221.

Karlin, R., 1990, Magnetite diagenesis in marine sediments from the Oregon continental margin, Journal of Geophysical Research, v. 95, pp. 4405-4419.

Kelley, V. C., and Silver, C., 1952, Geology of the Caballo Mountains: UNM Press Geologic Series, no. 4.

Khramov, A. N., Orientational magnetization of finely dispersed sediments, Izv. Acad. Sci. USSR Phys. Solid Earth, no. 1, pp. 63-66.

Kieling, M., 1993,

Kirschvink, J. L., 1980, The least-squares line and plane and the analysis of paleomagnetic data: Geophysical Journal of the Royal Astronomical Society, 62, p 699-718.

Lambert, P. W., 1968, Quaternary stratigraphy of the Albuquerque area, New Mexico: unpublished PhD dissertation, University of New Mexico, 329 pp.

LaRoche, T. M., 1980, Geology of the Gallinas Peak area, Socorro County, New Mexico: unpublished master's thesis, New Mexico Tech, 145 pp.

Larson, E. E., and Walker, T. R., 1975, Development of chemical remanent magnetization during early stages of red-bed formation in late Cenozoic sediments, Baja California: GSA Bulletin, v. 86, pp. 639-650.

Larson, E. E., Walker, T. R., Patterson, P. E., Hoblitt, R. P., and Rosenbaum, J. G., 1982, Paleomagnetism of the Moenkopi Formation, Colorado Plateau: Basis for long-term model of acquisition of chemical remanent magnetism in red beds: Journal of Geophysical Research, v. 87, pp. 1081-1106.

LoBello, P., Feraud, G., Hall, C. M., York, D., Lavina, P., Bernat, M., 1987, 40Ar/39Ar step-heating and laser fusion dating of a Quaternary pumice from Neschers, Massif Central, France: the defeat of xenocrystic contamination: Chemical Geology, v. 66, pp. 61-71.

Mack, G. H., and Grigsby, J. D., 1985, Mechanical and chemical diagenesis of the Haynor Ranch and Rincon Valley Formations (Santa Fe Group, Miocene), San Diego Mountain, New Mexico: New Mexico Geology, v. 7, pp. 45-48.

Mayerson, D., 1979, Geology of the Corkscrew Canyon-Abbe Spring area, Socorro County, New Mexico: unpublished master's thesis, New Mexico Tech, 125 pp.

McIntosh, W. C., 1991, Evaluation of paleomagnetism as a correlation criterion for Mogollon-Datil ignimbrites, southwestern New Mexico: Journal of Geophysical Research, v. 96, p. 13,459-13,483.

McIntosh, W. C., Chapin, C. E., Ratte, J. C., Sutter, J. F., 1992, Time-stratigraphic framework for the Eocene-Oligocene Mogollon-Datil volcanic field, southwest New Mexico: GSA Bulletin, v. 104, p. 851-871.

McIntosh, W. C., Geissman, J. W., Chapin, C. E., Kunk, M. J., Henry, C. D., 1992, Calibration of the latest Eocene-Oligocene geomagnetic polarity time scale using $^{40}Ar/^{39}Ar$ dated ignimbrites: Geology, v. 20, p. 459-463.

McIntosh, W. C., Sutter, J. F., Chapin, C. E., and Kedzie, L. L., 1990, High-precision 40Ar/39Ar sanidine geochronology of ignimbrites in the Mogollon-Datil volcanic field, southwestern New Mexico: Bulletin of Volcanology, v. 52, p. 584-601.

McIntosh, W. C., Sutter, J. F., Chapin, C. E., Osburn, G. R., Ratte, J. C., 1986, A stratigraphic framework for the eastern Mogollon-Datil volcanic field based on paleomagnetism and high-precision 40Ar/39Ar dating of ignimbrites--a progress report: NMGS Guidebook 37, pp. 183-195.

McIntosh, W. C., Kedzie, L. L., Sutter, J. F., 1990, Paleomagnetism and 40Ar/39Ar ages of ignimbrites, Mogollon-Datil volcanic field, southwestern New Mexico: NMBMMR Bulletin 135, 79 pp.

Morgan, P, Seager, W. R., and Golombek, M. P, 1986, Cenozoic thermal, mechanical, and tectonic evolution of the Rio Grande rift: Journal of Geophysical Research, v. 91, pp. 6263-6276.

Opdyke, N. D., 1972, Paleomagnetism of deep-sea cores: Reviews of Geophysics and Space Science, v. 10, pp. 213-249.,

Osburn, G. R., and Chapin, C. E., 1983, Nomenclature for Cenozoic rocks of the northeast Mogollon-Datil volcanic field, New Mexico: NMBMMR Stratigraphic Chart 1.

Ozdemir, O., and Dunlop, D. J., 1989, Chemico-viscous remanent magnetization in the Fe3O4-γFe2O3 system: Science, v. 243, p. 1043-1047.

Renne, P. R., Becker, T. A., Swapp, S. M., Turrin, B. D., and Onstott, T. C., 1989, The 40Ar/39Ar laser-probe applied to sediment provenance and Hinterland tectonics: an example from the Montgomery Creek Formation, California, EOS, v. 70, p. 488.

Reynolds, R. L., 1979, Comparison of the TRM of the Yellowstone Group and the DRM of some Pearlette ash beds: Journal of Geophysical Research, v. 84, p. 4525-4531.

Roberts, A. P., and Pillans, B. J., 1993, Rock magnetism of lower/middle Pleistocene marine sediments, Wanganui Basin, New Zealand: Geophysical Research Letters, v. 20, pp. 839-842.

Roberts, A. P., and Turner, G. M., 1993, Diagenetic formation of ferrimagnetic iron sulphide minerals in rapidly deposited marine sediments, South Island, New Zealand: EPSL, v. 115, pp. 257-273.

Seager, W. R., and Hawley, J. W., 1973, Geology of Rincon quadrangle, NMBMMR Bulletin 101, 42 pp.

Seager, W. R., and Mack, G. H., in prep,

Seager, W. R., Shafiqullah, M., Hawley, J. W., Marvin, R. F., 1984, New K-Ar dates from basalts and the evolution of the southern Rio Grande rift: GSA Bulletin, v. 95, p. 87-99.

Snowball, I. F., Magnetic hysteresis properties of greigite (Fe3S4) and a new occurrence in Holocene sediments from Swedish Lappland, Physical Earth Planetary Inter., v. 68, pp. 32-40.

Stacey, F. D., 1972, On the role of Brownian Motion in the control of detrital remanent magnetism of sediments: Pure Applied Geophysics, v. 98, pp. 139-145.

Swanson, D. A., Wright, T. H., ,1982,

Swisher, C. C., and Prothero, D. R., 1990, Single-crystal 40Ar/39Ar dating of the Eocene-Oligocene Transition in North America: Science, v. 249, pp. 760-762.

Verosub, K. L., 1977, Depositional and postdepositional processes in the magnetization of sediments: Reviews in Geophysics and Space Physics, v. 15, p. 129-143.

Walker, T. R., Larson, E. E., and Hoblitt, R. P., 1981, Nature and origin of hematite in the Moenkopi Formation (Triassic), Colorado Plateau: a contribution to the origin of magnetism in red beds: Journal of Geophysical Research, v. 86, pp. 317-333.

Walker, T. R., Waugh, B., and Crone, A. J., 1978, Diagenesis in first-cycle desert alluvium of Cenozoic age, southwestern United States and northwestern Mexico: GSA Bulletin, v. 89, pp. 19-32.

Waresback, D. B., and Turbeville, B. N., Evolution of a Plio-Pleistocene volcanogenic-alluvial fan: The Puye Formation, Jemez Mountains, New Mexico: GSA Bulletin, v. 102, pp. 298-314.

Welty, C. M., 1988, Petrology and diagenesis of the Ojo Caliente Sandstone (Miocene?), Espanola Basin, New Mexico: unpublished thesis, University of Colorado, Boulder, 105 pp.

Woodard, T. W., 1982, Geology of the Lookout Mountain area, northern Black Range, Sierra County, New Mexico, unpublished MS thesis, University of New Mexico, 95 pp.

York, D., Hall, C. M., Yanase, Y, Hanes, J. A., and Kenyon, W. J., 1981, 40Ar/39Ar dating of terrestrial minerals with a continuous laser: Geophysical Research Letters, v. 8, pp. 1136-1138.

Zielinski, R. A., Bloch, S., and Walker, T. R., 1983, The mobility and distribution of heavy metals during the formation of first cycle red beds: Economic Geology, 78, pp. 1574-1589.

Zijderveld, J. D. A., 1967, A. C. demagnetization of rocks: analysis of results; in Methods of Paleomagnetism, Collinson, D. W., Creer, D. W., and Runcorn, S. K. (eds.): Elsevier, New York, p. 254-286.

This thesis is accepted on behalf of the faculty of the Institute by the following committee:

_____

Adviser

_____

_____

_____

_____

_____

Date